DOCTOR OF PHILOSOPHY

Dynamics and characteristics of organo-mineral aggregates in shelf seas

McCreadie, Rebecca Jane

Award date:
2003

Awarding institution:
University of Wales, Bangor

Title: Dynamics and characteristics of organo-mineral aggregates in shelf seas

A thesis submitted in accordance with the requirements of the University of Wales for the degree of Doctor of Philosophy

By Rebecca Jane McCreadie

University of Wales, Bangor
School of Ocean Sciences,
Menai Bridge,
Wales,
LL59 5EY
Great Britain

July 2003

ABSTRACT

Suspended sediment characteristics, primarily size and concentration, were measured, in conjunction with temperature, salinity and turbulent dissipation at two sites: one in the northern North Sea (59° 20' N, 1°E; 14/10/98 – 09/11/98) and one in the Clyde Sea (55° 21' N, 5° 2' W; 21/05/00 – 22/05/00). An in-situ laser particle sizer (a LISST-100B) and a laboratory based time-of-transition particle sizer (a Galai) were used to obtain suspended particle size distributions. These instruments were evaluated against microscope and Coulter Counter measurements using spherical particles as well as directly comparing field results.

Both instruments performed well when measuring standardised particles in the laboratory and distributions obtained from the marine environment if the coarse part of the distribution was ignored. It was concluded that for mixed composition populations the Galai was likely to discard a proportion of the population if the optical properties varied greatly from the majority. For the LISST, it was concluded that the returned size distribution was representative of the population unless particles greater than 250 μm were present, when the coarse part of the distribution was "contaminated" by these particles.

At both study sites an apparent minimum in mass concentration (measured by a transmissometer) and a maximum in mean grain size occurred within the thermocline. The transmissometer results are found to be representative of the concentration of the fine portion of the population rather than the whole population. Using a simple aggregation model it is shown that the mass concentration minimum measured in the North Sea was not real, however in the Clyde Sea it is, although exaggerated. It is concluded that enhanced aggregation in the thermocline causes increased settling velocities, compared to the source particles, resulting a negative mass flux. These results are the first direct evidence that turbulence controls the equilibrium floc diameter in the marine environment.

ACKNOWLEDGEMENTS

My main thanks go to my supervisor Dr. Sarah Jones who provided guidance and advice throughout the study. Sarah always made time for me regardless of her other commitments and workload. Together with Dr. Colin Jago she taught me the procedures for collecting and processing suspended sediment data. My thanks also go to the other member of my research committee, Prof. Alan Elliott who made useful contributions at the annual committee meetings.

The work of the captain and crew of the *RRS Challenger*, *RRS Charles Darwin*, *Pelagia*, *Mitra* and *Belgica* was excellent and without then this study would not have been possible. Thanks are also due to Dr. Robin McCandliss, Mr. Malcolm Hearn and Mr. Neil Fisher who collected a lot of the data used in this study and became good friends. Thanks also to Dr. Tony Bale from the Plymouth Marine Laboratory for his training and guidance in the use of the Coulter Counter and Lasentec and to Alan Nield for his excellent technical advice. Thanks are also due to the turbulence group at UWB for supplying the turbulence data, BODC for supplying much of the data used in this thesis, NERC for the studentship and PROVESS for providing the fieldwork framework.

Finally, special thanks go to Adam McCreadie who provided constant encouragement and support.

To my parents

Table of Contents

Chapter 4: Comparison and Validation of Three Particle Sizers

Chapter 5: Northern North Sea

Chapter 6: Clyde Sea

Chapter 7: Discussion

Chapter 8: Conclusions and Further Work

List of Figures

Chapter 5: Northern North Sea

Chapter 6: Clyde Sea

Chapter 7: Discussion

List of Tables

Chapter 1

Introduction

1.1. Background and motivation for the study

Suspended particulate matter (SPM) occurs round the world's oceans in varying concentrations. Within shelf seas SPM concentration is generally greater than in the deep ocean or on the continental slope. As suspended particles tend to be small in size the dynamics of such sediments are vital in the understanding of chemical and biological processes that are occurring. Small particles have an affinity with nutrients and chemicals which make them effective transporters of both vital nutrients for biology as well as pollutants. Where SPM concentrations are high, light penetration is restricted and therefore so is productivity. The surfaces of these particles are also important sites for primary microbial activity.

Suspended sediment dynamics are not only important for biological reasons but also physical ones. Formation and maintenance of bedforms, such as sand banks, can be explained through resuspension processes and transport pathways of both SPM and bed load (Lees, 1983).

Resuspension of fine sediments is affected by currents and waves, both individually and through their interaction, as well as by biological processes. Therefore, to gain an understanding of resuspension both physical and biological processes must be considered. Such an insight may then provide solutions to problems such as the silting up of harbours and shipping lanes and aid environmental impact assessments.

Since the size of particles influences the transport method and the effects on optical, biological and chemical properties of the water column, the measurement of the size distribution of suspended sediments is an important parameter. Knowledge of the size distribution of SPM allows estimates of settling velocities to be obtained as well as estimates of erosion thresholds. Biological, chemical and physical models of both water column and near-bed

processes can be significantly improved with knowledge of the size distribution of the SPM.

Accurate measurements of SPM are, however, difficult to make, due to the characteristics of such sediments and instrument limitations. Various methods are available for the sizing of SPM, with most being either very time consuming or laboratory based. In recent years there has been a migration from previously used methods in the laboratory to in-situ techniques. The main advantage of in-situ measurements is the removal of the need to disturb the fragile flocs that make-up the vast majority of SPM.

Direct measurements of SPM characteristics such as SPM concentration and composition are well established. However, increasingly knowledge of particle size is also necessary to allow a greater understanding of particle related biological and chemical processes within an area. Recently developed optical methods have allowed faster sampling rates and in-situ measurements. Although the theory involved is well established for spherical particles the application to natural, non-spherical, particles is still in its infancy producing different results depending on the instrument used.

This study is closely linked to the PROcesses and Vertical Exchange in Shelf Seas (PROVESS) project (Howarth *et al.*, 2002) which aims at improving the understanding and quantification of vertical exchange processes in the water column, in the surface and benthic boundary layers and across the pycnocline in shelf seas. This was done through an extensive cruise programme aimed at providing a new, comprehensive and synoptic data set for two sites in the North Sea. Physical, biological and chemical measurements were made throughout the water column and at the seabed resulting in the development of both 1-D and 3-D models.

Figure 1.1 shows the location of the two contrasting PROVESS study sites, one in the northern North Sea and one in the southern North Sea. The northern site has a water depth of approximately 100 m, and experiences low tidal energy with the maximum amplitude of the M_2 tide being 0.15 m s^{-1} and the maximum

current is c. 0.6 m s^{-1}. The maximum wind speeds during the experiment are approximately 25 m s^{-1}, and the wave field has a maximum significant wave height of c. 10 m and maximum significant wave period of 10 s. A thermocline and halocline occurs between 35 and 100 m and there is a muddy sand seabed. This site was visited between September and November 1998.

In contrast, the southern site has a water depth of 16 m and is located within a region of freshwater influence (ROFI) and high tidal currents where the maximum M_2 tidal amplitude is 0.75 m s^{-1} and the maximum current speed is 1 m s^{-1}. The halocline at this site is between 5 and 10 m with a seasonal thermocline. The maximum wind speeds during the experiment are in the region of 20 m s^{-1} and the waves are significantly smaller than the northern site with maximum significant wave heights of c. 5 m and a maximum significant wave period of c. 8 s. Like the northern site the sediment type is muddy sand. This site was visited between April and May 1999.

Data was also collected during a cruise in May 2000 in the Clyde Sea as part of a much larger cruise campaign designed to estimate both the turbulence observed in fjords and the fluxes across the sills at their mouths. Due to this objective similar measurements were made to those carried out during the PROVESS campaign. It was also possible to carry out an extensive field comparison between two particle sizers.

All data collected has been used to validate the particle sizers used. However, only the processes observed in the northern PROVESS site and at one station in the Clyde Sea have been studied as they were found to be very similar. Interpretation of particle size data in the southern North Sea was complicated by episodic stratification, unquantified wind effects and plankton growth and so have not been pursued further as part of this thesis but results are presented in McCandliss *et al.*, (2002).

1.2. Aims and objectives

To examine suspended particle characteristics and dynamics at two shelf sea sites within the North Sea and Clyde Sea. In particular to show that in-situ suspended particle size distributions are variable over time and depth in response to both physical and biological forcing.

1) Validate a new in-situ particle sizer by comparison with other instruments under controlled laboratory conditions and in the field.
2) Characterise SPM in terms of size, composition and settling velocity.
3) Investigate, compare and contrast the temporal variability of SPM characteristics at the northern North Sea PROVESS site and one station in the Clyde Sea and relate this variability to physical and biological processes.

1.3. Thesis Layout

Following the introduction presented in this chapter, the remainder of this thesis is organised as follows:

Chapter 2: An overview of the main methods of determining the characteristics of suspended particulate matter and some of the main processes that SPM is subjected to.

Chapter 3: A description of the theoretical and operational concepts of the instrumentation used in this study.

Chapter 4: A comparison and validation of three laser particle sizers, including methods, results and discussion.

Chapter 5: An introduction to the northern North Sea PROVESS site, the observation programme and any specific data processing as well as the presentation of all the data collected that are pertinent to this study.

Chapter 6: An introduction to the Clyde Sea study site, the observation programme and any specific data processing as well as the presentation of all the data collected that are pertinent to this study.

Chapter 7: The results presented in the previous two chapters are discussed with particular emphasis on the particle size distributions and mid-water column SPM processes. The discussion draws on conclusions made in chapter 4 enabling a better interpretation.

Chapter 8: A presentation of the main conclusions drawn from this study and suggestions for further work.

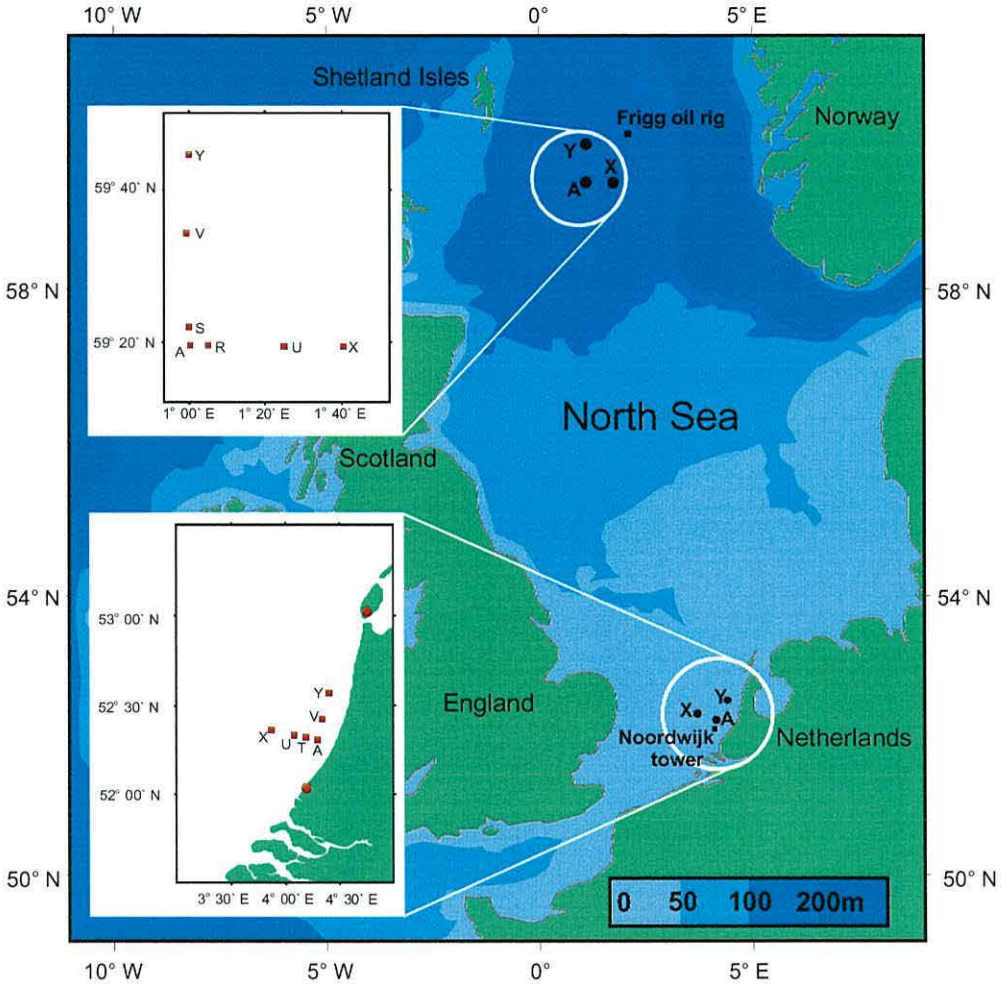

Figure 1.1. Map of North Sea with insets showing the mooring arrays at the northern and southern sites (From Howarth *et al.*, 2002).

Chapter 2

Background

2.1. Particle size

2.1.1. Introduction

The size distribution of suspended particles in the water column is an important characteristic in any study of sediment transport. Size and density are two of the primary factors in determining the fall velocity of a sediment particle, which in turn plays a major role in the distribution of sediment through the water column. Sediment size distribution is also important as large particles (i.e. sand grains) are efficient for transporting mass, while smaller particles are more important biochemically (e.g. as contaminant transporters).

Sediment size distributions can be determined through a variety of methods. However, until recently most methods were performed on water bottle samples in the laboratory. Although such techniques provide accurate measurements of the primary particle size they are prone to disturbing the fragile aggregates that exist in the marine environment (Kranck, 1973; Gibbs, 1981, 1982a,b; Gibbs and Konwar, 1982, 1983) and typically undersample the spatial and temporal variability.

Development of in-situ photographic imaging techniques have overcome the problems of disturbing the samples associated with laboratory techniques and have proven to be a powerful method of analysis. However, data processing of the photographic images for size distributions is a lengthy procedure.

In the past decade there has been a progression towards the adaptation of instruments which were previously laboratory based into in-situ instruments (Bale and Morris, 1987), as well as the development of non-intrusive in-situ instruments based mainly on laser diffraction (Agrawal & Riley, 1984; Agrawal *et al*, 1991) and time of transition techniques (Karasikov *et al.*, 1988; Jantschik *et al.*, 1992; Tsai, 1996). These two techniques have been used for two

decades as laboratory instruments, providing reliable results (Cooper *et al.*, 1984).

2.1.2. Sieving

This is a simple conventional technique that measures sediment size via sieve mesh size and sediment mass via weight. This technique has many biases, which are largely operational such as shaking time, clogging of sieves, and that elongated particles may pass through a sieve with a mesh size smaller than the longest dimension of the particle.

2.1.3. Microscopy

Microscopy is often used as an absolute method of particle size analysis since it is the only method in which individual particles are observed and measured and it also allows examination of the shape and composition of particles (Allen, 1981). However, as the technique is very time consuming only very small quantities of a sample are measured. Therefore, sub-sampling techniques used must ensure that the sub-sample is representative.

There are different methods of measuring particles by microscopy: optical microscopy using a variety of manual methods, transmission electron microscopy (typically used for the direct measurement of particles in the size range 0.001 to 5 μm), and scanning electron microscopy. As transmission electron microscopy and scanning electron microscopy are not relevant to this project they are not reviewed here. For a general review of these techniques refer to Allen (1981).

The image of a particle seen in a microscope is two-dimensional and from this an estimate of the particle size has to be made. There are six accepted diameters, described in Figure 2.1 and Table 2.1. Mean diameters from these measurements are all independent of particle orientation as they are either taken in some preferred direction or, in the case of the perimeter diameter and projected area diameter, are two-dimensional measurements. The projected

area diameter gives the best estimate of the true cross-sectional area of the particle, but does not rule out the use of the other diameters if they are conventionally measured, since the cross-sectional area diameter of a particle is not necessarily its optimum dimension (Allen, 1981).

	Accepted Diameter Measurement
1.	**Martin's diameter (M)** is the length of the line which bisects the particle image. The lines may be drawn in any direction which must be maintained constant for all the image measurements.
2.	**Feret's diameter (F)** is the distance between two tangents on opposite sides of the particle, parallel to some fixed direction.
3.	**Longest dimension.** A measured diameter equal to the maximum value of Feret's diameter.
4.	**Maximum chord.** A diameter equal to the maximum length of a line parallel to some fixed direction and limited by the contour of the particle.
5.	**Perimeter diameter.** The diameter of a circle having the same circumference as the perimeter of the particle.
6.	**The projected area diameter (d_a)** is the diameter of a circle having the same area as the particle viewed normally to a plane surface on which the particle is at rest in a stable position.

Table 2.1. The different accepted diameters when measuring an image of a particle seen in a microscope.

A frequently used manual method of measuring particle size, although not the method used in this study, is using a microscope fitted with an optical micrometer, a moveable crosshair, built into the ocular. The crosshair is moved by a calibrated micrometer drum to the edge of the particle. It is then moved to the other edge of the particle and the difference in readings is a measure of the size of the particle. As this method is very time consuming it has been largely superseded by the use of ocular scales.

The simplest form of manual measuring, and that used in this study, consists of a glass disc which is fitted on to the field stop of the ocular. This disc has a scale engraved on to it which is calibrated against a stage graticule at the required magnification. Once the disc has been calibrated the stage graticule is replaced by a slide with the particles on it and is examined in strips so as to give a complete coverage of the slide. As a particle image moves over the scale it is sized and recorded. Particles which overlap each other are neglected. As the

measurements are on a linear scale this method is best suited to particle populations with narrow size ranges.

2.1.4. Sizing using a Coulter Counter

A Coulter counter uses a resistive method for the sizing and counting of particles suspended in an electrolyte. The suspension is forced through a small orifice (12-1000 μm) in a dielectric barrier separating two electrodes. An orifice can measure particle sizes between approximately 2% and 60% of its size into 256 size intervals (by diameter) spaced linearly or logarithmically. As a particle passes through the orifice the resistance between the two electrodes increases. The change in the resistance is proportional mainly to the volume of the particle, but is also influenced by particle shape, the way it passes through the orifice and the composition of the particle. The main advantage of the resistance method is that the particle volume is determined. This is a unique property of particle size although the disadvantage, like all laboratory based methods, is that fragile flocs could be broken up at numerous stages of the process.

For a Coulter counter the resolution is not electronic accuracy but the ability to separate genuine characteristics that are very close together (Harfield and Cowan, 1988). These investigators showed that the Coulter counter was able to resolve a bimodal population whose modal sizes were only 1.9% different. For the purposes of most marine studies this resolution is more than required.

The Coulter counter used to be a popular method of measuring particle size (Kranck, 1980; McCave, 1983; Paffenhöfer *et al.*, 1980), partially because this method can be performed at sea and it is not a lengthy procedure like microscopy. However, as the suspended flocs are fragile they are likely to be broken up as they pass through the small orifice (Gibbs, 1982a). Other problems associated with the Coulter counter are clogging of the orifice (Jankschik *et al.*, 1992) and the inability to measure broad size populations.

2.1.5. Photographic Techniques

Photographic techniques allow direct, unobtrusive observation of suspended particulate matter and overcome almost all of the problems associated with the Coulter counter and sample disturbance associated with all laboratory based methods. They provide reliable results allowing visual verification of analytical results (Knowles and Wells, 1998). Many investigators have used photographic techniques for in-situ analysis of suspended material (e.g. Wells and Shanks, 1987; Knowles, 1998; Fennessy *et al.*, 1994; Zaneveld *et al.*, 1982). However, there are two major disadvantages with such systems. Firstly the resolution of most photographic assemblages is poor, only 50 μm in some cases (Tsai, 1996) and secondly such systems require excessive operator time for both the processing and verification of results. The second limitation constrains the sampling spatially and temporally, although not as severely as for discrete bottle sampling.

As photographic techniques allow direct visualisation of particles, the settling velocity of particles can be observed rather than estimated from size and density can be estimated. Fennessy *et al.* (1994) implemented a video camera assembly to directly measure both the size and settling velocity of flocs in an estuary. They showed that such a system does not disturb the fragile flocs yet allows accurate measurements of size and settling velocity, therefore allowing a more accurate estimate of floc density to be calculated. However, like all such techniques the processing is very intensive and therefore restricts sampling both spatially and temporally.

2.1.6. Particle sizing using lasers

All the methods of particle sizing described above have major disadvantages associated with them. In-situ laser particle sizers have begun, in the last decade, to replace these methods and overcome many of the associated disadvantages. These new instruments have utilised existing laser theory and in some cases new instruments have been developed (e.g. Agrawal *et al*, 1991; Agrawal & Pottsmith, 2000), whilst in others existing laboratory instruments

have been adapted for in-situ use (e.g. Bale and Morris, 1987). The theory of two different approaches to laser particle sizing are reviewed below.

Laser particle sizers have very wide operating size ranges, typically between 0.5 μm and 1000 μm (Tsai, 1996), the sampling and processing times are small, typically of the order of seconds, and being in-situ and non-intrusive they are suitable for measuring fragile flocs. They do still suffer from some major disadvantages which are primarily due to the fact that the theories applied are for spherical particles, something that is rarely seen in natural populations and their response to non-spherical particles is largely unknown. Also, these instruments rely on an inversion algorithm which has to make assumptions about the shape of the distribution, generally assumed to be normal. Therefore, they may not produce accurate results if the population displays a broad or multimodal distribution.

2.1.7. Time of transition

This theory states that the time a shadow persists on the detector due to the interaction between a rapidly rotating laser beam moving at a fixed velocity and a particle is directly dependent on the particle diameter (Tsai, 1996). This detection principle has virtually no lower concentration limit, although statistical confidence will essentially provide such a limit.

As the rotating laser beam interacts with the particles within the detection zone a detector measures the interaction pulses. The width of a pulse represents the time of interaction as the laser beam scans across the surface of the particle and the height represents the reduction in intensity of light reaching the detector as a result of the obscuring by the particle.

Again, there are problems associated with the technique. Firstly, the diameter of the laser beam varies along the beam and therefore an ambiguity may arise from particles interacting with the laser beam outside of the focus spot. These particles will produce a longer interaction pulse compared to the case where the same particle was within the focus spot. Secondly, the laser beam may not

interact with the particles along their diameter. With this method the beam can interact with particles along all chords depending on particle orientation with respect to the laser beam. However, such problems can be overcome as the resultant pulses associated with such situations are unique (Karasikov *et al.*, 1988) and can therefore be removed with an algorithm.

The other main problem associated with this technique is the assumption that the particles are spherical and the resultant diameters are equivalent spherical diameters. This problem does not apply to only this technique, all particle sizers utilising laser methods have to make this assumption. It can be expected however, that if the orientation of the particles is random and a large number of particles are measured then the associated error becomes negligible.

The accuracy and reproducibility of the time of transition method has been studied by a number of investigators. The results from such experiments range from concluding that the method is very accurate and results are reproducible (Jantschik *et al.*, 1992) through to concluding that the method is unreliable, producing inaccurate and non reproducible results (Allen and Davies, 1989; Tsai, 1996). However Tsai and Rau (1992) did conclude that the poor reproducibility of such a technique could be overcome by averaging a number of distributions obtained for the same sample. When analysing distributions averaged in this way, not only was the poor reproducibility problem addressed but the distributions were found to be more accurate in comparison with microscopy results of the same sample.

One further problem is associated with the change in the detected light intensity which is interpreted as a particle interaction. In general individual particles are only registered if the leading and trailing edges of the signal have a sufficiently sharp rise from the background noise. Therefore, if the composition of particles is such that this change in the light intensity is not great enough then such particles would not be sized, generating biased distributions.

2.1.8. Laser diffraction

Diffraction is a change in the directions and intensities of a group of waves after passing by an obstacle or through an aperture whose size is approximately the same as the wavelength of the waves. Fraunhofer diffraction occurs for a monochromatic light source, when the obstacle and receiver are far enough apart that all lines from the source to the obstacle can be considered parallel and all lines from the obstacle to a point in the pattern can also be considered as parallel.

The diffraction pattern caused by a circular aperture consists of a bright central spot, called an Airy disk, surrounded by a series of bright and dark rings (Figure 2.2). The intensity in the bright rings drops off very quickly with increasing angles. When the diameter of the aperture is much larger than the wavelength the intensity in the first ring is only 1.7% of the value at the centre of the Airy disk. This is usually the case in optical instruments. Optical particle sizing instruments using this theory then apply the theory of Mie scattering. Mie scattering theory states that for large particles, i.e. when the real part (m) of the complex refractive index, the size (ka), where $k=2\pi/\lambda$, is such that $(m - 1)ka >> 1$, the scattering at small forward angles appears nearly identical to the diffraction through an equal diameter aperture (Agrawal *et al.*, 1991).

According to Fraunhofer diffraction, the angle of diffraction from the centre of the Airy disk to the middle of the first dark ring occurs when u equals 3.83 where u is described by

Equation 2.1
$$u = \frac{2\pi \sin\theta}{\lambda}$$

and λ is the wavelength of the incident light and θ is the angle of diffraction (van de Hulst, 1957). Approximately 84% of the scattered light is within the Airy disk, i.e. within the bounds of the first dark ring and 91% is within the bounds of the second dark ring (Hecht and Zajac, 1974). The angle from the centre of the Airy disk to the middle of the second dark ring is when u equals 7.02.

Laser diffraction analysis is based on the fact that particles of a given size diffract light through a given angle which increases with decreasing particle size. A laser is used as the wavelength of the beam must be known accurately to enable reliable results. A parallel beam is passed through the suspension and the diffracted light is focused onto a detector with multiple rings which detects the angular distribution of the diffracted light intensity (Figure 2.3). The angular distribution of light intensity, $I(\theta)$ is given by:

Equation 2.2 $$I(\theta) = \frac{1}{\theta} \int r^2 n(r) J_1^2(kr\theta) dr ,$$

where θ is the diffraction angle, r is the particle radius, n(r) is the size distribution function, $k = 2\pi/\lambda$ (with λ being the wavelength of the light), and J_1 is a Bessel function of the first kind (McCave and Syvitski, 1991). This equation must then be inverted to obtain the size distribution (Agrawal and Riley, 1984; Riley and Agrawal, 1991; Traykovski *et al.*, 1999).

This method works for particles down to the order of a few microns, as they no longer diffract light in the same way. This is due to the Fraunhofer diffraction theory, on which the above relationship is based, becoming invalid as the particle diameter approaches that of the wavelength of light (de Boer *et al.*, 1987).

For particles that are not spherical the diffraction pattern will be different to the Airy disk. For elongated particles the pattern will produce streaks across the detector and therefore some light will be measured in each detection ring and result in an inaccurate particle size. This problem is not addressed by any of the currently available instruments that use this technique. Therefore, in populations where particles are not spherical the response of the instrument is not fully known.

2.2. *Suspended Sediment Concentration*

2.2.1. Introduction

Suspended particulate matter (SPM) in coastal and ocean waters can consist of mineral, biological and chemical components and, as such, are important in the transport of these components. Accurate measurements of the SPM concentration within the water column is vital as it directly affects many processes including photosynthesis (by limiting light penetration) and the distribution of contaminants. Therefore, in order to achieve a complete understanding of fluxes in the oceans, accurate SPM concentrations are required.

There are various methods of measuring SPM concentration both directly and indirectly. These include optical backscattering devices (OBS's), acoustical backscattering devices (e.g. ADCP's and ABS's), transmissometers and discrete sample collection with subsequent filtering and weighing. Transmissometers are reviewed here as they were the only method available in this study for obtaining SPM concentrations.

2.2.2. Transmissometers

Transmissometers are routinely used for the measurement of SPM concentration. The output from such instruments is in terms of percentage transmission and needs to be converted to SPM concentration by regression against simultaneously measured SPM concentrations. These are measured by discrete water sampling which are then filtered, dried and weighed. Therefore, the validity of the calibration depends on the researcher understanding both the specific particle characteristics and the instrument response.

The use of light attenuation for determining SPM concentration has been well documented over the last 30 years (Benns & Pilgrim, 1994; Bishop, 1986; Bartz *et al.*, 1978). Light attenuation in water is caused by the scattering, and absorbency by the constituents in the water and is an inherent property as it does not depend on the natural light field but solely on the composition of the

medium. The beam attenuation coefficient (referred to from here as the beam attenuation or attenuation) is described by Equation 2.3 and is the sum of absorption and scattering.

Equation 2.3 $$I(z) = I(0)e^{-cz},$$

where *I(z)* is the light intensity at a distance z from the light source and c is the beam attenuation coefficient.

Attenuation variations observed in seawater are mainly caused by the concentration, size, shape and absorption properties of the suspended particulates. Transmissometers measure the attenuation of a beam of light (usually with a wavelength ~ 660 nm which reduces the amount of absorption by yellow substance) over a known pathlength. The light detected on the receiver detector is then directly related to the optical properties of the suspension that the beam travelled through.

Particles in the path of the beam will scatter and absorb the light. Light scattering by particles is caused by diffraction, refraction and by external and internal reflection (Kirk, 1983). Diffraction depends on the size and shape of the particle, and for irregular non-absorbing particles it is similar to that of spheres. If particles are larger than the wavelength of the light, scatterance can be described on the basis of refraction and geometrical optics. For light at a wavelength of 660 nm the particle diameter must be greater than 0.6 μm for this to apply.

Although it is widely accepted that attenuation is highly dependent on particle size the application of this method is still widely used without much attention being given to this problem. However, within waters where the suspended particulate population is constant in terms of size and shape, the use of transmissometers are valid, as any changes seen in the beam attenuation can be confidently described by changes in suspended particulate concentration.

The effect of particle size on light attenuation has been extensively studied by many investigators (Baker and Lavelle, 1984; Moody *et al.*, 1987; Benns and Pilgrim, 1994). Baker and Lavelle (1984) studied the effect of particle size ranging from 6.6 μm to 106 μm on α', where $c = \alpha'C + \alpha_0$ (where c is beam attenuation, C is mass concentration, α' is the slope of the line and α_0 is the intercept on the y-axis). They found that α' was very dependent on particle size, varying by more than a factor of ten and being bigger at smaller size classes. Figure 2.4 shows the beam attenuation calculated using the theoretical α' calculated by Baker and Lavelle (1984) for different size classes. This illustrates how much a change in particle diameter would result in underestimating the beam attenuation if concentration remained constant. With the use of one α' over a range of particle populations it would be possible to interpret a decrease in c as a decrease in concentration, whereas it is possible that the concentration may have increased or remained constant and the decrease in beam attenuation is due to an increase in particle size.

Most of the light that is scattered from a particle is in the near-forward direction. Both the angle of acceptance of the transmissometer and the size of the particles being measured are important parameters in the interpretation of data obtained from a transmissometer. A description of Fraunhofer diffraction is given in section 2.1.8, however it is worth repeating that approximately 84% of the forward diffracted light is within the Airy disk and 91% is within the bounds of the second dark ring.

Figure 2.5 illustrates the effect of increasing particle size on the angle of forward diffraction, using Equation 2.1 with a wavelength of 660nm, which is the same as the SeaTech transmissometers used in this study. These transmissometers have an angle of acceptance of 1°. From Figure 2.5 it can be seen that for particles with a diameter greater than approximately 45 μm, 84% of the total diffracted light falls within a 1° angle and by approximately 80 μm, 91% of the total diffracted light falls within a 1° angle. Therefore in the presence of particles greater than approximately 45 μm, changes in beam attenuation due to concentration alone will be relatively small as so much light is being scattered.

With particles of approximately 150 μm in diameter and greater, all the scattered light falls within 1° making the transmissometer "blind" to such particles (pers. comm. Agrawal, 2001).

Investigators who have looked at the response of the transmissometer to changes in natural populations have reported a variety of responses. Volten *et al.* (1998) concluded that the use of Mie theory for measuring phytoplankton size results in poor approximations of size, as phytoplankton usually have internal or external structures too complex to justify using Mie calculations. Bunt *et al.* (1999) concluded that the presence of phytoplankton may increase the transmissometers response by a factor of four compared to similar concentrations of minerogenic grains. They also concluded that grain size changes may affect the transmissometer response by over a factor of 100 and that with the exception of smooth grains, sediment texture and surface roughness can increase the response by a factor of 10.

Therefore, data obtained from transmissometers must be treated with caution in regions where the particle population consists mainly of large particles (diameters greater than 45 μm). The quality of SPM concentration data maybe improved if particle aggregation is negligible. Where particle aggregation is likely, the most accurate determination of particle size distributions is gained from the in-situ use of floc cameras or laser particle sizers. Repeated field calibration of transmissometers can help to account for changes in beam attenuation as a result of change in the grain size. Therefore, the importance of good calibration data cannot be stressed enough and where the composition of the particle population varies, different calibrations may need to be applied to ensure an accurate interpretation of the SPM concentrations.

2.3. Particle Settling

Determining the flux of suspended sediment requires a knowledge of the particle settling velocity. The accuracy in calculating such fluxes depends critically on the settling velocity of the sediment in suspension. Grain size,

shape and density determine settling velocity. For sands and coarse silts these parameters may be estimated by direct examination of recovered bottom sediment. Finer silt and clays, however, tend to aggregate into flocs of variable size and density that sink at rates much greater than the component grains (Syvitski and Murray, 1981). Flocs lack resilience, so settling velocities of disturbed and disrupted flocs bear little resemblance to in-situ settling velocities (Alldredge and Gotschalk, 1988). The floc dominated settling velocity of finer grained sediment must therefore be measured in-situ. Most instruments developed to measure settling velocity of flocs in-situ utilise some form of camera assembly to observe the settling velocities (eg. Fennessy *et al.*, 1994; Hill *et al.*, 1998). Hill *et al.* (1994) demonstrated the importance of such measurements as part of the STRESS programme where they measured a bimodal distribution of fine sediment suspended in the water column and concluded that this indicates that insufficient time has passed since formation of the suspension for aggregation to blur modal peaks as suggested by McCave (1984).

The simplest interaction between sediment particles and a fluid is a single grain of density ρ_s falling in a static fluid of density ρ. Assuming $\rho_s > \rho$ then the sphere will accelerate until it reaches its terminal velocity (V_g) which occurs within a distance of a few grain diameters (Dyer, 1986). For a sphere falling at a speed where viscous forces dominate, the Navier- Stokes equation (Equation 2.4) can be simplified as follows:

Equation 2.4 $$\frac{D\underline{u}}{Dt} = \frac{-\nabla P}{\rho} + \nu\nabla^2\underline{u},$$

Equation 2.5 $$\Rightarrow \nabla P = \mu\nabla^2\underline{u},$$

where ν is the kinematic viscosity, ∇P the pressure gradient, and μ the molecular viscosity.

Equation 2.5 is known as the equation of creeping motion. For low Reynolds number flow (i.e. viscous forces dominating over inertial forces) past a sphere, surface drag, *D*, can be derived:

Equation 2.6 $$D = 2\pi\mu d V_g ,$$

where *d* is the sphere diameter, V_g the velocity and μ the molecular viscosity. Drag is defined as the force applied by the fluid on the body, i.e. the force exerted by the fluid on an obstacle in the opposite direction to the flow (Tritton, 1988).

For a sphere to be falling at its terminal velocity there must be an equal and opposite force exerted by the body on the fluid. At a low particle Reynolds Number (R_{e^*}), where the equation of creeping motion (Equation 2.5) is valid, flow round a sphere is reversible and there is no wake. Therefore, the forces acting on a sphere falling at its terminal velocity, at low R_e, are drag (opposing) and the weight of the sphere (Equation 2.7).

Equation 2.7 $$Weight = \frac{4}{3}\pi\left(\frac{d}{2}\right)^3(\rho_s - \rho)g$$

Combining Equation 2.6 and Equation 2.7 the terminal fall velocity of a sphere at low R_e is described by Stokes' settling law:

Equation 2.8 $$V_g = \frac{d^2 g}{18\nu}\left(\frac{\rho_s}{\rho} - 1\right)$$

Stokes Law is valid for particles whose particle Reynolds number (R_{e^*}) is < 0.5 which corresponds to silt-size and finer (<62.6 μm) quartz density particles in water (Leeder, 1982). Stokes Law becomes invalid at $R_{e^*} > 0.5$ as particles with a Reynolds number greater than this develop wakes due to boundary layer separation at increased velocities.

Application of Stokes Law to naturally settling particles must be cautious due to many factors. Firstly, particles are not spherical and hence do not fall like spherical particles. Braithwaite (1973) observed that unhindered falling carbonate grains have four fall regimes: straight falling, spinning, spiralling, and erratic tumbling. For such particles an exact terminal velocity can only be obtained through careful experimental analysis of each individual grain which is impractical. Work with specific samples has been performed, each resulting in empirical formulae specifically for those samples (Braithwaite, 1973; Hallermeier, 1981).

Secondly, particles usually settle as a population. Due to the action of viscosity being felt far away from the particle, hindered settling and increased drag results in decreasing individual particles fall velocity compared to its velocity in a grain free fluid (Leeder, 1982). The presence of other particles does not always result in hindered settling. The bulk of sedimentation for fine grained particles only occurs because of aggregation which increases the particle size by one or two orders of magnitude (Hillier, 1995). In concentrations of up to several tens g l^{-1} settling rates tend to increase because of the greater chance of particle-particle collisions leading to the formation of aggregates. Only when concentrations begin to increase above these levels do settling rates begin to decrease due to hindered settling (Hillier, 1995).

Thirdly, particles rarely settle in a static fluid and turbulence is usually present affecting the drag on the grains. Therefore, unless turbulence is absent from a flow, particles will be affected as they will be subject to forces acting both in an upwards and downwards direction.

Finally, as small sediment grains tend to flocculate forming large aggregates that sink at speeds several orders of magnitude faster than their component grains but slower than their equivalent spherical sized particle, the application of Stokes Law is invalid. Hill *et al.* (1998), along with other previous investigators, showed that floc settling velocities can be related to diameter with a proportionality of the form:

Equation 2.9 $$w_s \propto d_f^n,$$

where w_s is settling velocity, d_f is floc diameter, and n is an exponent that typically falls between 0.5 and 1.5 (ten Brinke, 1994). The value of n is less than two, which is predicted by Stokes Law, because the inclusion of water within the aggregate causes a reduction in density with increasing diameter. The settling velocity of flocs is individual to each floc as variability in floc shape and composition will affect the effective density (density of the floc minus the water density) and therefore the settling velocity. Changes in the proportion of organic matter and mineral grains will have profound effects on the effective density. Flocs that have large relatively rare silt grains will have greater masses, effective densities, and sinking rates than those that do not. The settling of flocs is discussed in greater detail in section 2.4.

In summary, the settling velocity of suspended particles is a function of the particle size, shape and composition. For particles which are spherical or near spherical and their densities are known Stokes Law can be applied with some degree of confidence. However, this is rare within the natural environment where particles are rarely spherical and their size and density are often unknown. Various instruments have been developed for the measurement of particle size and settling velocities in-situ allowing more accurate measurements and estimates of particle fluxes in the marine environment.

2.4. Flocculation/De-flocculation

A floc is defined as an aggregate of smaller particles that maybe either organic or inorganic (Lick *et al.*, 1993). Krone (1978) separated flocs into orders based on their constituent particles. First order flocs consist of primary particles, i.e. "building blocks", second order are termed conglomerates and are made up of first order flocs, and third order, agglomerates, consist of second order and first order flocs. Such ordering has been proposed by many other authors, however

some are based on floc size, such as Luettich *et al.* (1993) who defined macroflocs as flocs with a diameter greater than 125 μm and consisting primarily of loose agglomerations of small aggregates or microflocs. Microflocs were then defined as flocs whose diameter is less than 125 μm.

Flocculation of fine-grained sediments is often the cause of deposition of such sediments (van Leussen, 1988; Hillier, 1995). This is a result of increasing the settling velocities of the primary particles by increasing the overall particle size and therefore the settling velocity (McCave, 1984; van Leussen, 1988). van Leussen (1988) demonstrated the importance of understanding aggregation of fine particles within estuaries with regards to the formation of a turbidity maximum and transportation of absorbed pollutants. If aggregation is important within estuaries then it is probably an important process on the continental shelf where fine sediments are acted on by both waves and currents, and where biology can have a dominant affect on both suspended and deposited sediments.

Flocculation does not only affect settling velocities of sediments but also determines the erosional properties of a bed, as these are governed by the properties of the constituent particles and various properties of the surrounding water. With regards to erosion, aggregates and their properties have an important influence, with their inter-grain cohesive strength and their resistance to crushing or reshaping with depth within the bed being vital to the bed's erosional properties (van Leussen, 1988). Optical properties of the water are affected by floc formation as flocculation by differential settling (see below) has been found to cause rapid water column clarification during slack water periods (van Leussen, 1988).

Formation of flocs occurs when particles collide and stick together. Particle collisions are caused by; (1) Brownian motion, (2) fluid shear (velocity gradients) and (3) differential settling. Brownian motion, which is random and a function of the absolute water temperature and dynamic viscosity, is only important in the initial stages of floc formation, i.e. formation of primary flocs,

when it is the dominant process in causing collisions (van Leussen, 1988). Therefore, for modelling of aggregation within natural systems where there are measurable velocity gradients and turbulence, Brownian motion can be neglected (Partheniades, 1993). Lick & Huang (1993) concluded that the collision rate due to Brownian motion is proportional to d^2, where d is the average diameter of the colliding particles.

Velocity gradients or fluid shear, due to both laminar and turbulent flows, has proved to be an important mechanism in formation as well disaggregation of flocs. It has been suggested by many investigators that shear acts as a limiting factor in the size of a floc (Eisma, 1986; Luettich *et al.*, 1993; Burban *et al.*, 1989). Lick *et al.* (1993) demonstrated that in a system experiencing shear, particle collision due to shear dominated over Brownian motion and therefore Brownian motion can be ignored in modelling of floc formation in such a system (van Leussen, 1988). Unlike Brownian motion, collisions due to velocity gradients are not a function of temperature and viscosity, but only a function of the flow speed. Turbulence is considered as one of the main floc formation mechanisms (Hillier, 1995; Johansen & Larsen, 1998) and therefore in regimes where turbulence is great, flocculation may prove to be an important process in determining the properties of suspended matter. van Leussen (1988) demonstrated that properties of suspended aggregates are determined by the turbulence in a narrow near bed zone, with the smallest turbulent eddies being of greatest importance. This is not, however, specific to turbulent induced flocs, each mechanism alone results in different floc properties.

Differences in particle size cause suspended particles to settle at different rates. This mechanism is called differential settling and causes particles to collide as faster settling particles collide with the slower settling particles, resulting in aggregation and more rapid deposition (Partheniades, 1993). The collision rate due to this mechanism is proportional to d^{α} where α varies between 2 and 4 depending on the density variation of the floc (Lick *et al.*, 1993) and a function of the properties that govern the settling velocity of the individual grains. Differential settling is important in high SPM concentrations such as estuaries

(Johansen & Larsen, 1998) and has been proved to be important in systems ranging from estuaries to the deep ocean (Hillier, 1995).

Therefore, formation of flocs is brought about by three main mechanisms, each one dominating in different situations. Where there is measurable fluid shear Brownian motion can be neglected. Partheniades (1993) concluded that, in general, collisions in flows are controlled by velocity gradients whereas in quiescent waters differential settling dominates.

Other less accepted processes have been suggested for aggregate formation such as salinity-induced flocculation and various biological processes (e.g. Rhoads & Boyer, 1982), which include the production of faecal pellets by both deposit and suspension feeders resulting in particles of much different sizes and densities from that of the primary particles (Nowell *et al.*, 1981).

Many mechanisms cause particles within an aggregate to "stick together", for example biological processes and electrochemical bonds. Most muddy deposits are aggregates held together by various biological mechanisms (Rhoads & Boyer, 1982). Wheatcroft & Butman (1997) found that on the mid Californian Shelf (~100 m) much of the larger particles were bound together in biological aggregates. Like most mechanisms that influence aggregation, biological processes cause aggregation and disaggregation. Mucopolysacharides produced by bacteria and algae act as "glue" sticking particles together. These are present in faeces and maintain the faecal pellets as a collection of aggregated particles.

Salt flocculation, i.e. flocculation due to charges on particle surfaces, is often thought of as an important process in the formation of flocs, especially in estuaries. Charges originate in two ways; (1) from substitutions within the mineral structure and (2) from surface reactions (Hillier, 1995). Most clay particles have a negative charge, a result of their structure, and in that respect would repel each other. However, surface charges are a function of pH with positive charges at high pH and negative charges at low pH. As suspended clay particles move from fresh to salt water the counter ions around the clay particles

that repel other particles become compressed closer to the particle. Therefore, as particles are surrounded by water of a higher pH they can come closer together before feeling any repulsion. If they are able to get sufficiently close the van de Waals attraction may be strong enough to counteract the repulsion from the surface and ionic structure of the particles and cause them to stick together (Hillier, 1995). Van de Waals attraction is the weak attractive forces between molecules caused by the uneven distribution and movement of electrons in the atoms of the molecules.

The process of salt flocculation is not disputed. However, its importance is. Gibbs (1983) found that salt flocculation occurs in salinities of as little as 0.05 to 0.1 which suggests that changes in salinity in a shelf and oceanic setting would have no affect on the flocculation processes and therefore size of aggregates. Eisma (1986) concluded that salt flocculation is not important, playing only a minor role if any, in the formation of flocs in the natural environment and only affects particles smaller than 1 μm. Lick and Huang (1993) studied the effect of salinity on particle size and found an appreciable difference between deionized water, fresh water and seawater and concluded that salt flocculation was an important process. However, the only significant difference between freshwater and salt water is that a steady state is reached sooner in seawater and that steady state particles are smaller in seawater as compared to freshwater (Lick & Huang, 1993). Therefore could be suggested that as particles come into contact with saltwater at an estuarine front disaggregation occurs as a smaller steady state is achieved.

Maximum size, density and strength of an aggregate is influenced by the collision mechanism (Krone, 1978; Partheniades, 1993), the strength of the bonds between particles and properties of the surrounding fluid and component particles. Flocs formed by both Brownian motion and differential settling only are formed in conditions where there is little stress on the aggregates resulting in weak, low density, non-spherical flocs, whereas those formed by velocity gradients are much more spherical and have stronger bonds than those formed by other mechanisms (van Leussen, 1988). Traditionally, the properties of the

surrounding fluid and component particles which are thought to be important are suspended sediment concentration, interparticle bonds, salinity of the surrounding fluid and fluid shear. The size of the flocs produced and how they are held together through biological processes is controlled by the binding strength of the organic matter (Hillier, 1995).

Floc density will change not only as a function of primary particles but also as a function of packing of the particles. As the packing changes so does the amount of pore water, thus affecting the density as found by Gibbs *et al.*, (1971) who reported that increasing pore water resulted in a decrease in bulk densities.

It is not only hydrodynamic forces that influence maximum floc size. The composition of the sediment in suspension also plays an important role. It has been shown that particle adhesion and floc stability depend on the effect polymer concentration has on particle sizes (Milligan & Hill, 1998) and the maximum floc size increases with increased concentrations of flocculent.

Aggregation theory predicts that higher concentrations of particles lead to further aggregation. However, concentration has also been shown to have a negative effect on maximum floc size (Tsai *et al.*, 1987; Lick & Lick, 1988). Lick and Lick (1988) concluded that collisions between flocs are more important than fluid shear for disaggregation under some conditions, and added a break-up term due to particle collisions to their aggregation model. Hillier (1995) suggested that for concentrations up to several tens of g l^{-1} settling rates increased, resulting from a greater chance of particle collision. It was also suggested that because of mutual particle hindrance, at higher concentrations the settling rates begin to decrease. However, Burban *et al.* (1989) concluded that formation of large flocs does not require high suspended sediment concentrations, but time. Lick & Huang (1993) also found that in a system where differential settling was the only formation mechanism floc size is only weakly dependent on concentration. However, in a system where there is weak fluid shear high concentrations appear only to decrease the time taken to reach the steady-state median particle size. They also concluded that a floc formed only by differential settling has a different shape, a result of the influence of flow

round the floc during settling. Johansen & Larsen (1998) however, argued that at low turbulent shear the floc size and settling velocity increase with increasing suspended sediment concentration, as the number of collisions increases.

If a correlation exists between suspended sediment concentration and median particle size then floc size distributions obtained from different geographical areas with the same concentration but differing sedimentological properties should be similar. Kranck *et al.* (1993) found that particle size distributions from the Amazon Shelf, Nith River (ON), San Francisco Bay, and Skagitt Bay (WA) had similar floc size distributions suggesting a common controlling mechanism in turbid waters. Therefore, although suspended sediment concentration has been shown in laboratory experiments not to have an influence on the steady-state particle size, it is possible that it does determine which collision mechanism dominates in the formation of flocs.

The equilibrium size distribution of suspended flocs can be considered a balance between particle aggregation and disaggregation. Floc formation rate increases with turbulence due to increased contact, and yet the same hydrodynamic forces limit floc growth. Laboratory studies by many investigators (eg. Tambo & Hozumi, 1979; Spicer & Pratsinis, 1996) have shown a strong negative correlation between floc size and turbulence or shear rate for latex beads and pure clay suspensions. This inverse relationship has also been shown in both fresh and salt water (Tsai *et al.*, 1987; Burban *et al.*, 1989).

Van Leussen (1997) studied the effect of turbulence on flocs sizes of suspended fine grained sediment in estuaries. He concluded that in the interaction of flocs and turbulence, the turbulent eddies with dimensions in the same order of the flocs are most important. This means that the smallest turbulent eddies dominate the floc dynamics. As turbulence stimulates both floc growth and floc break-up the final size of aggregates is governed by the destructive properties of the turbulence field, and only when floc growth is very slow would the maximum size limit not be reached. Examples of this are in low sediment concentration conditions or where the sediment has a low cohesivity. Van Leussen (1997) showed that the Kolmogorov micro scales, being a

measure of the smallest eddies in the turbulent flow, are a good reference for the maximum sizes of the fragile macro flocs.

Turbulence, as well as being a mechanism for floc formation, is also one that causes disaggregation and therefore can be considered as a limiting factor. Wheatcroft & Butman (1997) found that by treating the sediment with ultra-sound and dispersants, the number of particles less than 20 μm increased by 20-25% in the disaggregated sample compared with the untreated sample. Although ultra-sound is an extreme form of turbulence there are applications for the handling of water samples that are to be analysed by laboratory particle sizers. Flocs lack resilience, therefore floc-dominated settling velocity must be measured in-situ (Hill *et al.*, 1994) (section 2.3). This has also been seen by other investigators who have found that for more fragile flocs turbulence will break up aggregates (eg. van Leussen, 1988).

Milligan and Hill (1998) studied the importance of turbulence and particle concentration on limiting the floc size using mud samples from the Scotian shelf. They concluded that turbulence and sediment composition dominate the behaviour of flocculated suspensions and that concentration plays a part only in the initial development of aggregates or when turbulence decreases. Unlike Lick and Lick (1998) they suggest that including a floc break-up term due to concentration in models of particle aggregation on the continental shelf is not necessary. They clearly demonstrated the negative effect of increasing turbulence on the maximum floc size but concluded that although turbulence appears to dominate the maximum floc size, it cannot be considered in isolation when predicting floc size. The maximum floc size was smaller at high turbulence, but compositional effects were also found to be highly significant in the comparison of size between materials in suspension and in the settling behaviour of the flocs formed.

Empirical studies on the effects of turbulence and concentration have also been performed (e.g. Dyer & Manning, 1999; Manning & Dyer, 1999; Burban *et al.*, 1989). These studies were conducted in estuarine, or similar, situations where

relatively high turbulent shears and mass concentrations are experienced. All demonstrated that median floc size decreases was shear stress increases and as the suspended sediment concentration increases but all propose different empirical solutions. Burban *et al.* (1989) also concluded that disaggregation due to shear was negligible and that the dominant mechanism for disaggregation is collision between particles. Dyer & Manning (1999) also showed that the concentration of SPM has a larger effect than turbulent shear on the floc size.

The compositional effects on the maximum floc size eluded to by Lick & Lick (1998) include biological factors. Rhoads and Boyer (1982) showed that both spatial and temporal variation in floc size and density can occur as a result of biological patchiness (Wheatcroft & Butman, 1997). Therefore, measurements made simultaneously, but not at exactly the same location, may suffer from effects of biological patchiness. With regards to bottom sediment, Wheatcroft & Butman (1997) concluded that biological repackaging of muddy bottom sediments can significantly change the particle size distribution, and that the resuspension of sediments was not a reason for the observed fining of sediment particles towards the sediment-water interface from deeper down in the sediment.

Application of the generally accepted settling velocity equations for non-cohesive particles must be with caution when flocs are involved. Often a density must be assumed and therefore, unless this is known it is unlikely that an accurate settling velocity will be calculated. Laboratory settling experiments on bottom sediments collected from the California Shelf showed that the average settling velocity (W_s) for the untreated aggregated sample was 20% faster than that of the treated disaggregated sample (Drake & Cacchione, 1989), suggesting that either flocs have a higher density than their component particles causing faster settling, or that the size increase is great enough to cause an increase in settling velocity even if the density was less. Syvitski & Murray (1981) also found that aggregated particles had settling velocities several orders of magnitude greater than the primary particles.

As aggregates are often loosely bound, density is usually less than the component particles, therefore the observed increase in W_s is probably a result of the increase in diameter. Hillier (1995) suggested that combined with the increase in particle size, the increase in settling velocity was also in part due to larger aggregates trapping silt and fine sand particles between the clay particles, thus increasing the settling velocities.

As previously mentioned, pore water between particles also affects floc density, an increase in pore water results in a reduction in density. Therefore, all these factors mean that the relationship between particle diameter and settling velocity applied through Stokes Law is inappropriate for calculating the settling velocity of aggregates. Hill *et al.* (1998) show that floc settling velocity is proportional to particle diameter in the form of Equation 2.9 and that n typically falls between 0.5 and 1.5 thus reflecting the change in density from the assumed density used for Stokes Law (section 2.3) where n is usually ~2.

In summary, flocculation and de-flocculation are both important processes in shelf seas. The processes associated with flocculation and de-flocculation are many, with relative importance varying in different environments. The properties of flocs also vary widely, being influenced by the processes that formed them. However, all flocs consist of many smaller mineral particles and microflocs and are not as resilient as the primary particles that go into making up the flocs, resulting in difficulties with the sampling of such particles. Flocs also contain varying amounts of pore water depending on how tightly packed the constituent particles are. This results in the density of the flocs being less than that of the constituent particles and therefore affecting their settling velocity. Therefore, in the presence of flocs sampling must be such as to minimise disturbance. Also, interpretation of results must allow for the presence of flocs and their varying properties.

2.5. Stratification

Stratification of the water column can be caused by of a number of factors, such as warming of the surface resulting in a thermocline (Simpson & Hunter, 1974; Simpson & Rippeth, 1993), the influx of a different water mass (Simpson, 1997; Simpson & Rippeth, 1993), or high sediment concentrations (Adams & Weatherly, 1981). Such stratification results in energy transfer between the upper and lower layers of the water column being significantly reduced.

In shelf sea regions seasonal stratification is often observed with a thermally stratified water column during the summer months and a vertically homogenous water column in the winter. In these stratified waters the stabilizing heat flux at the sea surface in spring and summer is capable of overcoming the mixing due to wind and tide (van Aken, 1986). Such stratification has the effect of decoupling the surface mixed layer from the bottom mixed layer resulting in little energy transfer between the two layers (Burchard *et al.*, 2002; McCandlis *et al.*, 2002). Stratification also acts a means of preventing an upward flux of suspended material (McCandlis *et al.*, 2002) and can result in different populations of SPM above and below the pycnocline.

Stratification of the water column has been shown to have observable effects on the velocity profile. Villaret & Trowbridge (1991) showed that, like with thermal stratification, stratification caused by suspended sediment results in larger gradients in the mean velocity profile than the corresponding profile in a flow of clear water.

Stratification due to high concentrations of suspended matter stabilise the water column and therefore suppress turbulent motion (Adams & Weatherly, 1981). However, Lavelle *et al.* (1984) concluded that the excess density caused by this higher SPM was so small that it would not cause significant stratification and was therefore unlikely to modify the velocity profile. Glenn & Grant (1987) dispute the result of Lavelle *et al.* (1984) as they found that sediment induced stratification of the boundary layer does occur and its inclusion within a near bottom combined wave and current flow model is vital as it can capture the

most important physical processes affecting the near bottom flow field on the continental shelf during storms. Jago *et al.* (1993) also conclude that such a process must be important in shallow water, fine sediment areas during storms.

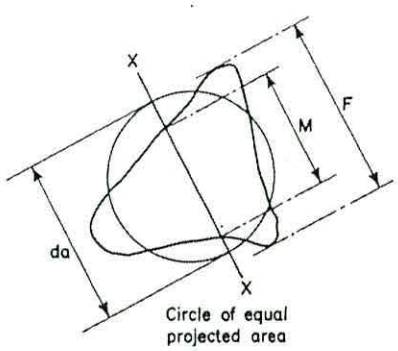

Figure 2.1. Representative two-dimensional diameters (from Allen, 1981)

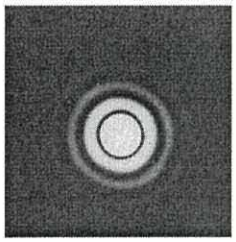

Figure 2.2. The diffraction pattern formed by a circular aperture (diameter of 1mm). From Young and Freedman (1996).

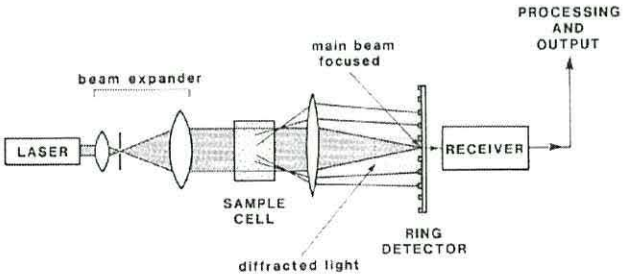

Figure 2.3. Diagram of a laser particle size analyser showing the primary components of light source, sample, focusing lens, detector and processing system. From McCave *et al.* (1986).

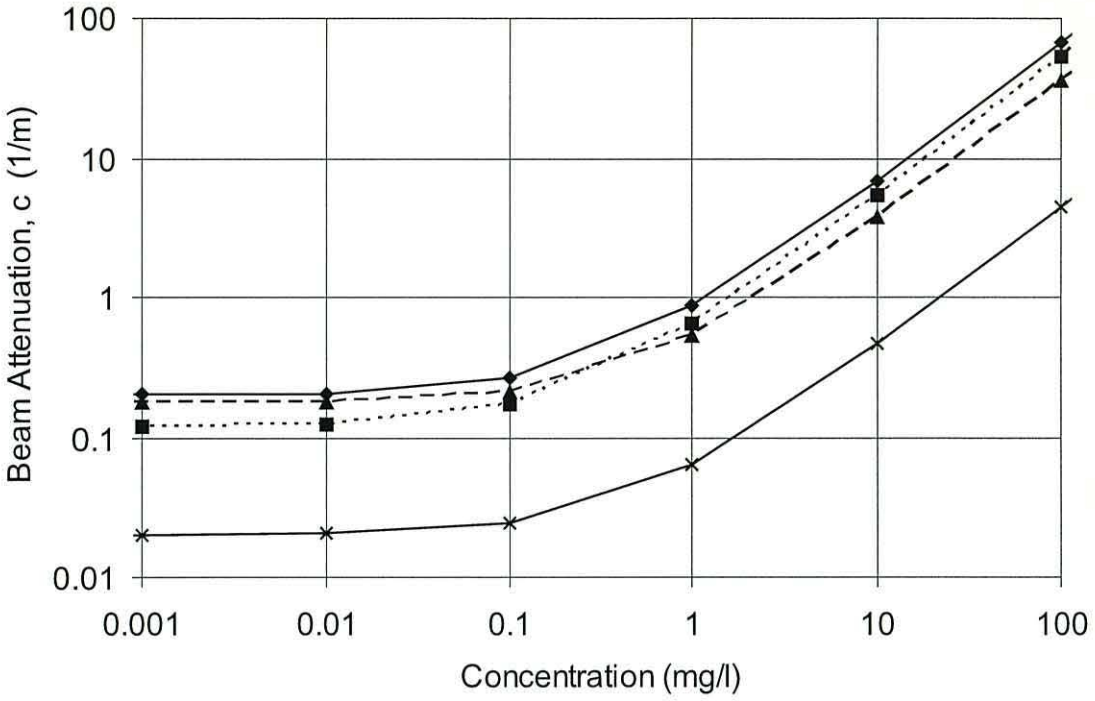

Figure 2.4. Effect of particle size on beam attenuation with increasing concentration. —◆— 8.5μm, ----■---- 15.1μm, - -▲- - 20.8μm and —x— 48μm. (After Baker & Lavelle, 1984).

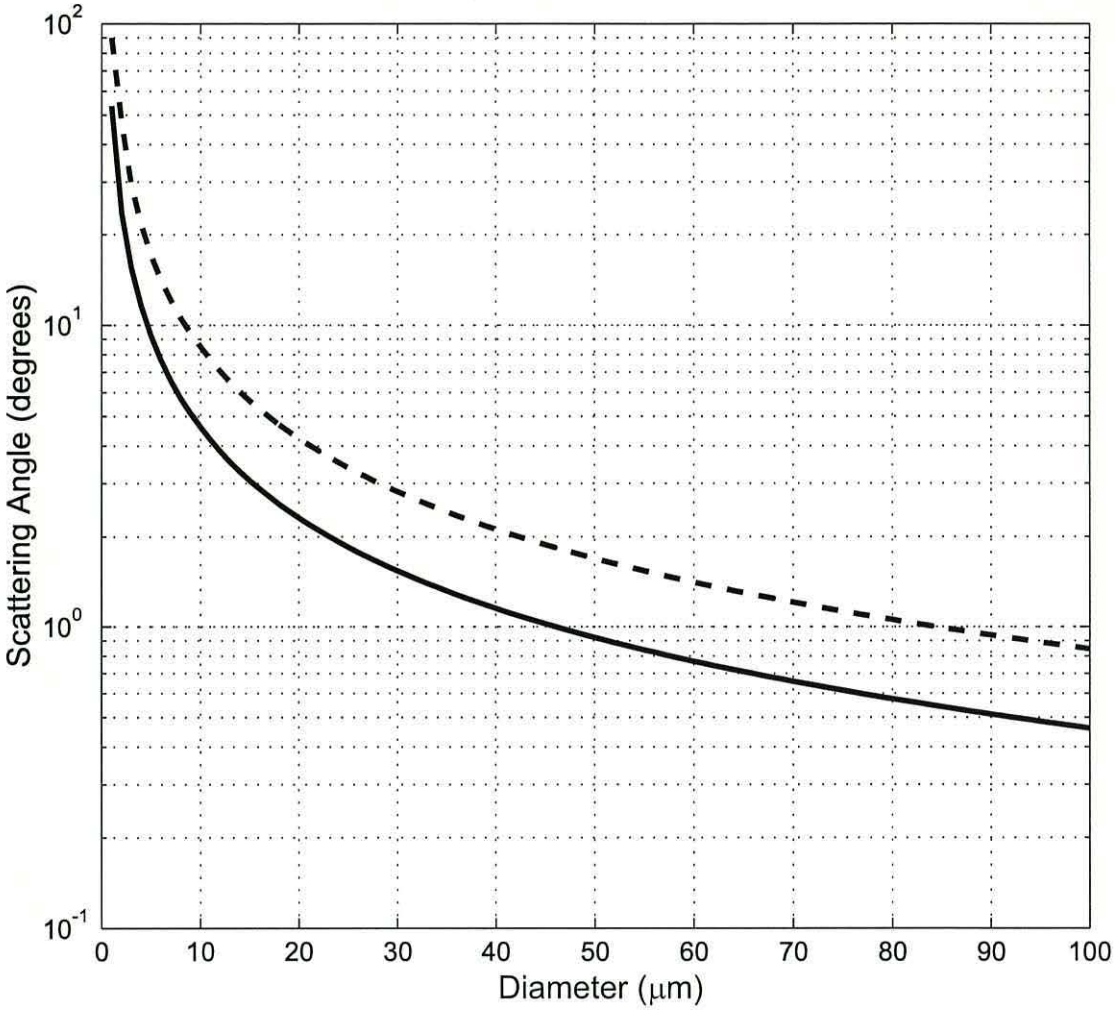

Figure 2.5. Angle of diffraction for increasing particle diameter. First dark ring (———) and second dark ring (----------).

Chapter 3

Observations and Instrumentation

3.1. Observations

Observations used to address the first stated aim are listed in Chapter 4.

Aim:

- Validate a new in-situ particle sizer by comparison with other instruments under controlled laboratory conditions and in the field.

Observations used to address the second and third stated aims.

Aims:

- Characterise SPM in terms of size, composition and settling velocity.
- Investigate, compare and contrast the temporal variability of SPM characteristics at the northern North Sea PROVESS site and one station in the Clyde Sea and relate this variability to physical and biological processes.

Ships	*R.V. Dana* (D1198) *R.R.S. Challenger* (CH140)	*R.R.S. Charles Darwin* (CD122)
Dates of cruises	14/10/98 – 26/10/98 (D1198) 22/10/98 – 09/11/98 (CH140)	21/05/00 – 22/05/00: 24 hour study
Site	59° 20' N 1° E	55° 21' N 5° 2' W
Observations	LISST (34 Profiles) Transmissometer (145 profiles) Gravimetric (130 samples) CTD (145 Profiles) ADCP (17/10/98 – 02/11/98) Wind and wave (From the Frigg oil platform: 17/10/98 – 08/11/98)	LISST (136 Profiles) Transmissometer (136 profiles) Gravimetric (110 samples) CTD (136 Profiles) Fluorometer (136 Profiles) Millport tides ADCP (12/05/00 – 21/05/00)

Table 3.1. Observations made at the northern North Sea and Clyde Sea sites.

3.2. *Measuring Particle Size*

3.2.1. Galai Cis-100 laser system

This laboratory based laser particle sizer uses the 'time-of-transition' theory to estimate particle size distributions of samples (Chapter 2). This theory states that the duration of a shadow on the detector due to the interaction between a rotating laser beam moving at a fixed velocity and a particle, is directly dependent on the particle diameter (Karasikov *et al.*, 1988; Jantschik *et al.*, 1992; Tsai, 1996) (Figure 3.1). Particle-laser interactions can be interpreted to give an equivalent spherical diameter size for each interaction. Three operating ranges are available; 0.5 - 150 μm, 1 - 600 μm and 10 - 3600 μm. The 1 - 600 μm range was used during all field measurements considered here. Each water sample can also be directly viewed by video microscope during analysis and recorded, allowing re-examination frame by frame for subsequent 2-D particle shape analysis.

The Galai stores raw data as a number frequency distribution using linearly spaced size classes ranging from 1 μm to 600 μm increasing by increments of 1 μm. As the other particle sizer (LISST-100, see section 3.2.2) used in conjunction with Galai has logarithmically spaced size classes ranging from 1.25 μm to 250 μm increasing with a factor of $200^{(1/32)}$ the Galai data was converted into the same logarithmic size classes extending to 600 μm. The size classes and the median of each size class can be seen in Table A1.1 (Appendix A). In each Galai size class the % of the total number of counts is known. A percentage cumulative frequency graph is drawn and the slope and intercept (*c*) of the line between each point is calculated. For each LISST size class limit a cumulative value can be obtained (Equation 3.1).

Equation 3.1. $\text{Cumulative \%} = (\text{LISST Limit} \times \text{slope}) + c$

The number of counts measured by the Galai in the LISST size class can then be calculated by

Equation 3.2.

$$\text{Counts} = \left(\left(\text{Cumulative}\%_{\text{upper}} - \text{Cumulative}\%_{\text{lower}}\right)/100\right) \times \text{Total Number of Counts}$$

The volume of particles in the LISST size class measured by the Galai is then calculated assuming that the particles are spherical (Equation 3.3). By dividing by the total volume of particles a normalised volume of particles for each size class can then be calculated.

Equation 3.3.

$$V = \left(\pi \times \text{Median of LISST Size Class}^3 \div 6\right) \times \text{Number of Counts in Size Class}$$

For sample analysis the sample is retrieved into a stainless steel sleeve (referred to as the Galai sample sleeve) with a hole at one end leading to a piece of plastic tubing which was clamped shut until sample analysis. For sample analysis the sample sleeve was clamped in the upright position above the sampling chamber of the Galai and the tubing from the bottom of the sleeve was attached to the top of the sampling chamber which was filled with distilled water. This prevented air bubbles moving through the sample and disturbing it when the clamp on the tubing was removed. A peristaltic pump located downstream of the sampling chamber was then turned on to gently pump the sample through the sampling chamber while the Galai was measuring the particles moving past the laser beam (Figure 3.1). During all cruises there was a fault with the computer running the Galai which meant that on occasions it crashed during a sample run. If possible the pump was stopped while the computer was set to run again and in these cases all files from the same sample were summed together to give one size distribution for the whole sample, as this is what was obtained when the computer did not crash.

3.2.2. LISST-100 (Laser In-Situ Scattering and Transmissometry)

The LISST-100B (hereafter referred to as LISST), which measures particles in the range of 1.25 - 250 μm, is a relatively new instrument developed by Agrawal and adapted for commercial use by Sequoia Scientific, Redmond, WA. It is an in-situ laser particle sizer that uses laser diffraction analysis based on particles of a given size diffracting light through a given angle which increases with decreasing particle size. A parallel beam is passed through the suspension, with a pathlength of 5 cm, and the diffracted light is focused onto a detector with multiple concentric rings which detects the angular distribution of scattered light intensity (Figure 2.3). The underlying mathematical model assumes that light is scattered only once from the laser beam (i.e. there is no multiple scattering). This single scattering is generally prevalent until the optical transmission over the instrument sensing path drops below c. 30% (Sequoia Scientific, 2001a). As the instrument relies on light scattering patterns a very low concentration will result in high signal-to-noise ratios. This occurs in waters which have optical transmission greater than 98%, although averaging over more scans can overcome this problem (Sequoia Scientific, 2001a). The technical specifications are listed in Appendix A.

Fraunhofer diffraction, which describes the diffraction pattern utilised here, is described in Chapter 2, section 2.1.8. For an extensive description of the equations and inversion used by the LISST to obtain the size distribution the reader is referred to (Agrawal & Riley, 1984; Riley & Agrawal, 1991; Traykovski *et al.*, 1999).

During all cruises the LISST was deployed mounted horizontally on to a CTD frame to prevent particles settling on the detector window, and lowered at a rate no faster than 1 m s^{-1}.

The LISST instrument can be turned on by three different triggers; 1) Using an on/off switch; 2) Pressure triggered to turn on at 2 m; 3) Time trigger. Collected data is stored in the onboard memory and downloaded after retrieval to a PC using an R232 connection. It is possible to view and log the data on a PC in

real-time although this feature was not used. Prior to data processing a reading in clear water is required (zscat). This is done by placing the LISST in a calibration chamber (provided by the manufacturers). Primary processing is undertaken using the WINDOWS based program provided by the manufacturers and is summarised in Figure 3.2. This program applies the calibration factors and accounts for the readings obtained in clear water as well as inverting the data, and outputs 74 columns of data, the first 32 being the volume concentration ($\mu l\ l^{-1}$) in the 32 size classes (see table A1.1 for size classes and table A1.2 for a description of each data column).

All further processing, including any averaging and de-spiking, was performed using my own MATLAB programs specific to each experiment. A description of the de-spiking and averaging applied to the LISST data can be found in the appropriate experimental chapters.

3.2.3. Lasentec

The Lasentec is an in-situ laser particle sizer developed from a commercially available non-submersible probe, Par-tec 100 (Law *et al.*, 1997). Lasentec utilises a monochromatic laser diode with a width of less than 0.5 nm. Such a narrow beam is used because the principle of operation depends on being able to measure the amount of light scattered from a single particle and as such requires a highly focused beam whose cross-section is at least as small as the smallest particle. The laser is focused on the measuring point by means of a precision micrometer and in all cases in this experiment the focal length was approximately 0.8 mm.

As suspended particles move at different random velocities the time of transition would vary according to the flow velocity. For this reason the laser beam is rotated at very high velocity so that it is moving faster than the particles. When measurements are taken both the transmitter and receiver are stationary while the focusing lens rotates at a very high velocity. Any particle that intercepts this scanning beam will scatter light back to the photo-detector. Therefore, by

measuring how long it takes for the beam to sweep across the particle, taking into account the velocity of the beam, the size of particle is directly measured.

Data is downloaded in real-time to a PC. After data collection the data is imported into MS EXCEL and a macro provided by Dr. A. Bale (Plymouth Marine Laboratory) is run. This macro calibrates the data using Equation 3.4 which is an improved version of the calibration factor (*sf*) (Bale *pers. comm.*) suggested by Law *et al.* (1997).

Equation 3.4. $$sf = -9.46\times10^{-6}\times M_o^{\,2} + 8.414\times10^{-3}\times M_o - 0.213,$$

where M_o is the original mean size. The calibration factor is then applied to obtain the actual mean size and adjusts the size classes accordingly. Therefore the size classes for Lasentec are never the same. However, as they are logarithmically spaced the means and distributions obtained can be directly compared with those from LISST and the adjusted values from Galai.

3.3. Measuring SPM Mass Concentration

3.3.1. Theory of a Beam Transmissometer

Transmissometers measure the transmission of a collimated beam of monochromatic light (usually with a wavelength of ~660 nm) through a known volume of sample. The light detected on the receiver detector is then directly related to the optical properties of the suspension that the beam travelled through. The transmission of light through a volume of water is affected by the scattering and absorption properties of the medium and is described in detail in Chapter 2, section 2.2.2.

The percentage of the initial light received by the receiver (i.e. the percentage transmission) is:

Equation 3.5 $$T(z) = \frac{I(z)}{I(o)},$$

where I(z) is the light intensity at a distance z from the source and is given by:

Equation 3.6 $$I(z) = I(0)e^{-cz},$$

where c is the beam attenuation coefficient which is the sum of absorption and scattering which is computed by:

Equation 3.7 $$c = -\ln(T)/z$$

The total beam attenuation coefficient, c, is a result of attenuation by water, c_w, suspended particulate matter, c_p, and by dissolved materials (yellow substance), c_y and can therefore be described by $c = c_w + c_p + c_y$ with each component having distinct spectral characteristics. Absorption by yellow substance is greatest in the blue part of the spectrum, decreasing exponentially with increasing wavelengths with the attenuation at 660 nm being negligible (Jerlov, 1976). As the beam attenuation due to water is constant the main changes observed in c are caused by variations in the suspended particle population. For a given suspended particle population, c_p is linearly dependent on particle concentration. Therefore c can be converted to concentration using calibration coefficients obtained by linear regression analysis with gravimetric concentrations taken simultaneously. Attenuation due to suspended particles is affected by particle composition, shape, size and refractive index and the calibration will vary according to both the nature of the suspended particles and their size distribution, resulting in both spatial and often temporal variation in the calibration coefficients. All transmissometers used were SeaTech transmissometers with a 20 cm pathlength and wavelength of 660 nm.

3.3.2. Gravimetric Calibration of a Beam Transmissometer

Mass concentration of SPM was directly measured at the northern North Sea site and at the Clyde Sea site for the purpose of calibrating the beam transmissometers for the estimation of SPM concentration throughout the water column.

Water samples were obtained from known depths (details of sample collection are given in chapters 5 and 6) and known sample volumes were filtered by vacuum through pre-weighed 47 mm diameter Whatman GF/C glass microfilters with 1.2 μm retention capabilities. When the entire sample had passed through the filter, approximately 150 ml of distilled water was filtered through in order to rinse through any salt. Approximately every twentieth sample an additional GF/C filter was inserted beneath (i.e. two filters were used, one on top of the other) thereby acting as a blank. As much moisture as possible was removed from the filter before switching off the vacuum. The used filters were frozen until return to the laboratory.

In the laboratory, the GF/C's were oven dried overnight at 60 ^{o}C, then brought to room temperature under ambient humidity before re-weighing. The weight of the material on the filter was then determined using the pre and post filtration filter weights, having first subtracted the mean blank weight, and then converted into SPM mass concentrations using the filtered sample volumes. A linear regression analysis between the measured mass concentrations and corresponding beam attenuations was then performed.

3.4. Calculating the Dry Particle Density

As the LISST measures volume concentration, where dry mass concentration has been obtained independently, by gravimetric measurements, the dry particle density can be calculated. However, there are limitations associated with this, a result of the dry mass concentration being over the whole size spectrum. Firstly, density may vary with particle size resulting in the dry particle density being an average for the whole particle population. Secondly, the total

volume concentration measured by the LISST is not accurate if there are particles with diameters greater than 250 μm present. These two limitations can lead to large errors in the estimation of the dry particle density and must be taken into account when performing such calculations.

The mean, dry particle density, i.e. over the whole size spectrum as measured by the LISST, was calculated using Equation 3.8 in the northern North Sea and the Clyde Sea. Particle densities were obtained for each site for the surface waters (within the top 5 m), the thermocline region and the near-bed region (within 8 m above the bed).

Equation 3.8. $$\rho = \frac{gravimetric\_concentration\_(g/l)}{volumetric\_concentration\_(cm^3/l)}$$

3.5. CTD Packages

3.5.1. Northern North Sea (RRS Challenger, Cruise Number CH140)

Hydrographic casts were performed by lowering an instrument package consisting of a Neil Brown Mk IIIB CTD incorporating a pressure sensor, conductivity cell, platinum resistance thermometer and a 20 cm pathlength SeaTech transmissometer (wavelength of 660 nm). Data were transmitted in real time on both the down and upcasts via a single conductor armoured cable. A General Oceanic rosette sampler equipped with twelve 30-litre water bottles was fitted above the CTD unit. The base of the bottles were 0.75 m above the pressure head with their tops being 1.55 m above it. Temperature was calibrated with two calibrated digital reversing thermometers attached to one bottle. Salinity was calibrated from bottle samples taken throughout the cruise and measured on a Guildline 55358 AutoLab Salinometer. These calibrations were carried out by RVS personnel and the data were initially quality controlled by the British Oceanographic Data Centre (BODC).

3.5.2. Clyde Sea (RRS Charles Darwin, Cruise Number CD122)

Hydrographic measurements were made by lowering an instrument package consisting of a Neil Brown Mk IIIB CTD unit, a Chelsea Mk3 fluorometer and a Seatech 20 cm pathlength, 660 nm, transmissometer. A General Oceanic rosette sampler equipped with twelve 30-litre water bottles was fitted above the CTD unit. Temperature was calibrated with a reversing thermometer attached to one bottle and salinity was calibrated from bottle samples taken throughout the cruise. These calibrations were carried out by RVS personnel. The data was supplied, with initial quality control flags by Dr. C. Janzen (UWB).

Due to the unavailability of an accurate calibration coefficient for the fluorometer a linear relationship was assumed between volts and chlorophyll-a concentration using a range of 0.01 – 100 $\mu g\ l^{-1}$ as specified by Chelsea Instruments. Therefore, chl-a concentration ($\mu g\ l^{-1}$) = 20 x volts. It is stressed that the chl-a concentration values presented in this thesis should be treated with caution if absolute values are required.

3.6. Turbulence Measurements

Turbulence dissipation rate measurements were made by the turbulence group at UWB using a turbulence profiler (FLY-IV profiler) and is described in detail by Dewey *et al.*, (1987). This instrument uses a pair of piezoelectric sensors (sensor 1 and sensor 2) to measure the vertical shear in the horizontal velocity field. In addition the probe is equipped with fast and slow thermistors, a conductivity cell and a pressure gauge. The pressure case contains two tilt gauges, signal amplifiers and the power supply. Floats are attached to the top of the case to allow control of the fall velocity and ensure that the profiler remains vertical.

The profiler free falls to the bed at ~80 cm s^{-1}, sampling the shear 274 times each second. Once at the seabed the profiler is winched back to the surface. The number of profiles measured depends on the water depth but it is

approximately one profile every four minutes. Valid results are obtained from 10 m below the surface to 15 cm above the bed.

For processing, the water column is subdivided into bins. In the interior, bin length is ~1.6 m with shorter bins used in the high shear zone near the bed in order to reduce the effects of non-stationarity. A fast Fourier transform is performed on the shear signal from each bin to obtain the power spectrum and the dissipation rate spectrum. Transfer functions are then used to compensate for deterioration in probe performance at high frequencies. Low and high frequency cut-off are applied to isolate noise and the signal is then boosted to account for the energy lying beyond these cut-offs. Over 80% of the dissipation spectrum is observed directly. The Epsilon (W m^{-3}) (turbulent dissipation rate) profiles are then interpolated to give a result every 15 cm. Details on the calculation of Epsilon from the velocity gradient are described by Dewey and Crawford (1988).

Data was supplied by BODC and required no processing as this had already been performed.

3.7. ADCP Measurements

Acoustic Doppler Current Profilers (ADCPs) use sound waves to determine vertical profiles of currents. They transmit sound bursts into the water and particles carried by the water currents scatter the sound back to the transducer. As echoes return from further way from the sensor, the instrument assigns different water depths to the returning signals. Motion of the scattering particles relative to the sound source causes a change in the frequency of the sound (known as Doppler shift). The ADCP measures this change to produce vertical profiles of water velocity at up to 128 depths throughout the water column.

An upward looking 150 kHz broadband ADCP was deployed by the Proudman Oceanographic Laboratory prior to the study period and was recovered during the study period. The data was supplied by BODC and therefore no processing or quality control was required as this had already been performed.

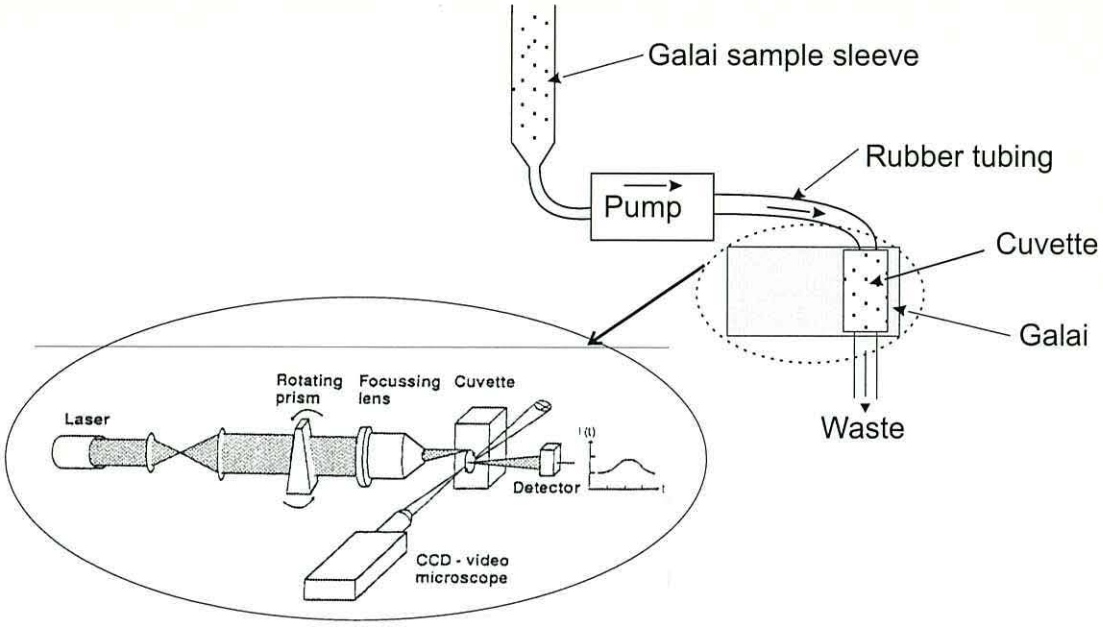

Figure 3.1. Schematic of the experimental setup and measurement principle of the Galai laser system (adapted from Jantschik *et al.*, 1992).

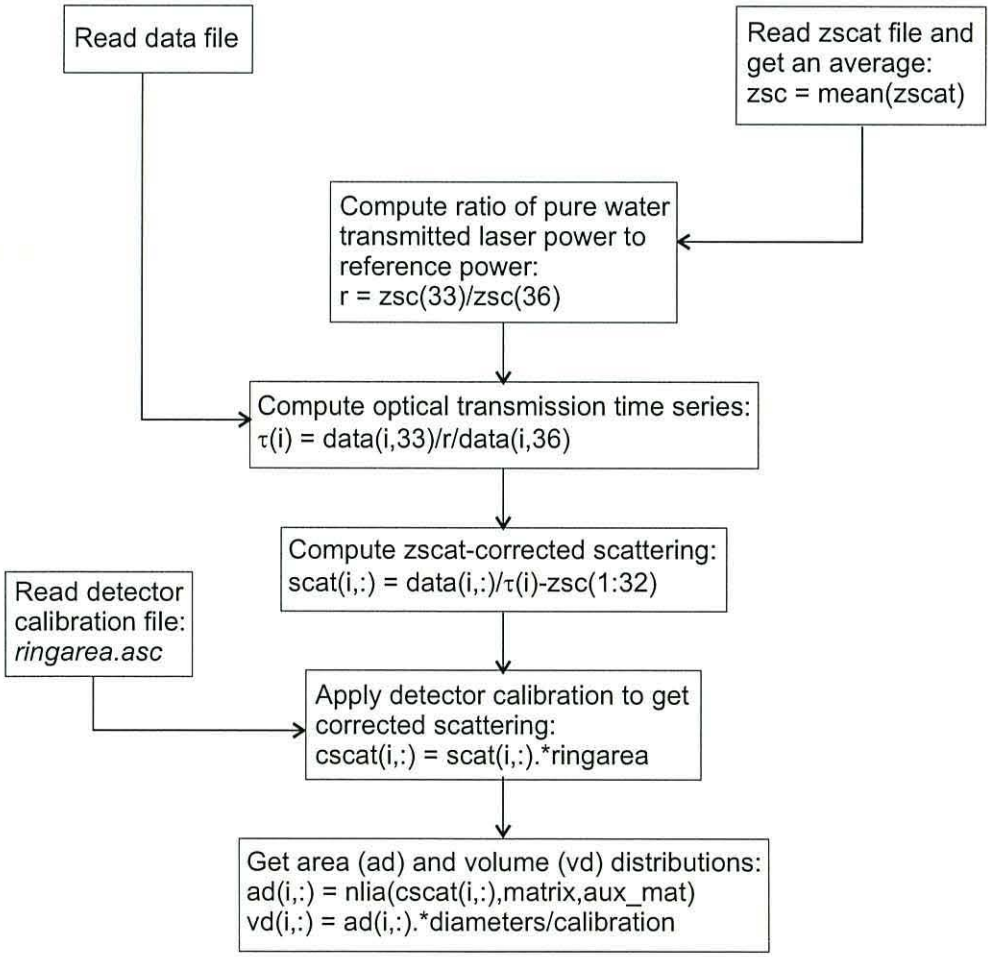

Figure 3.2. Flow-diagram of the LISST processing programme where nlia is the inversion routine.

Chapter 4

Comparison and Validation of Three Particle Sizers

4.1. Introduction

Two particle sizers were deployed during the field studies of this project (LISST 100-B and Galai Cis-100). As described in Chapter 3, these each employ different methods for determining the particle diameter. Also the LISST is an in-situ instrument and therefore does not have the sampling problems associated with the Galai due to the latter being a laboratory based instrument (Chapter 3). In order to validate the field results some basic laboratory experiments using standardised glass and latex particles were conducted. The aims of these experiments were to establish whether, given the same materials, the results from both instruments were similar, thus enabling a more informed view to be taken when evaluating results from the field. A Lasentec, an in-situ laser particle sizer, was also used in the laboratory experiments to provide a third comparison (see chapter 3 for a detailed instrument description).

As the aim was to determine whether the instruments were giving accurate particle size information the actual distribution within the samples analysed had to be established. This was achieved using a Coulter Counter and microscopy, depending on the size being measured. These methods are widely accepted as giving accurate results if performed correctly (e.g. Law, 2001).

After comparisons between the LISST and the Galai in the laboratory, field data collected on a number of cruises were compared. This gave a further understanding of the abilities and limitations of the instruments before interpretation of the field results.

A set of experiments was also conducted to help determine the minimum operating range of the LISST.

4.2. Methods and Data Processing

4.2.1. Instrument Comparisons (Laboratory)

Standardised particles (Duke Scientific) were used to allow direct comparisons between the LISST, Lasentec and Galai. These particles consisted of 1 – 35 μm glass beads, 10 – 95 μm glass beads and 100 – 500 μm latex beads, although the latex beads were not analysed by the Lasentec as it is unable to detect these (Law *et al.*, 1997). The 100 – 500 μm beads were divided by dry sieving into ½ ϕ intervals. There were not enough particles that went through the 150 μm sieve to allow analysis to be carried out and therefore the smallest beads used from the 100 – 500 μm beads were those collected on the 150 μm sieve. Actual distributions for both 1 – 35 μm and 10 – 95 μm particles were determined using a Coulter Counter. The apertures chosen were based on the guidelines set out in the manual, that is that Coulter Counter apertures can measure between approximately 2% and 60% of the aperture size. Therefore the 1 – 35 μm particles were analysed using a 100 μm aperture and the 10 – 95 μm measured using a 280 μm aperture. Each sample was sub-sampled by coning and dividing until a suitable amount of sub-sample had been selected. The sub-sample was then mixed with a small drop of detergent and distilled water and ultrasonically dispersed for ten minutes. Each sub-sample was then analysed a minimum of three times and a minimum of three sub-samples were obtained for each sample. The Coulter Counter logged both number and volume distributions with logarithmically spaced size classes, allowing direct comparison with the LISST, Galai and Lasentec.

Actual distributions for the 150 – 500 μm ½ ϕ samples were obtained through microscopy. Sub-samples of each size class were obtained by dipping adhesive tape into the sample and then a minimum of 50 particles were sized. These particles were chosen by randomly choosing a starting place and then measuring each successive particle, moving in a downwards direction if more than two particles neighboured the same particle on the same side. Each particle was then put into the correct size class using the LISST size classes (see Appendix A) before a volume distribution was obtained.

The Lasentec and LISST were mounted in the same calibration tank and stirring was applied to ensure homogeneity of the sample throughout the chamber (Figure 4.1). The samples were run independently through the Galai and where possible the same sub-sample was used that had been used for the Lasentec and LISST. To maintain a constant concentration for the Galai the sample was stirred whilst in the reservoir before being pumped through the sampling chamber by a peristaltic pump located downstream.

Samples were prepared for analysis using the Lasentec and LISST in the same way that they were prepared for analysis by the Coulter Counter. If a known concentration was required then the sample was weighed before the addition of a drop of detergent and 10 ml of distilled water. Each sample was then ultrasonically dispersed for ten minutes before being added to three litres of distilled water. To ensure accurate results the distilled water used as the suspending fluid was scanned one hundred times by the LISST prior to addition of the sample and this was used as the zscat file required by the processing package (see Chapter 3). This was not performed with either the Galai or Lasentec as the particle count in distilled water was always too low to be significant.

Before measurements commenced a real-time reading of greater than 1000 counts was required by the Lasentec. Resultant data from both the Lasentec and the LISST were averaged over all the scans performed to produce one distribution per sub-sample for each instrument. At least five sub-samples were run per sample. Sub-samples from the same sample were then run through the Galai at least five times. As the Galai analyses the whole sub-sample, giving one distribution, no averaging was required. However, as the Galai returns results on a linear scale these were converted to the same logarithmic scale as the LISST (Chapter 3). As each instrument gave results in different units all were converted to normalised volume to allow easy comparison. This conversion was done using the median of the size class as the size used to obtain a volume of particles and the total number of counts in each size class.

4.2.2. Instrument Comparisons (Field)

The LISST and Galai were deployed during four separate cruises, details of which are outlined in Table 4.1. Different sampling methods and storage of the Galai water samples were employed on each cruise due to different CTD configuration and instrument reliability. In all cases the samples were retrieved into the Galai sample sleeve and analysed from this using the method and instrument set-up described in section 3.1.1.

Survey	SNS1	SNS2	SNS3	CLY1
Ship	*Pelagia* PE136	*Mitra* MT0499	*Belgica* BG9912	*Charles Darwin* CD122
Date	29/3/99-9/4/99	19/4/99-30/4/99	17/5/99-21/5/99	12/5/00-23/5/00
Site	S. North Sea	S. North Sea	S. North Sea	Clyde Sea

Table 4.1. Cruise details where the LISST and Galai were deployed where SNS is the Southern North Sea (Figure 1.1).

Survey SNS1

Samples were collected from near-bed and near-surface using the rosette sampler on the CTD. This rosette consisted of twenty-four 12 litre NOEZ sampling bottles. These operate on a vacuum system sucking the water in when triggered. Sample retrieval was through plastic tubing, 0.5 cm diameter, attached to a nozzle located at the base of the sampling bottle into the Galai sample sleeve.

Samples were stored in the sample sleeve, which was held upright, for up to one hour prior to analysis, during which time care was taken not to disturb them. A video was also used to record the sample passing through the sample chamber for subsequent analysis.

Surveys SNS2, SNS3 and CLY3

During survey SNS2 Galai water samples were collected using 1 litre Niskin bottles, on the CTD bottle rosette, fired at known depths. For analysis the Galai

sample sleeve was carefully inserted into the bottle. The tubing was then clamped shut and the bottle and sleeve rotated through 180° into an upright position. This was done carefully minimising any disturbance. The sample was then run through the Galai in the standard manner. Due to an analysing backlog some samples were left to sit in the upright position for up to one hour before being analysed.

Sampling during the SNS3 and CLY1 surveys was similar to that of the SNS2 survey except that during the SNS3 survey samples were stored in the sleeve upside down and therefore required turning through 180° directly before analysis. During the CLY1 survey samples were stored in the CTD bottle until they were analysed when they were transferred into the stainless steel sleeve which is then inverted carefully for analysis.

4.2.3. LISST Concentration Operating Range

The minimum concentration for which the LISST can produce reliable results was determined using the following method. Three litres of distilled water was put into the calibration chamber and 100 scans taken to be used as the background scatter file. A small sub-sample of particles (both 1 – 35 μm and 10 – 95 μm were used in separate experiments) was weighed. Then one drop of detergent and 10 ml of distilled water was added and the sub-sample ultrasonically dispersed for ten minutes.

After the sub-sample had been dispersed a mechanical stirrer was started in the calibration chamber and the sub-sample added. After thirty seconds the LISST was turned on and allowed to measure for one minute before being turned off and another known amount of sample added and the procedure repeated. This was repeated until the concentration was deemed to be well within the recommended operating range.

4.3. Results

4.3.1. Instrument Comparisons

The Coulter Counter volume distributions for 1 – 35 μm and 10 – 95 μm diameter particles are shown in Figure 4.2. These are an average of all the distributions obtained from all the sub-samples as the individual distributions were very similar and consistent with the commercially supplied distributions for the samples. The mean size of the 1 – 35 μm particles is 22.29 μm (standard deviation = 8.19 μm) and for 10 – 95 μm particles the mean size is 68.26 μm (standard deviation = 11.91 μm). The volume size distributions and mean sizes obtained by microscopy are shown in Figure 4.3.

Figure 4.4 shows the average size distributions measured by the LISST, Galai and Lasentec with the actual distributions (i.e. measured by Coulter Counter / microscopy). The mode measured by the Lasentec for the 1 – 35 μm particles is 20 μm greater than that measured by the other methods. The Lasentec was unable to detect latex particles (Law *et al.*, 1997), therefore there is no data from the Lasentec above the 10 – 95 μm particles. Also the LISST was only used up to 250 – 300 μm as its upper measuring limit is 250 μm.

The microscopy distributions, when compared against the distributions obtained from the LISST and the Galai, are distributed over a much smaller size range (Figure 4.4(c-h)). Both the LISST and the Galai have "tails" in the distribution extending into much finer size classes than measured by microscopy resulting in the mean size of the distributions measured by the LISST and Galai being consistently smaller than the mean size suggested by the microscopy results (Figure 4.5). However, the mode of the distributions measured by the LISST and Galai are always within one size class of the mode measured by microscopy (Figure 4.4).

Both the LISST and the Galai were used on four separate cruises in the southern North Sea and Clyde Sea (Table 4.1). During all cruises near-bed and near-surface water samples were taken for the Galai. Both distributions and

mean sizes from the Galai were compared with the corresponding LISST data. Subsequent plots do not include data collected on the Pelagia cruise for reasons discussed later.

For all cruises the LISST mean sizes were consistently much greater than those from the Galai (Figure 4.6) and the correlation between the two was poor (correlation coefficient = -0.2674). This is explained by the fact that the Galai size distributions from all the cruises rarely showed any material greater than 100 μm, however the LISST size distributions indicate a large volume concentration of material greater than 100 μm, with few exceptions (Figure 4.7). Only twice did the LISST and Galai report similar size distributions (Figure 4.8) and this occurred during two casts on the SNS2 survey. On both casts the distributions were similar at both the near-surface and near-bed.

If the LISST results are recalculated by ignoring the part of the distribution coarser than the last size class that the Galai registered non zero particle counts, then very similar distributions to the corresponding Galai distribution are obtained (Figure 4.7). The mean size calculated by the LISST for this truncated distribution then becomes very similar to that by the Galai (Figure 4.9) and the correlation co-efficient becoming significant ($r^2 = 0.8331$).

Videos of the suspension that passed through the Galai sampling chamber were analysed manually for particle type, composition and size. Shape analysis was not possible as this function was not working at the time. Footage from the SNS1 survey showed few large particles. Footage from the other three cruises show the presence of four main particles, *Phaeocystis, Eucampia sp., Rhizosolenia sp.* and copepods (Figure 4.10) with *Phaeocystis* and *Rhizosolenia sp.* being the most dominant. *Phaeocystis* was present in most frames analysed and is spherical, semi-transparent (Figure 4.10) with sizes ranging from c. 170 μm to 550 μm diameter. Most frames also contained a range of particles with sizes greater than 100 μm, including those greater than 250 μm.

4.3.2. LISST Concentration Operating Range

1 – 35 μm and 10 – 95 μm particles were used to test the minimum beam attenuation for which the LISST can return meaningful size distributions and means. The results of this experiment are shown in Figure 4.11. For 1 – 35 μm particles the smallest increment in mass concentration used still resulted in correct estimate of mean size. For 10 – 95 μm particles the mean size was not correctly estimated until the beam attenuation was c. 0.8 m^{-1}.

4.4. Discussion

4.4.1. Instrument Comparison

Using spherical, standardised particles, the Lasentec overestimates both the mode and mean size for the 1 – 35 μm size range, a result also seen by Law *et al.* (1997) who concluded that the Lasentec overestimates for particles less than c. 100 μm using a focal distance of 0.8 mm. This may be improved if a focal length nearer 0.2 mm was used as suggested by Law *et al.* (1997). With the 10 – 95 μm glass particles the Lasentec performed much better, reporting nearly identical size distributions and mean diameters to those obtained from the Coulter Counter.

Although the calibration factor equation used (Equation 3.1) was an improvement on that suggested by Law *et al.* (1997) it appears that this still needs to be improved for small particles. However, this was not pursued further in this project as many more samples, differing in composition and size, would be needed.

Both the LISST and Galai were in good agreement in measuring particles from 1 to 250 μm. This is expected as both instruments have been designed to work with spherical particles, as the theory and mathematics utilised assume this (see Chapter 3). The best agreement of the LISST and the Galai was obtained for the finer size classes (1 – 35 μm and 10 – 95 μm), compared with the

Coulter Counter. These have a relatively large number of size classes and all three instruments agreed reasonably well in mode, distribution and mean grain size. For the coarser samples (150 – 180 μm, 180 – 212 μm, 212 – 250 μm and 250 – 300 μm) there was agreement to within one size class in mode but the Galai and especially the LISST indicated a fine "tail" which was not apparent in the microscopy results. The cause of this discrepancy is unknown but could be due to contamination of the suspending fluid or the presence of bubbles, or to the inversion algorithm used to fit the size distribution to the data. This fine "tail" produced a finer mean diameter than that measured by microscopy, hence deviating beneath the 1:1 line in Figure 4.5 as the mean diameter increases. For the 250 – 300 μm sample the LISST produces a distribution which is truncated at 250 μm hence the mean is significantly underestimated. Finally, the two coarsest samples (g) and (h) show that the Galai data is truncated at 600 μm.

In the presence of particles greater than 250 μm LISST produces a distribution and a mean size (Figure 4.4f). As it can only measure up to 250 μm both the distribution and mean size in such situations are obviously incorrect. As particles larger than 250 μm will diffract light into the 250 μm detection ring a population containing such particles would give anomalous results in the larger size classes. This will also mean that the volumes in the larger size classes may be wrong because the >250 μm signal is effectively increasing their concentration. This finding has also been reported by other investigators (e.g. Traykovski *et al.*, 1999).

As the laboratory experiments show, both the LISST and Galai produce more or less the same results for spherical particles within their operating range. Therefore, it may be expected that they would return the same results in the field using a diverse population of particles. However, it has been shown (Figure 4.6) that this is not the case. They measure neither the same mean size nor size distribution. The Galai size distributions rarely showed any material greater than 100 μm in size yet both the LISST and the Galai video footage indicate a near uniform presence of large particles. However, by re-normalising the LISST

data to the maximum size class that the Galai measures any material in both the distributions and mean sizes are similar. Therefore, the LISST and Galai were in reasonable agreement up to a maximum of c. 100 μm during these field studies.

As the LISST and the Galai produce similar size distributions with suspensions measured in the laboratory, up to 250 μm, the reason for the apparent discrepancy must be due to a factor that is only present in the field, such as sampling techniques or particle characteristics. The LISST measures in-situ whilst the Galai requires discrete water sampling. As a result they are not measuring exactly the same water and therefore some inconsistencies may be expected due to this. However, this cannot account for the major discrepancies observed.

Due to the Galai requiring discrete water sampling some particle break-up may occur during the Galai sample collection and subsequent pumping process. This would be particularly important in regions where the majority of the particles are fragile flocs. As the LISST measures in-situ, such break-up would not occur.

Analysis of the Galai video data from SNS2, SNS3 and CLY1 indicated that particle break-up was not responsible for the differing distributions as large numbers of particles greater than 100 μm were seen in all but two cases. For these two cases the LISST and the Galai reported no particles greater than 165 μm (Figure 4.8). This eliminates the proposition that particle break-up was caused by the peristaltic pump and confirms the findings of Jantschik *et al.* (1992). However, Galai video footage from SNS1 showed very few particles greater than 100 μm. The sampling method for the Galai samples was far from gentle during this cruise as the water bottles used (NOEZ sampling bottles) work by a vacuum method, sucking in the water. Also subsequent drainage through the nozzle into the sample sleeve could again have caused disturbance. It is highly likely therefore, that particles were broken up during

collection. It is for this reason that no further results from the SNS1 survey are reported here.

The findings from the SNS1 survey highlight the problems associated with laboratory based instruments where water samples have to be collected. Many investigators have reported such problems (e.g. Jantschik *et al.*, 1992; Gibbs, 1982a).

As particle break-up was largely not responsible for the differing distributions seen between the LISST and the Galai data in all the other cruises the other main cause is likely to be due to particle composition and / or shape. Of the four main large particle types observed only one is spherical (*Phaeocystis*) (Figure 4.10). As the LISST and the Galai assume that particles are spherical only a rough estimation of their size will have been obtained. In fact, the presence of thin cylinders, such as *Rhizosolenia sp.*, would result in streaks across the face of the LISST ring detector as diffraction theory predicts that thin cylinders produce streaked scattering in a plane normal to the plane containing the cylinder (Agrawal & Pottsmith, 2000). This diffraction pattern will only affect the LISST measurements. As the Galai estimates the diameter from the time of transition, it is likely to underestimate the equivalent spherical diameter for such particles.

However, *Phaeocystis* was present in most frames and is spherical (Figure 4.10) ranging from c. 170 μm to 550 μm diameter, well within the size limits of Galai. Galai accepts or rejects particles based on the difference in light detected. If there is not a sharp change the particle is rejected. As *Phaeocystis* is semi-transparent it is likely that the shadow formed on the detector is not of sufficient contrast when compared with the ambient light to be accepted. Therefore, the Galai is likely to be rejecting the majority of the larger particles in these samples. Jantschik *et al.* (1992) reported that the Galai could measure such particles in open water environments. However for this study the populations contained a mixture of constituents with very different opacity. In its statistical handling of the data the Galai rejects cases with very different

properties (e.g. contrast, rise-time of shadow) so with a mixture of different opacities transparent particles are more likely to be rejected. This would result in the Galai rejecting less opaque particles. Jantschik *et al.* (1992) also illustrated the difficulties in obtaining accurate measurements in the presence of large particles. They concluded that large volumes were required to be measured to produce good statistics for the large particles. Although relatively large volumes were measured in this study the Galai does not sample a large volume at the beginning of the analysis to set its tolerance level. This could mean that if the few large, more opaque particles are not included when it is setting the tolerance level they will be rejected during the measuring of the distribution.

Consequently, the Galai is likely to be both underestimating the equivalent spherical diameter of the non-spherical particles present and rejecting a large majority of the large, spherical, semi-transparent *Phaeocystis* cells, resulting in a size distribution that does not correctly represent the larger diameters of the population. The LISST is apparently able to detect the presence of large particles, however it is limited by the upper size limit of the instrument being much smaller than the maximum size seen on the video footage. It is also limited by the way the light is diffracted from the particles which may lead to an inaccurate description of the size distribution.

Therefore, it is probable that while the LISST and the Galai were in reasonable agreement in measuring the finer part of the size distribution, they were both, to a different degree underestimating the true mean size of the SPM populations they were measuring in these field samples.

4.4.2. LISST Operating Range

For the 1 – 35 μm particles it was not possible to determine the minimum beam attenuation (Figure 4.11a). Sequoia Scientific recommend that with 98% transmission or higher the LISST begins to produce noisy estimates of size distribution from single scans. However, noise reduction can be achieved through averaging. For 10 – 95 μm particles the mean size was not correctly

estimated until the beam attenuation was c. 0.8 m^{-1} (97% transmission) (Figure 4.11b) even with averaging large number of scans, slightly less than that recommended by Sequoia Scientific. Therefore, all data collected for this thesis has been averaged over a minimum of 4 scans and any data with a percentage transmission greater than 97% have been discarded.

4.5. Conclusions

A laboratory comparison between three laser particle sizers (LISST, Galai and Lasentec) was performed as well as a comparison between the field results from the Galai and the LISST. Results from using standardised particles in the laboratory indicate that all three instruments can correctly resolve size distributions of particle populations within their respective size ranges. It was found that despite using an improved empirical calibration factor to that suggested by Law *et al.* (1997) the Lasentec still overestimates both the mean and mode size of particles less than c. 100 μm.

Both the LISST and the Galai agreed well when measuring standardised particles whose populations had sizes within the respective size ranges of the instruments. It was found that in the presence of particles greater than 250 μm the LISST returned erroneous results for the higher size classes. This finding has also been reported by other investigators (e.g. Traykovski *et al.*, 1999) and is likely to be a result of the part of the diffraction pattern of larger particles falling on to the inner concentric detector rings of the LISST.

The LISST and the Galai were both deployed during four cruises in the Southern North Sea and Clyde Sea. Results showed the importance of the sampling procedure for the Galai samples. As a result of rough sampling procedures during one cruise (SNS1) all the Galai data had to be discarded due to the evidence of particle break-up occurring.

Mean sizes from the LISST and Galai field deployments were found to be dissimilar in all cases with the LISST measuring mean sizes an order of

magnitude greater than those of the Galai. Limitations of both instruments have been identified with regards to particle composition and instrument measuring theories. The Galai discards all particles that do not produce a distinct change in received signal and as a result has probably ignored the main large particle present (*Phaeocystis*) which is semi-transparent. The LISST does detect these particles to some extent but is limited by the size range it can detect. By re-normalising the LISST distributions up to the largest size class that the Galai sees particles in, it is found that the LISST and Galai size distributions and mean sizes were in reasonable agreement. Therefore, it is concluded that for SPM populations similar to those seen during this project neither the LISST nor the Galai is accurately resolving the size distribution, rather they are both underestimating the actual mean size due to the limitations outlined above. However, it is also concluded that for the smaller, less transparent particles both instruments agree reasonably well.

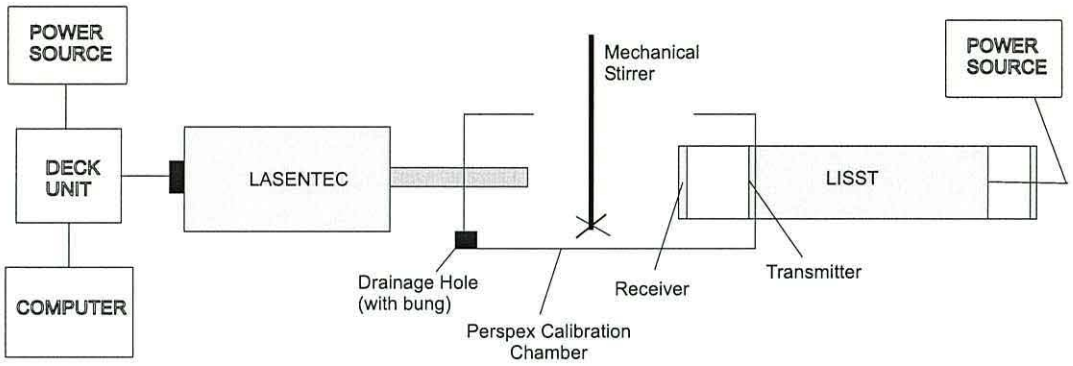

Figure 4.1. Laboratory set-up for the Lasentec and the LISST.

(a)

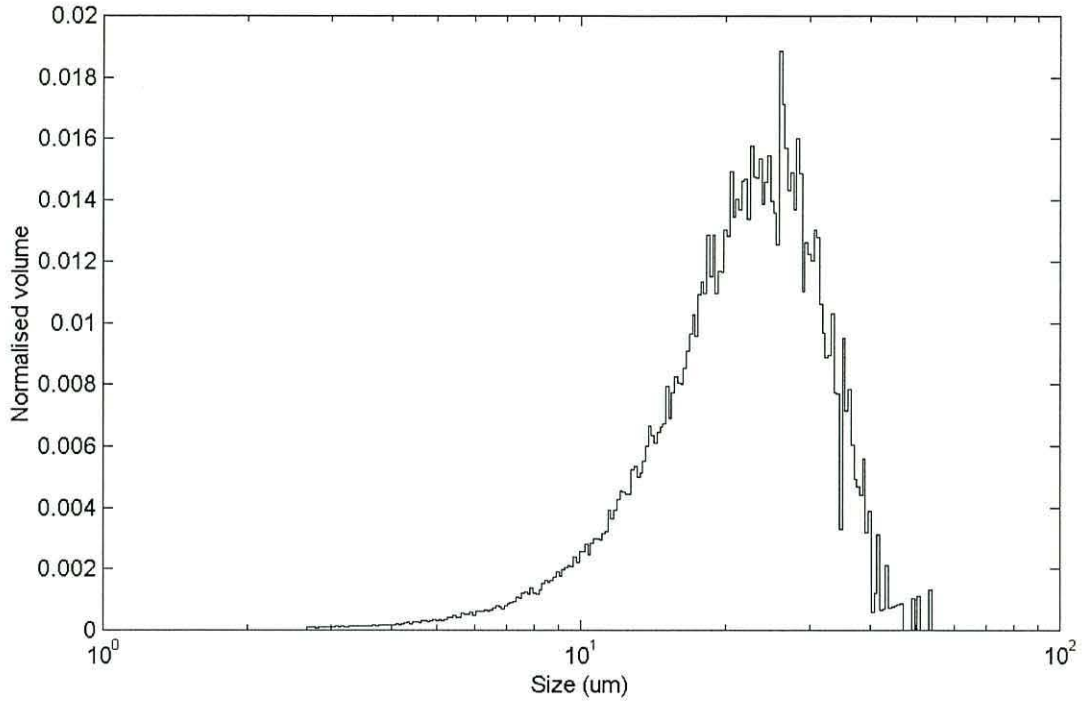

(b)

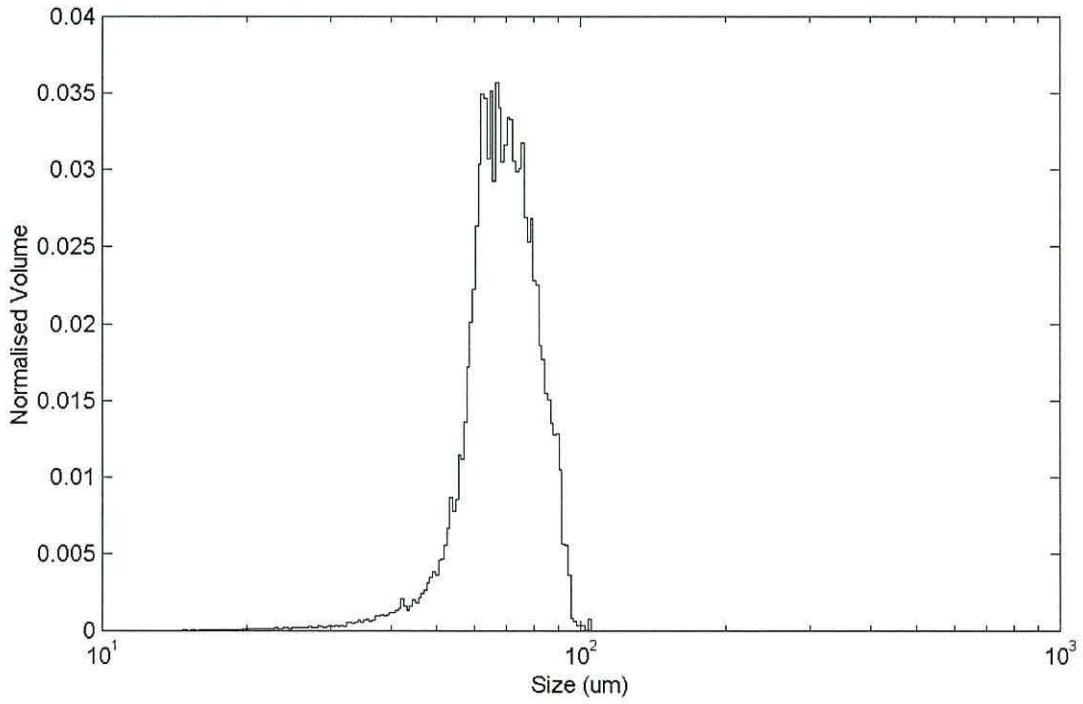

Figure 4.2. Average volume size distribution of standardised glass particles from the Coulter Counter. (a) 1-35 μm diameter particles and (b) 10-95 μm particles.

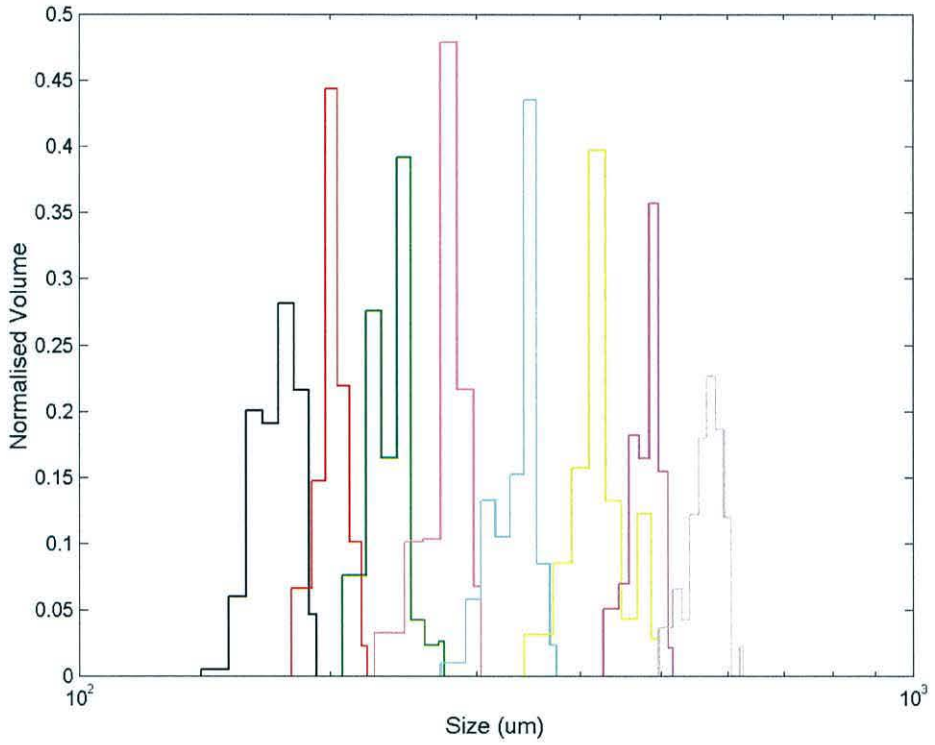

Figure 4.3. Size distributions (volume) and mean sizes from microscopy analysis. 150 - 180 μm (——), 180 - 212 μm (——), 212 - 250 μm (——), 250 - 300 μm (——), 300 - 355 μm (——), 355 - 425 μm (——), 425 - 500 μm (——), 500 - 600 μm (——).

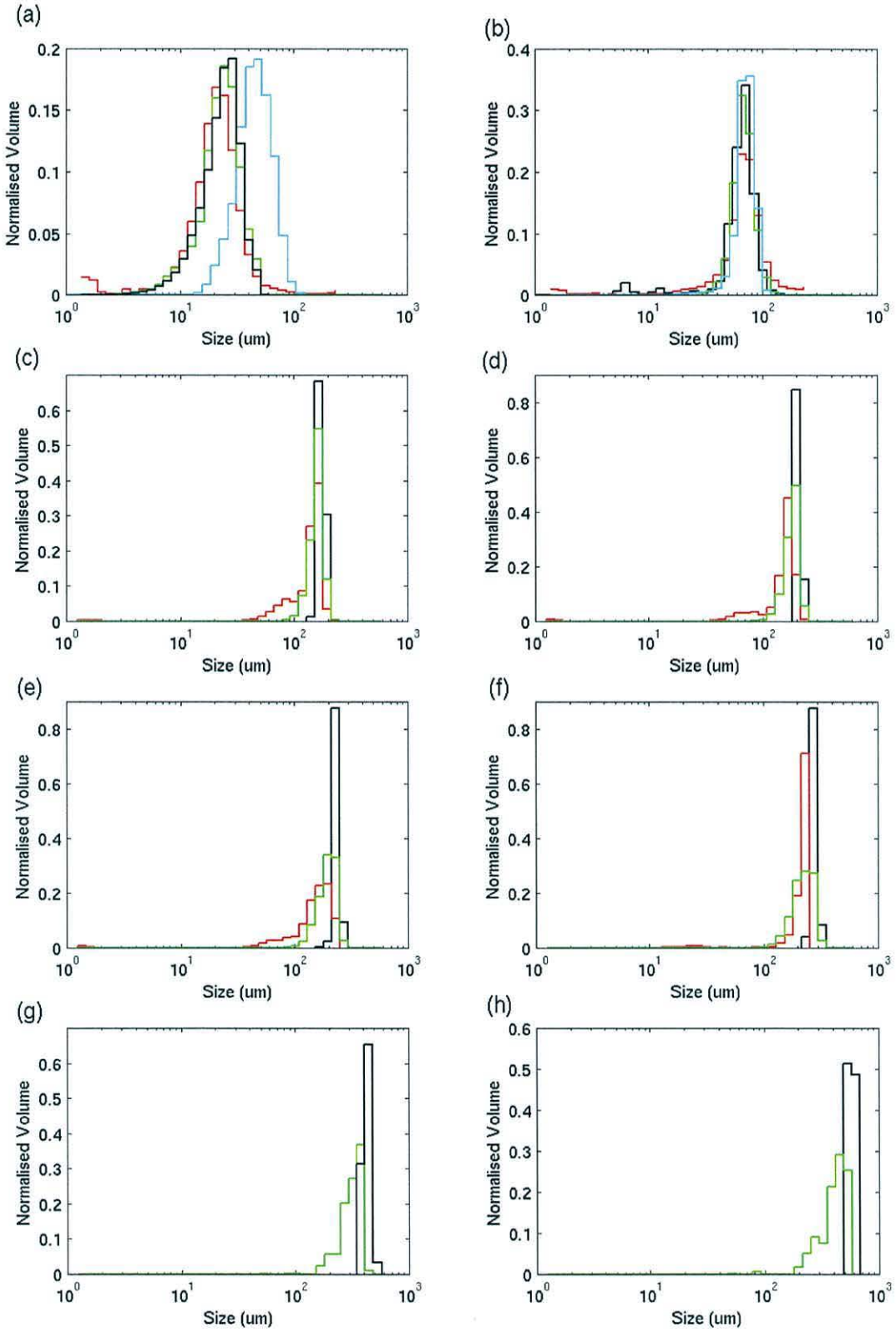

Figure 4.4. Average size distributions of calibration particles measured by LISST (——), Galai (——), Lasentec (——) and Coulter Counter / microscopy (——). (a) 1 - 35 μm, (b) 10 - 95 μm, (c) 150 - 180 μm, (d) 180 - 212 μm, (e) 212 - 250 μm, (f) 250 - 300 μm, (g) 355 - 425 μm, (h) 500 - 600 μm.

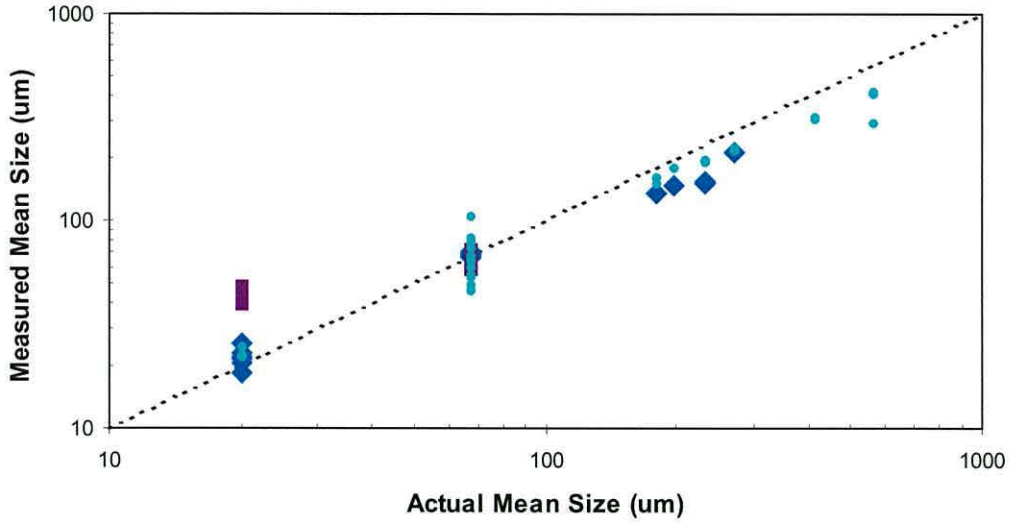

Figure 4.5. Mean sizes as measured by LISST (◆), Lasentec (■) and Galai (●) compared the Coulter Counter and microscopy results.
A 1 to 1 relationship is also shown (----).

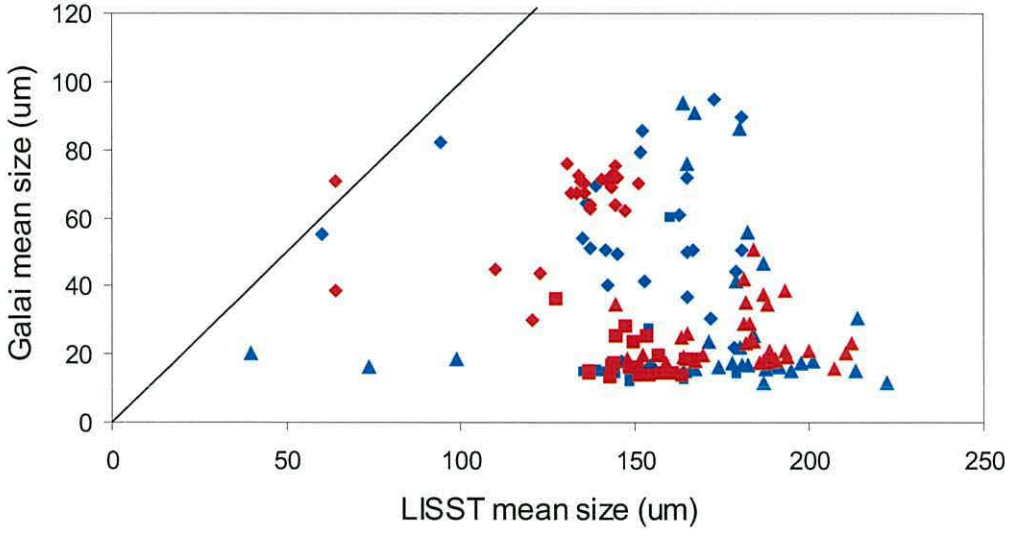

Figure 4.6. Mean sizes from LISST and Galai (Field results before re-normalisation of LISST).◆Surface (SNS2),■ surface (SNS3), ▲surface (CLY3), ◆near-bed (SNS2),■ near-bed (SNS3),▲near-bed (CLY3), (——) LISST = Galai.

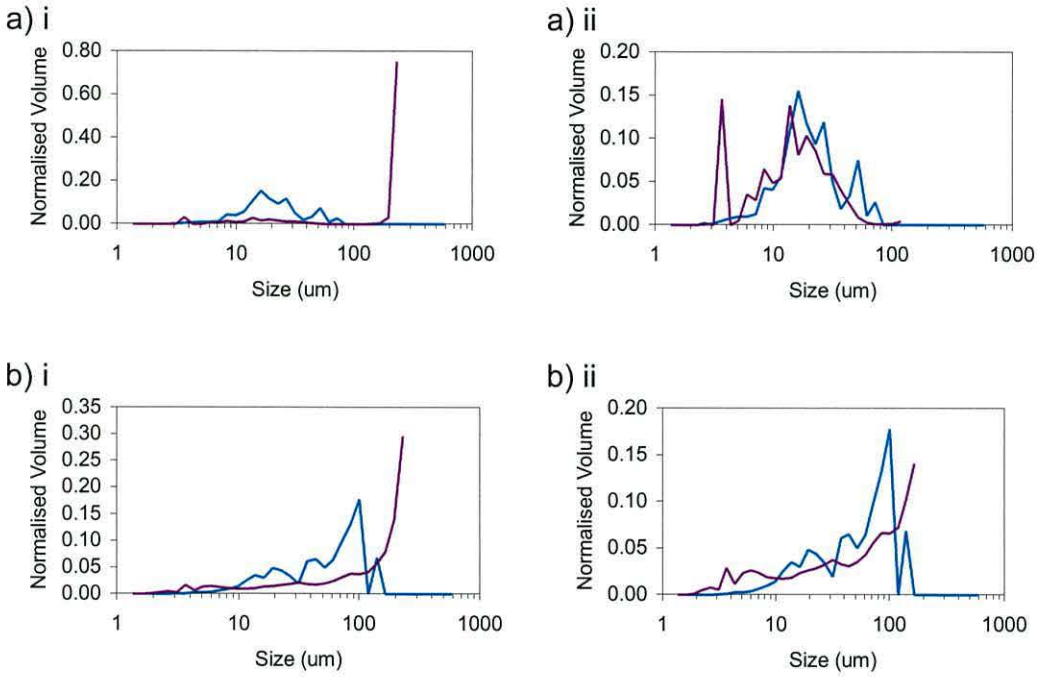

Figure 4.7. Size distributions from LISST (——) and Galai (——).
(a) CLY1: Cast 33 near-bed sample (i) All 32 LISST size classes,
(ii) LISST data corrected by ignoring median sizes > 118.67 μm,
(b) SNS2: Cast 14 near-bed sample (i) All 32 LISST size classes,
(ii) LISST data corrected by ignoring median sizes > 165.25 μm.

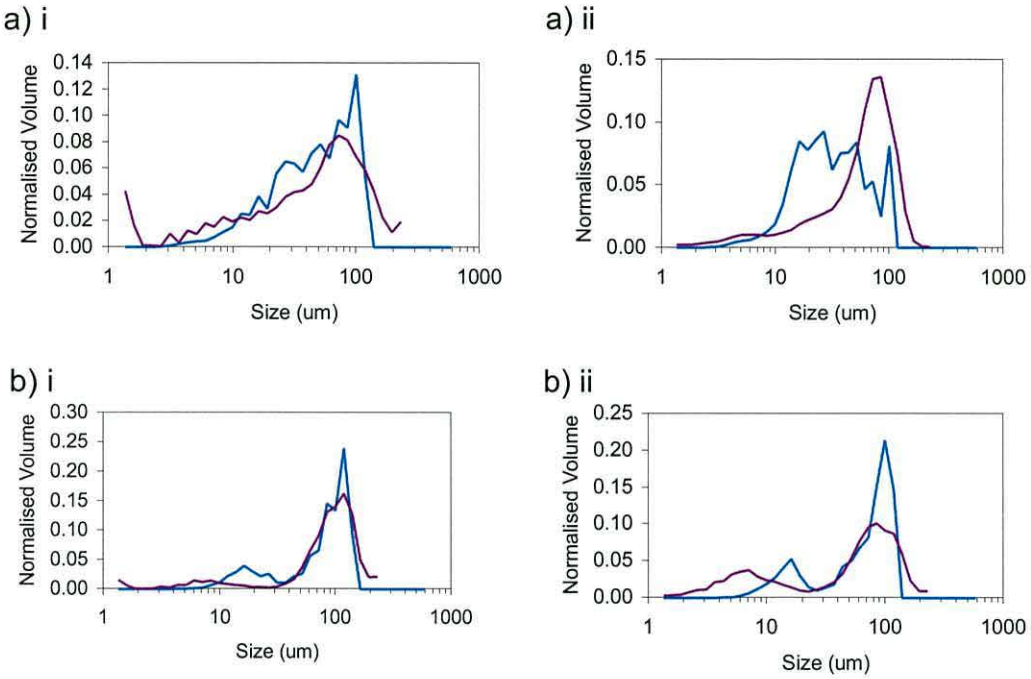

Figure 4.8. Size distributions from LISST (——) and Galai (——).
(a) SNS2, cast 19 (i) near-surface, (ii) near-bed.
(b) SNS2, cast 147 (i) near-surface, (ii) near-bed.

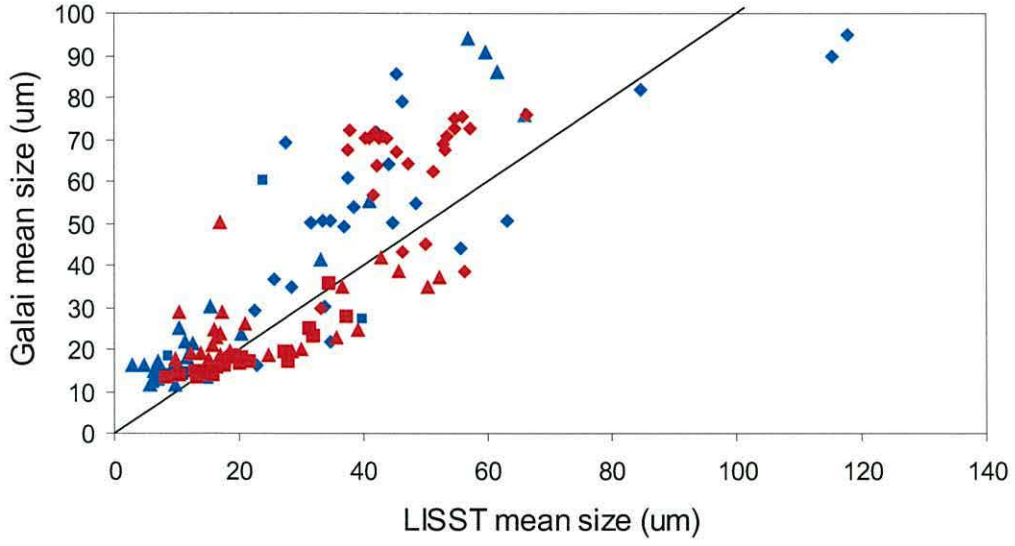

Figure 4.9. Mean sizes from LISST and Galai (Field results after re-normalisation of LISST).◆Surface (SNS2),■ surface (SNS3), ▲surface (CLY1), ◆near-bed (SNS2),■ near-bed (SNS3),▲near-bed (CLY1), (——) LISST = Galai.

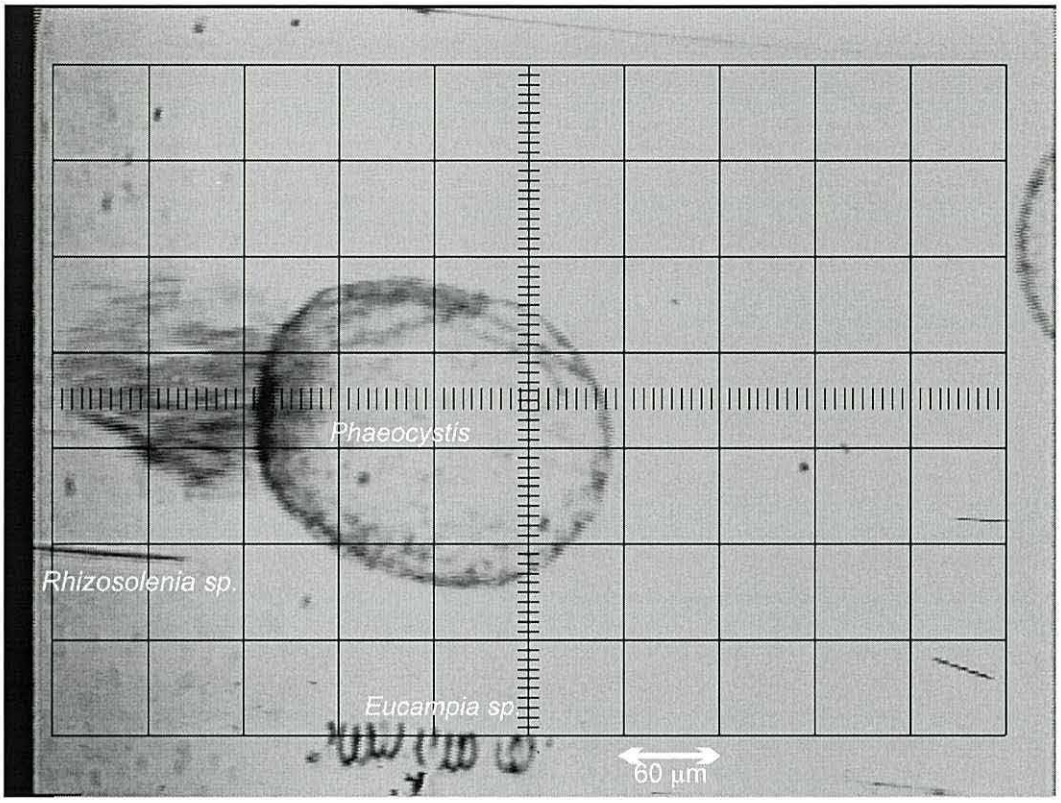

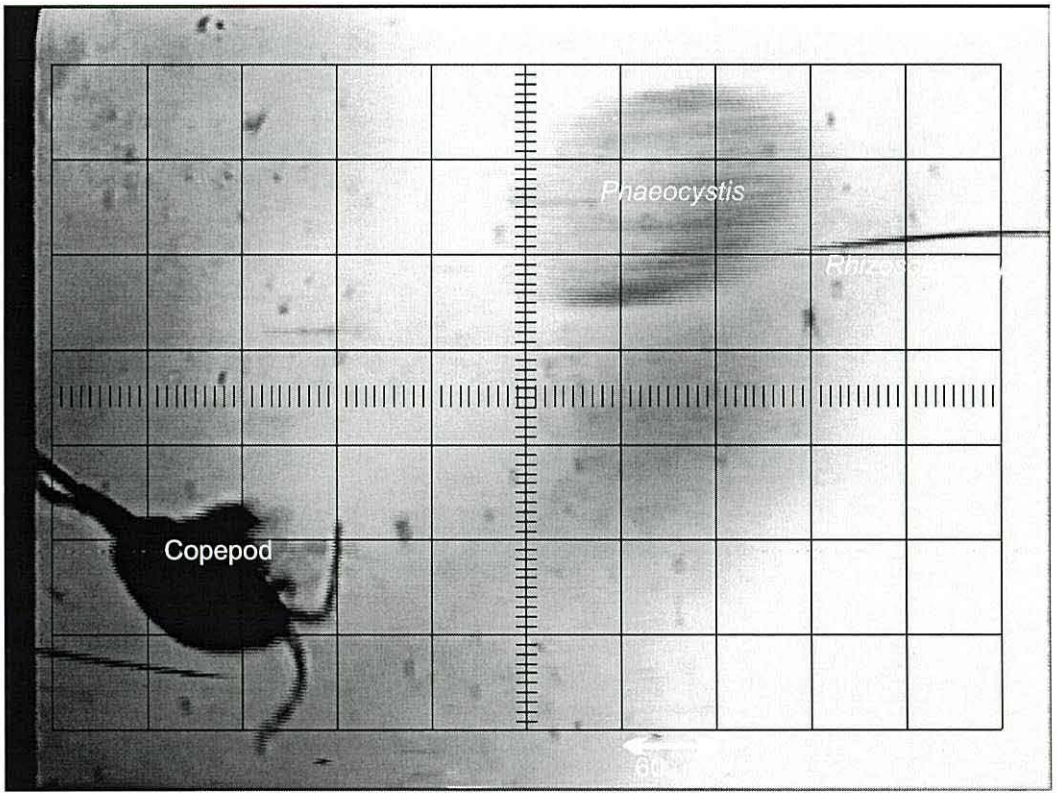

Figure 4.10. Typical Galai video microscope images.

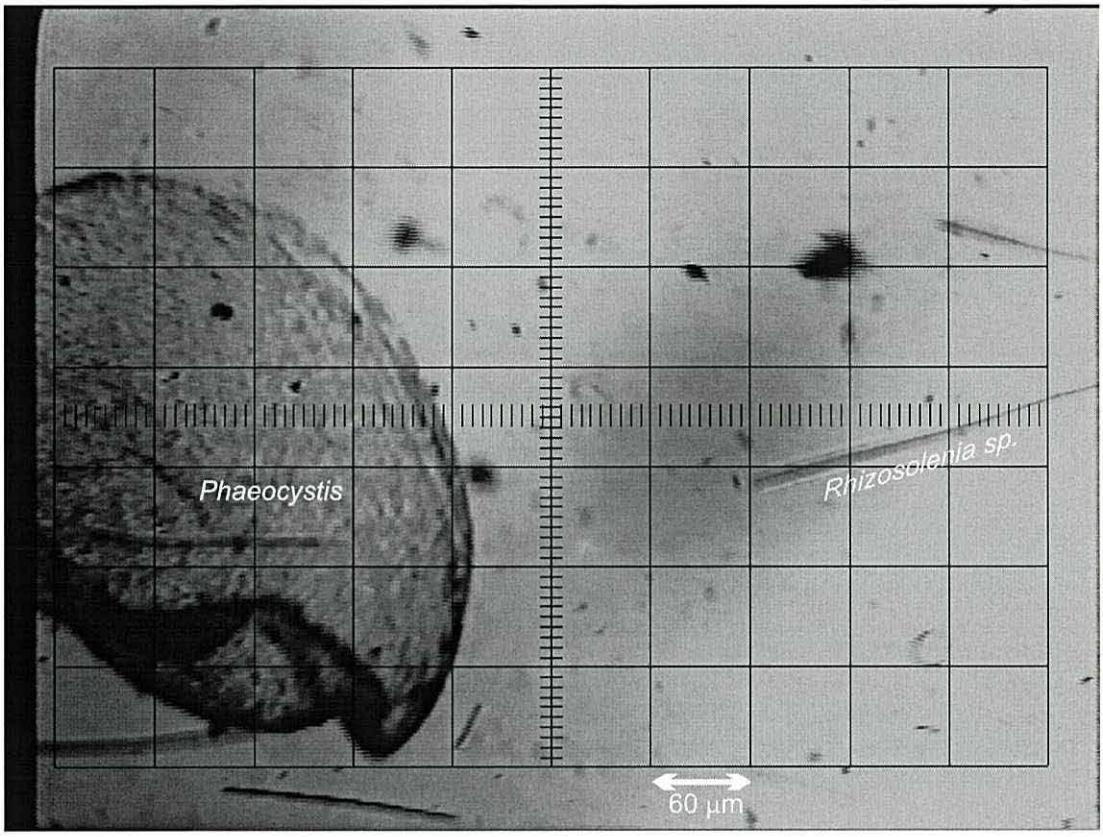

Figure 4.10. (Cont.) Typical Galai video microscope images.

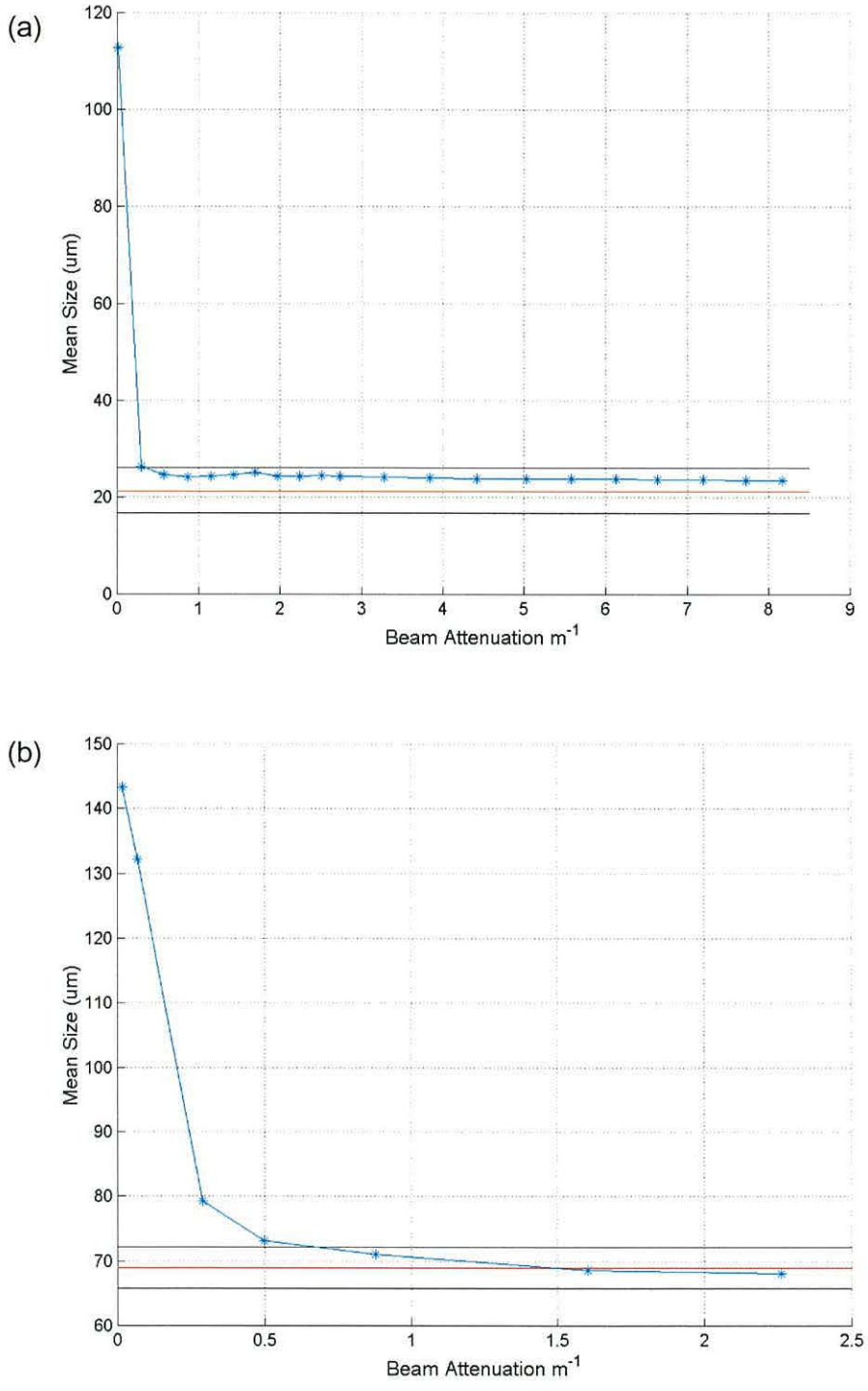

Figure 4.11. Mean size measured by LISST with increasing percentage transmission. (a) 1 to 35 µm, (b) 10 to 95 µm. (——) mean size of the particles, (——) +/- 2 standard deviations, (—*—) mean size measured by the LISST with changing beam attenuation.

Chapter 5

Northern North Sea

5.1. Introduction to the Study Site

Measurements were made during autumn 1998 at a low energy site in the northern North Sea (59° 20' N; 1°E) where the water depth was approximately 110 m (Figure 5.1). The position of the site minimised the significance of horizontal gradients, topography and fronts and was located away from coasts and the Norwegian Trench (Howarth *et al.*, 2002). It also avoided the main circulation paths in the region which follow the 100m isobath and the shelf edge or are associated with the Norwegian Trench and the Norwegian Coastal Current (Howarth *et al.*, 2002). This site is located at the southerly extreme of the northern North Sea as defined by Otto *et al.* (1990) (Figure 5.1).

Figure 5.1 shows the dominant circulation pattern in the northern North Sea and the major inflow of water into the region, the Orkney-Shetland inflow. The water circulation in this area is strongly influenced by wind stress which can result in current velocities of up to 40 cm s^{-1} (Eisma, 1990).

Suspended matter in the North Sea has a number of sources; the Atlantic, the English Channel, seafloor erosion, the Norwegian Channel and rivers, with the first three being the most important (Eisma, 1990). The fate of suspended sediment entering the North Sea has been observed and modelled, the direction of transport following the general residual water circulation (Eisma, 1990). Using Sellafield discharge, Prandle (1984) showed, by tracing Sellafield discharge, that after introduction through the Orkney-Shetland channel the spread of particles is south-westerly. This was confirmed by Kautsky (1987) through observations of the radioactive components in the sediment, as well as by the numerical model data calculated by Hainbucher *et al.* (1987).

In general, suspended matter in the North Sea is dispersed by mixing of high salinity water from the North Atlantic and the Channel with low salinity water

from the Baltic and freshwater from the land (Eisma, 1990). Transport is restricted by the formation of separate water masses of differing densities and the development of fronts between them, resulting in a concentration of material near-shore (Eisma, 1990).

The northern North Sea can be divided into four distinct hydrographic regimes according to the vertical structure of the water column (Figure 5.1). The study site for this project is located between regions B and C. During summer the water column in region B is both haline and thermally stratified, becoming vertically well-mixed during the winter months. In contrast the water column in region C has a permanent pycnocline, with thermal stratification in the summer months (Otto *et al.*, 1990). Lee (1980) also split the North Sea into hydrodynamically distinct regions with the present study site again located between two regions, with North Atlantic water occupying all or part of the region (depending on season) to the west whereas to the east it only occupies the deeper layers of the water column.

5.2. Observation Programme

Observations were made from the *RRS Challenger* (cruise CH140) over the period from 26/10/98 (day number 299) to 6/11/98 (day number 310). LISST, CTD and transmissometer (see Chapter 3) data were collected and the periods of particle size data collection are listed in Table 5.1.

Prior to cruise CH140, CTD and transmissometer measurements were made from *RV Dana* starting on 14/10/98 (day number 287) (Chapter 3, Table 3.1). A moored upward looking broadband ADCP was also deployed at the site (Chapter 3). Meteorological data (wind speed and direction) and wave data were also made available from a Marine Weather Station located on the Frigg oil platform (Figure 1.1). This data was collected and supplied by the Norwegian Meteorological Institute.

	Date/Time *Decimal Day*	Number of Samples
Period 1	26/10/98 (12:13) – 27/10/98 (02:52) *299.51 – 300.12*	10
Period 2	28/10/98 (15:26) – 28/19/98 (21:42) *301.64 – 301.90*	5
Period 3	1/11/98 (17:27) – 2/11/98 (03:07) *305.73 – 306.13*	9
Period 4	2/11/98 (18:35) – 6/11/98 (18:26) *306.77 – 310.77*	9

Table 5.1 Times when LISST and CTD data were collected in the northern North Sea during CH140.

The LISST was mounted horizontally to the CTD frame and was configured to start sampling at a measured depth of c. 2 m, turning on to check the depth every 20 seconds until a depth of 2 m or greater was measured. The frame was lowered to a depth of approximately 10 m where it was left for a few minutes before being brought back to just below the surface. In some instances this caused the LISST to turn itself off again before the cast resulting in some casts having no surface LISST data. The CTD frame was then lowered continuously at 0.5 to 1 m s^{-1} to the closest comfortable proximity to the sea floor. The upcast was done in stages between bottle firing depths.

Water samples were taken for gravimetric analysis and subsequent gravimetric calibration of the transmissometer (Section 3.3.2). Due to the low concentrations experienced 5 litres of water sample were filtered through each GF-C filter before rinsing with approximately 150 ml of distilled water.

5.3. Data Processing

Due to the low concentrations measured and the presence of large particles the LISST data was quite noisy. To despike the data a running mean of beam attenuation over 16 LISST scans (i.e. over a 4 second period which is equivalent to approximately 2 to 4 m in the vertical) was calculated. Any points in the raw data with values outside two standard deviations either side of this

mean were flagged as spikes and removed. Any obvious spikes which were not automatically removed by this method were removed manually afterwards.

The de-spiked LISST data was then averaged over half meter depth bins resulting in two data points per meter. Half meter depth bins were chosen to ensure that a minimum of three scans were used to produce one averaged data point while retaining good spatial resolution.

5.4. Results

5.4.1. Meteorological Data

Throughout the study period a series of storms tracked across the site with maximum wind speeds in excess of 15 m s^{-1} (Figure 5.2), resulting in waves with periods of 4 to 7.5 seconds and heights between 2 m and 5 m (Figure 5.3). These high energy events were interspersed between calmer periods, however, wind speeds were in excess of 10 m s^{-1} with wave periods greater than 5 seconds, and wave heights greater than 3 m for most of the sampling period.

5.4.2. ADCP

A spring tide was experienced just prior to the sampling period with sampling occurring during the transition from springs to neaps and the main sampling occurring during neap tide. Figure 5.4 shows the total current speed measured by the ADCP. A spring tide was experienced from the beginning of the record until day 300. During this period maximum speeds alternated between above and below the thermocline on a 5 day cycle. The total current is the sum of the tidal currents, which had a 12.5 hour period, and the inertial currents which had a 14 hour period and were 180° out of phase around the thermocline (Knight *et al.*, 2002). This cycle becomes less evident after day 300 when the tidal current is reduced due to it being a neap tide. Inertial currents are produced in response to wind forcing over a relatively thin surface layer above a sharp

thermocline. The wind forcing must not last for more than half of the inertial period (2π/coriolis parameter).

5.4.3. Turbulence

Figure 5.5 shows a tidally averaged profile of turbulent dissipation rate measured by the FLY at the study site, centred on day 299.3. Turbulence clearly decreased within the thermocline region with the minimum turbulence associated with the base of the thermocline. The maximum turbulence was measured at the bed, a result of the friction caused by the sea bed.

5.4.4. Temperature

The water column at the survey site was well stratified into two layers with a thermocline region fluctuating between 60 m and 40 m above the bed although there was a general deepening of the thermocline during the survey period (Figure 5.6). Throughout the study period water above the thermocline decreased in temperature gradually from c. 11 ^{o}C to c. 9 ^{o}C whilst below the thermocline temperature remained constant at approximately 7 ^{o}C.

5.4.5. Salinity

A halocline region occurred over c. 10 m of the water column between 60 m and 40 m above the bed and with fluctuations in depth mirroring those seen in the thermocline positioning (Figure 5.7). The salinity below the halocline remained constant throughout at ~35.2 with only minor fluctuations (maximum of 0.2) occurring above the halocline (Figure 5.7).

5.4.6. Suspended Particulate Matter Concentration

A linear regression analysis was performed using the beam attenuation measured by the transmissometer and gravimetric concentrations (minus the blanks as described in Chapter 3) measured during the study period (Figure 5.9) which produced a regression of

Equation 5.1 SPM (mg l^{-1}) = 2.5467(beam attenuation) – 0.6996,

with r^2 equal to 0.326 and a p-value of 1.34×10^{-12}. Therefore this regression equation explains a low but statistically significant part of the observed variation in beam attenuation.

Figure 5.10 shows the SPM concentration in mg l^{-1} converted from beam attenuation using Equation 5.1 and combines data from the *Dana* (days 289 – 298) and *Challenger* cruises (days 299 – 311). In general a two layer structure was present with the SPM concentration less in the surface waters compared to the bottom waters. Periodic increases in the gravimetric concentration occurred near-bed between day 294 and 298 as well as an increase throughout the water column below the thermocline on day 302. A concentration minimum is evident in the transmissometer data between 60 m and 40 m above the bed, which is within the thermocline region, throughout the measurement period, becoming less well defined from day 299.

In contrast, the total volume concentration measured by the LISST for the period from day 299 does not show a decrease in concentration at the thermocline but an increase (Figure 5.11 & Figures 5.14i – 5.18i) with total volume concentration above the thermocline approximately 7 - 9 µl l^{-1} and below the thermocline approximately 12 - 14 µl l^{-1}. Individual profiles of the total volumetric concentration show this two layer structure but also show "spikes" in volume concentration in the transition between the surface and bottom waters (Figure 5.14i, Figure 5.15i, Figure 5.16i, Figure 5.17i and Figure 5.18i). These profiles also indicate that the greatest volumetric concentration is present within and at the base of the thermocline, decreasing towards the bed. The marked increase observed in gravimetric concentration on day 302 was not apparent in the total volumetric concentration measured by the LISST (Figure 5.11).

5.4.7. Particle Size

In-situ particle size distributions were measured using the LISST from day 299 (26/10/98) until day 310 (7/11/98). Figure 5.12 shows the size distributions near the surface, within the thermocline and near the bed measured by the LISST for five representative casts, two from the first sampling period and one from each subsequent sampling period. These sampling periods are listed in Table 5.1. In most cases a tri-modal size distribution prevailed throughout the water column with peaks occurring in the 3.11μm - 3.67 μm and 16.27 μm - 19.20 μm size classes (Figure 5.12). The smallest mode in the size distribution (3.11 μm – 3.67 μm) was observed in every distribution. A similar mode was also observed by Gartner *et al.* (2001) who suggested that it may be a result of the Fraunhofer diffraction technique beginning to loose application. It is also possible that the background scattering value used was incorrect in this size class. Although an exact cause of this mode is not known it can be concluded that it should be treated with caution.

The size class of the largest mode is unknown as it is greater than 250 μm, the upper limit of the LISST. The presence of this mode is indicated by large increases seen in all the size distributions at the upper limit of the size distribution (Figure 5.12). The actual values in this size class generally range between 5 and 10 $\mu l\ l^{-1}$ and therefore could not easily be plotted on the graphs if the rest of the distribution was to be seen.

The individual distributions all indicate a large volume of particles present that are greater than 250 μm. As discussed in Chapter 4 this leads to distortion of the measured volume concentrations of the larger size classes and therefore caution must be exercised when interpreting these data.

As the individual size distributions show, the distributions are dominated by large particles which greatly effect the mean size. Figure 5.13 shows the mean size measured by the LISST over the whole sampling period. It is likely that the mean size calculated here is an underestimate for the overall population as it is restricted by the measuring limits of the LISST. However, relative variation in

apparent mean size can still be interpreted in terms of variation in mean size of the population. During the whole sampling period the apparent mean particle size became smaller in the surface waters, decreasing from c. 205 μm to c. 165 μm, and to a lesser extent below the thermocline where the decrease was from c. 205 μm to c. 177 μm. Also, an increase in mean particle size is seen between 40 m and 60 m above the bed, coinciding with the thermocline region and decrease in mass concentration.

During the first sampling period (day 299) the mean size of particles in the surface waters remains constant at 200 μm to c. 50 m above the bed where the size increased to c. 210 μm. Figure 5.14ii is a typical profile from this period and clearly shows that this increase in mean particle size occurs rapidly and at the top of the thermocline. The mean size then gradually decreases towards the bed becoming similar to that at the surface (Figure 5.13 and Figure 5.14).

By the second sampling period (Figure 5.15) both the surface and near-bed mean particle size decreased to c. 180 μm. However, the increase in mean size at the thermocline that was observed during period 1 had become more pronounced, increasing by at least 20 μm (Figure 5.15ii). Through the thermocline and down towards the bed mean particle size decreases to c. 180 μm (Figure 5.13 and Figure 5.15ii).

After the storm that occurred between days 300 and 305 (Figure 5.2) the mean sizes both at the surface and near-bed are similar to those at the end of sampling period 2 (Figure 5.13). The increase in mean size occurring at the thermocline was also still present with the mean size increasing by c. 25 μm (Figure 5.16). As with all the mean size profiles throughout the whole sampling period large spikes occurred within the thermocline region.

For the remainder of the sampling period the near-bed mean size remained constant at approximately 180 μm. However above the thermocline the mean size continued to decrease (Figure 5.13). As the mean size above the thermocline continued to decrease the maximum in mean particle size occurring

at the top of the thermocline continued to prevail with a maximum size of c. 200 μm, similar to that observed throughout the whole sampling period (Figure 5.17ii). By day 309 when both wind and wave activity had increased again, (Figure 5.2 and Figure 5.3) the increase observed at the thermocline diminishes with maximum mean sizes of c. 185 μm (Figure 5.18ii). There is also a less marked decrease in the mean size of particles near the bed at this time (Figure 5.18ii).

As Figure 5.14 to 5.18 clearly illustrate, the increase in mean particle size observed at the top of the thermocline coincides with a rapid increase in total volume concentration which then remains constant at this maximum value to the bed. To investigate why the mean size was varying the distribution was split into those of size greater than 78.45 μm (PGT) and particles less than 78.45 μm (PLT). 78.45 μm was chosen as the size to divide the distribution at because this is where the distributions show an obvious split between the smaller particles and the larger particles (Figure 5.12). Volume concentration profiles of these fine and coarse sub-populations are presented in Figure 5.14 – 5.18.

At the end of day 299 the total volume distribution was dominated by PGT with approximately 6 times more volume of large particles compared with small particles in the surface (Figure 5.14). Between 40 m and 60 m above the bed this domination increased to 10 times more PGT than PLT, coinciding with the increase seen in mean size and total volume concentration. As the mean size decreased below this maximum the volume concentration of PGT decreased but the volume concentration of PLT increased.

By day 301 the total volume concentration had increased in both the surface and near-bed regions. This increase was due to an increase in the volume concentration of PLT, the volume concentration of PGT had remained constant (Figure 5.15). In the thermocline region the volume concentration of the PLT did still decrease with an increase in the PGT.

Just after the storm (Figure 5.16) no significant change in total volume concentration compared to before the storm was evident. The increase in mean size at the thermocline was slightly less pronounced than prior to the storm. However, the decrease in volume concentration of PLT seen in all the profiles prior to the storm was not present. The volume concentration of PGT did still increase at the thermocline and decrease below the thermocline as the volume concentration of PLT increased.

Towards the end of the sampling period (Figure 5.17 and 5.18) the decrease in volume concentration of PLT within the thermocline did return but was within a small, well defined region at the top of the thermocline region.

5.4.8. Dry Particle Density

Dry particle densities for the whole population (measured by the LISST) were calculated, using the method described in Chapter 3, in the surface, near-bed regions and combined surface and near-bed. As there was no thermocline gravimetric data it was not possible to perform these calculations for the particles in the thermocline. The results are shown in Table 5.2.

These results clearly indicate that there is no significant difference in the mean size, volumetric concentrations or the particle densities between the near-surface and near-bed measurements. There is however a small significant difference between the near-surface and near-bed gravimetric and volumetric concentrations.

For particles larger than 250 μm to be maintained in suspension in this relatively low energy environment they must have a low density, and therefore may not contribute significantly to the mass concentration measured by gravimetric analysis. If this were the case then mass concentration should be best correlated with volume concentration of finer particles only, rather than with total volume concentration. To test this hypothesis correlation analysis of mass concentration against volume concentration with larger size classes excluded was performed, but there was no improvement in the correlation coefficient.

	Average Depth (m)	Mean Size (μm)	Gravimetric Concentration ($g\ l^{-1}$)	Volumetric Concentration ($cm^3\ l^{-1}$)	Particle Density ($g\ cm^{-3}$)
Combined n = 39	48.85 ± 18.09	180.6 ± 3.39	$9.42 \times 10^{-4} \pm 1.74 \times 10^{-4}$	$0.991 \times 10^{-2} \pm 0.056 \times 10^{-2}$	$9.23 \times 10^{-2} \pm 1.42 \times 10^{-2}$
Surface n = 17	5.94 ±0.598	179.8 ± 5.00	$7.59 \times 10^{-4} \pm 1.80 \times 10^{-4}$	$0.815 \times 10^{-2} \pm 0.036 \times 10^{-2}$	$9.39 \times 10^{-2} \pm 2.50 \times 10^{-2}$
Near-bed n = 22	105.7 ± 4.285	181.3 ± 4.68	$11.1 \times 10^{-4} \pm 2.13 \times 10^{-4}$	$1.13 \times 10^{-2} \pm 0.045 \times 10^{-2}$	$9.11 \times 10^{-2} \pm 1.61 \times 10^{-2}$

Table 5.2. Dry particle densities for the whole particle distribution measured by the LISST in the surface and near-bed regions. ± is 95% confidence limit and n is the number of samples.

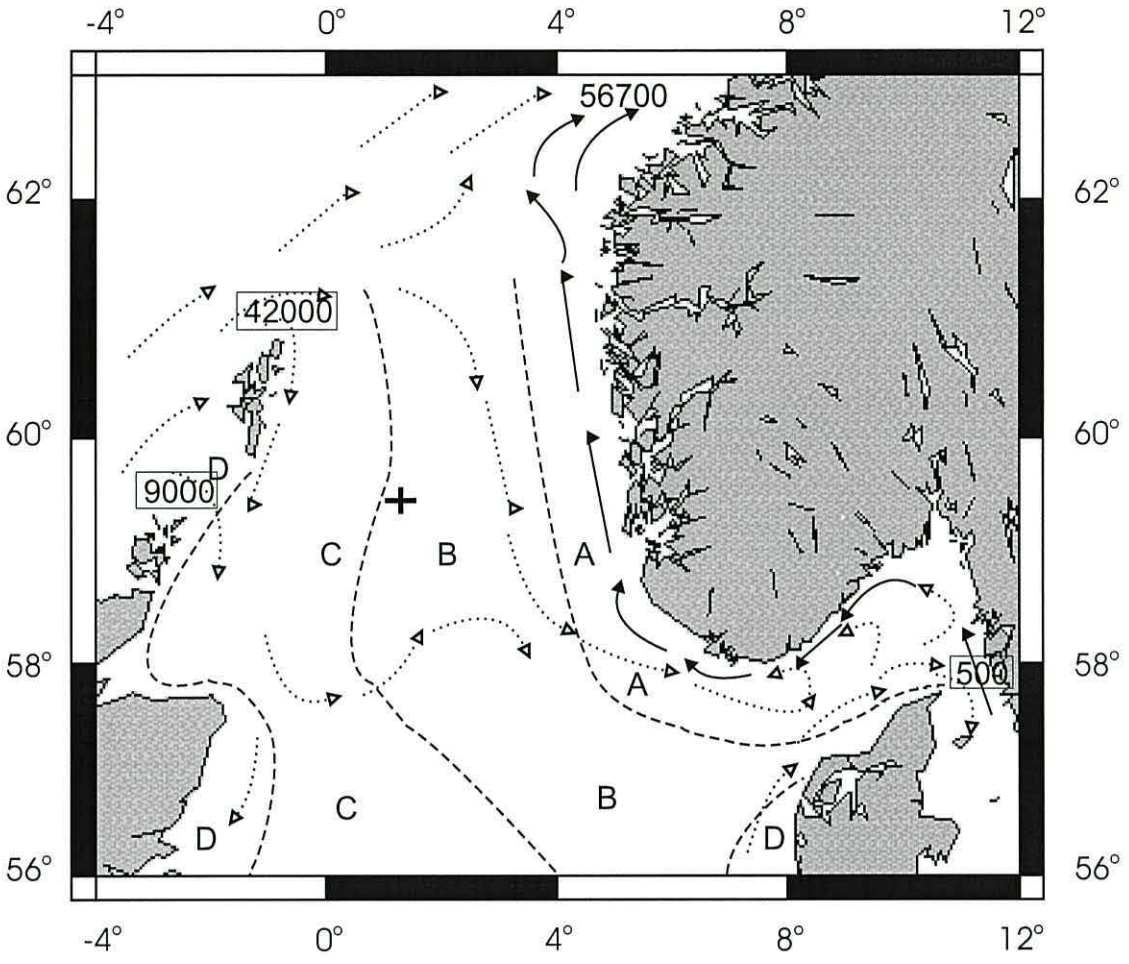

Figure 5.1. Site map of the area of study (+) in the northern North Sea illustrating the residual circulation pattern and sub-regions of the area.

⋯⋯▸ Atlantic / North Sea water, ⟶ Baltic / Norwegian coastal water.

▭ Inflow/outflow ($km^3 yr^{-1}$).

A) Whole year haline and thermally stratified. B) Haline and thermally stratified during the summer, vertically homogeneous during the winter. C) Whole year pycnocline, thermally stratified during the summer. D) Whole year vertically homogeneous. (Modified after Otto *et al.*, 1990 and Eisma, 1990).

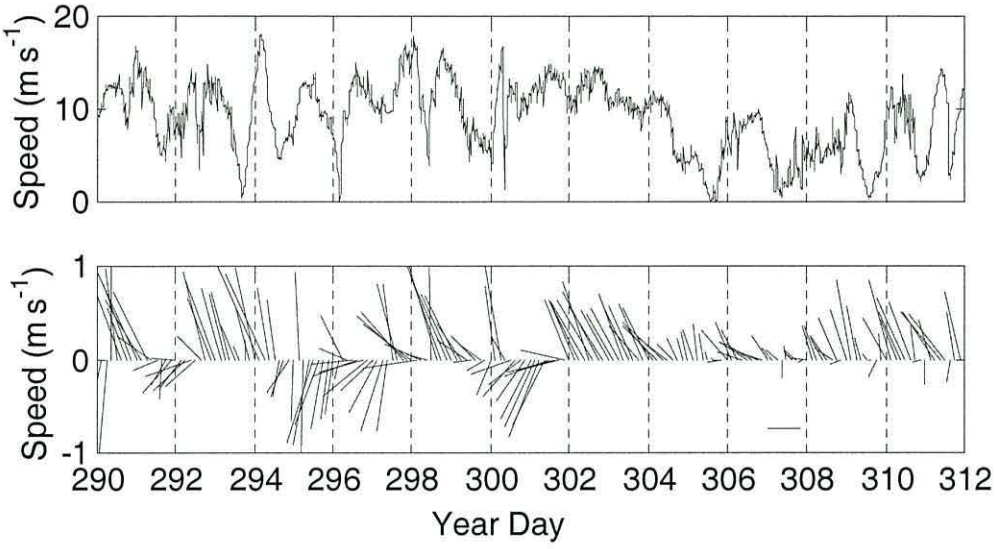

Figure 5.2. Wind speeds (a) and direction (b) at the northern North Sea site during the survey period.

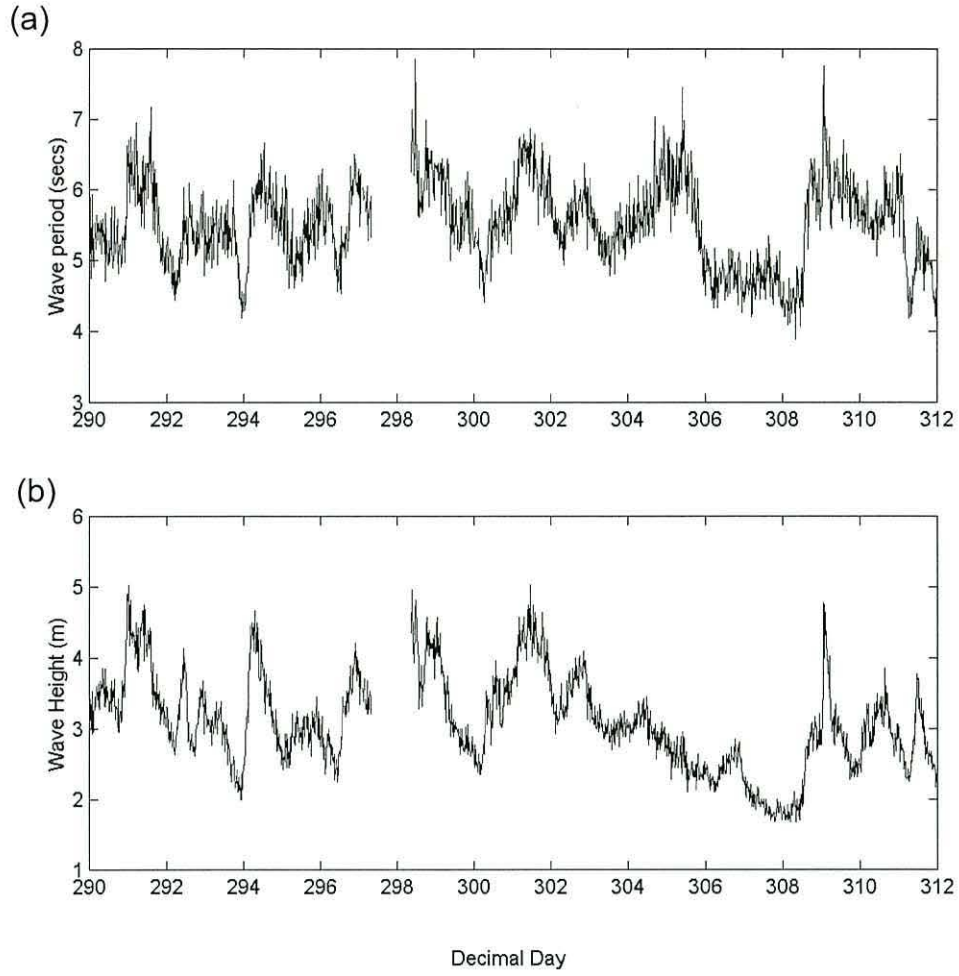

Figure 5.3. (a) Wave periods, and (b) wave heights at the study site during the survey period.

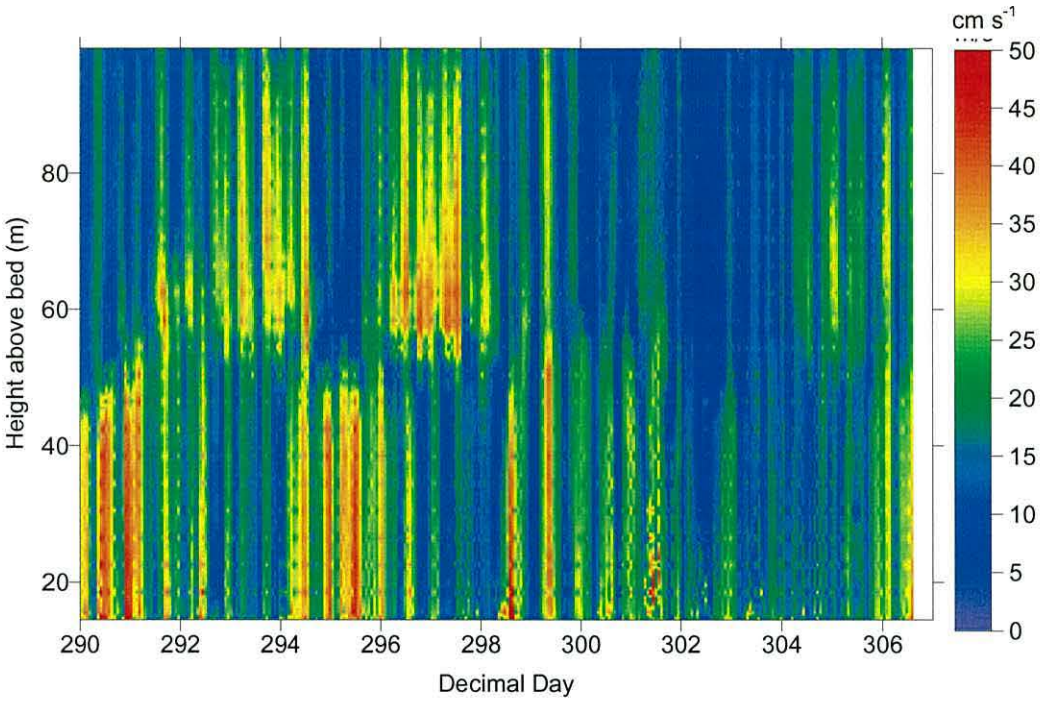

Figure 5.4. Current speed (cm s^{-1}) measured by a broadband ADCP.

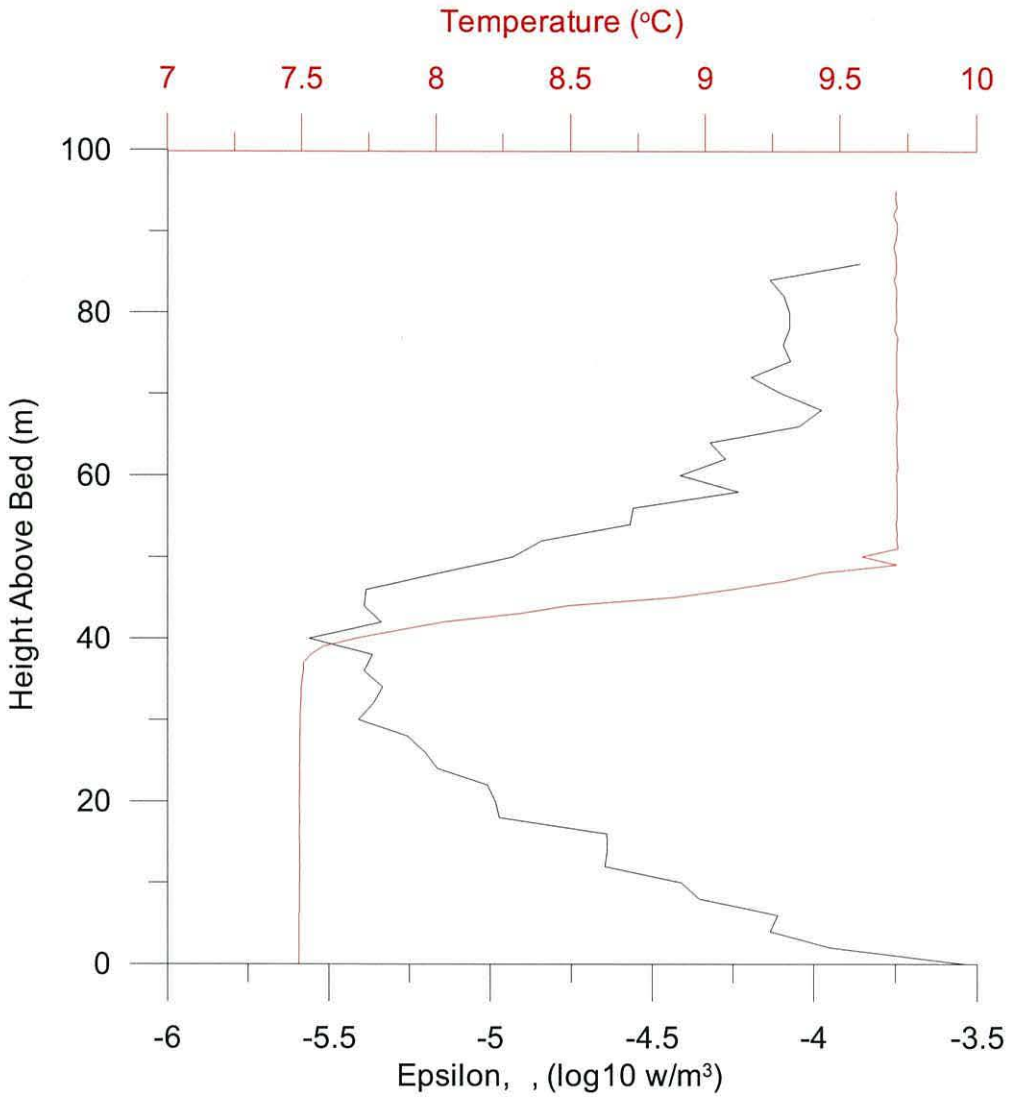

Figure 5.5. Turbulence profile measured by the FLY on day 299 (26/10/98 23:00).

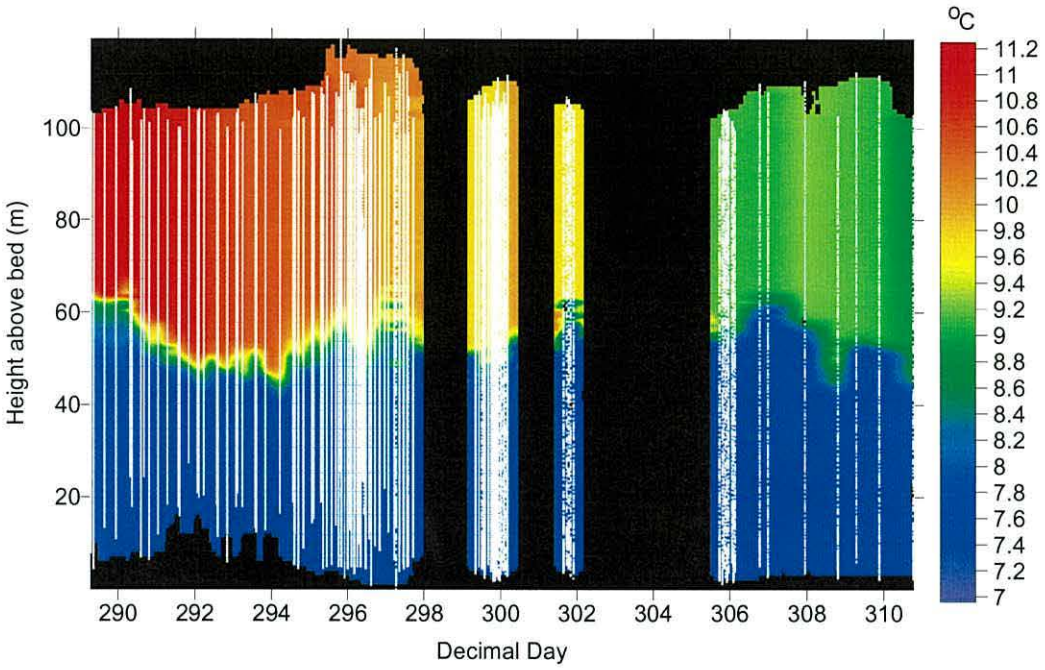

Figure 5.6. Temperature at the northern North Sea site. Day 290 is 17th October 1998.

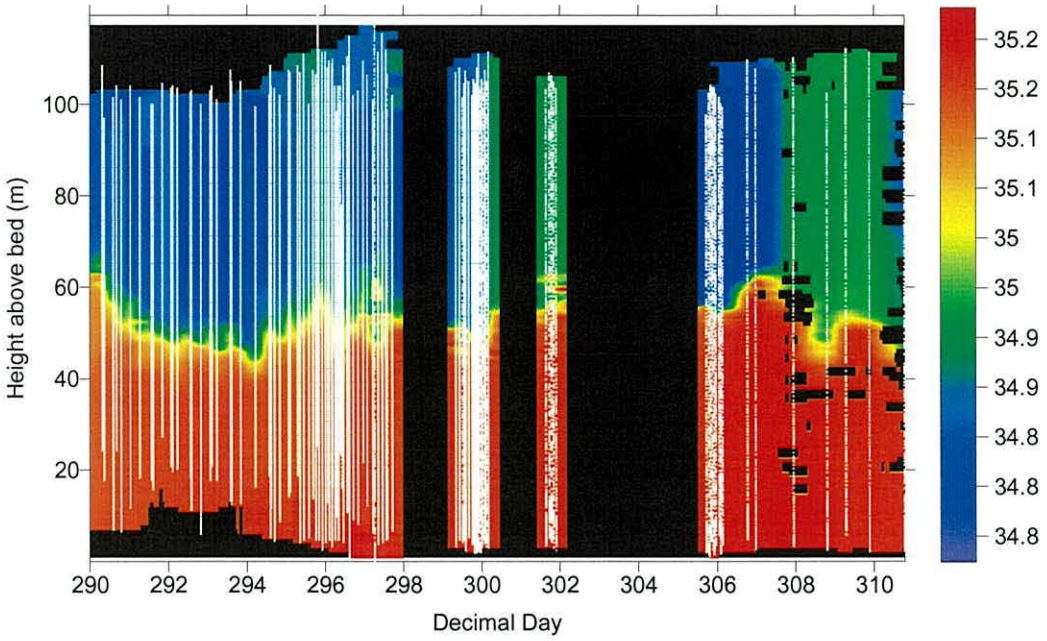

Figure 5.7. Salinity at the northern North Sea site. Day 290 is 17/10/1998.

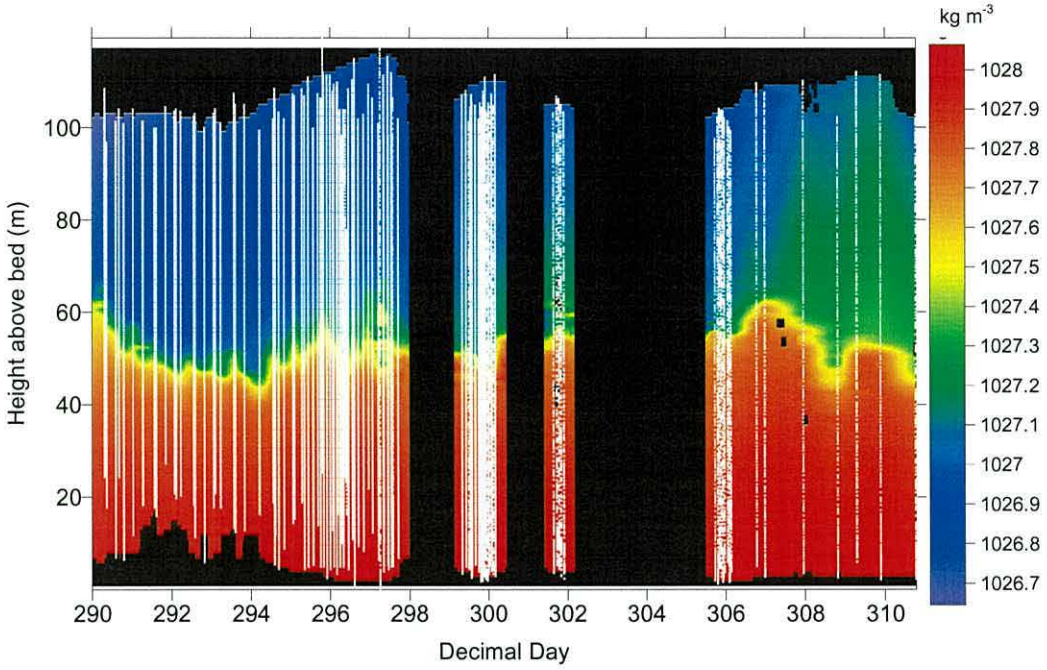

Figure 5.8. Density at the northern North Sea site. Day 290 is 17/10/1998.

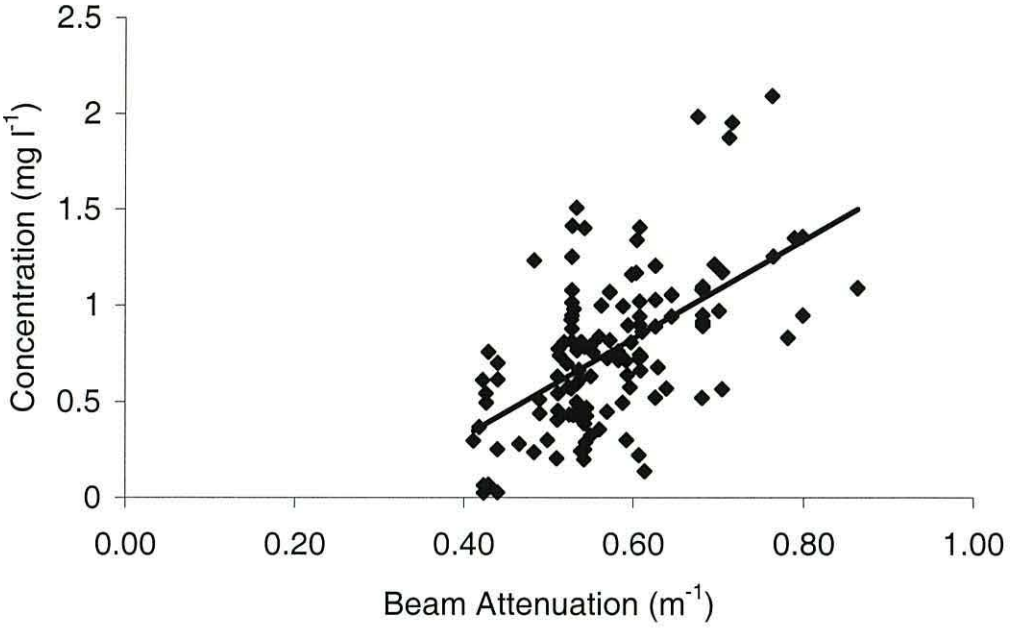

Figure 5.9. Linear regression plot of gravimetric concentration against beam attenuation. Observed values (♦), regression line (——).

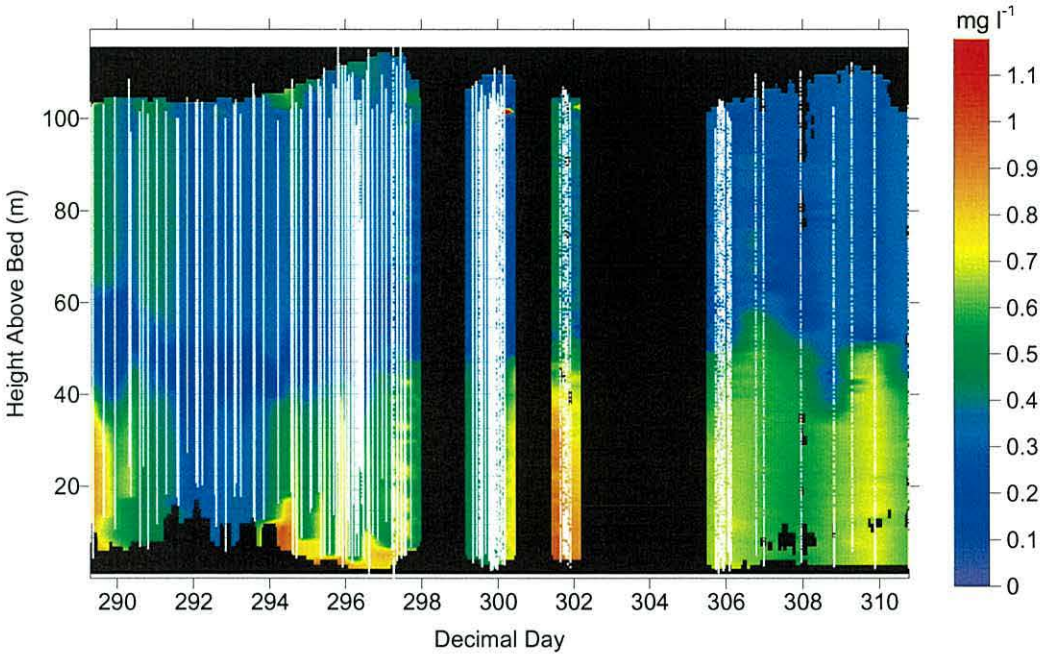

Figure 5.10.(a) SPM concentration at the northern North Sea site. Day 290 is 17/10/1998. White points indicate where the measurements were made.

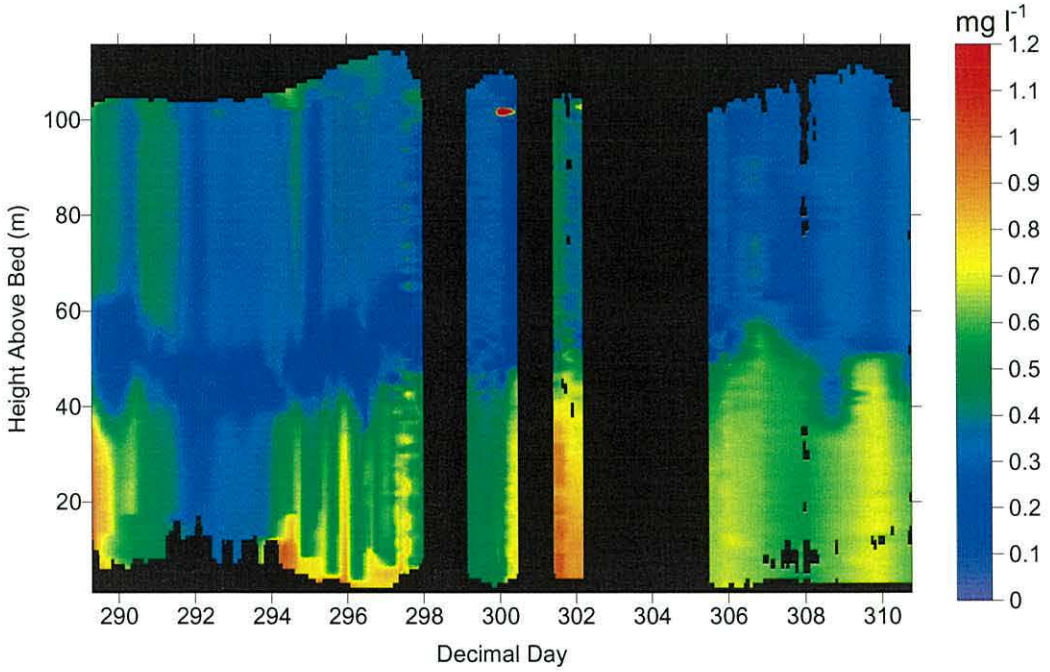

Figure 5.10.(b) SPM concentration at the northern North Sea site. Day 290 is 17/10/1998. Same as Figure 5.10a but without the measurement positions.

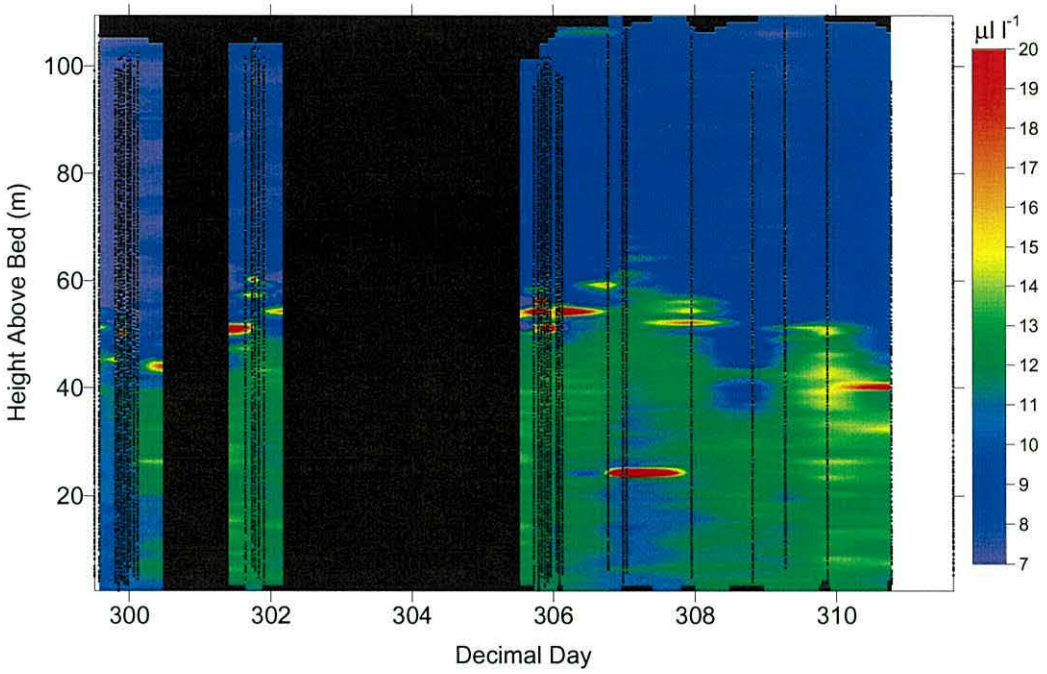

Figure 5.11. Total volume concentration (µl l^{-1}) measured by the LISST at the northern North Sea site. Day 299 is 26/10/1998.

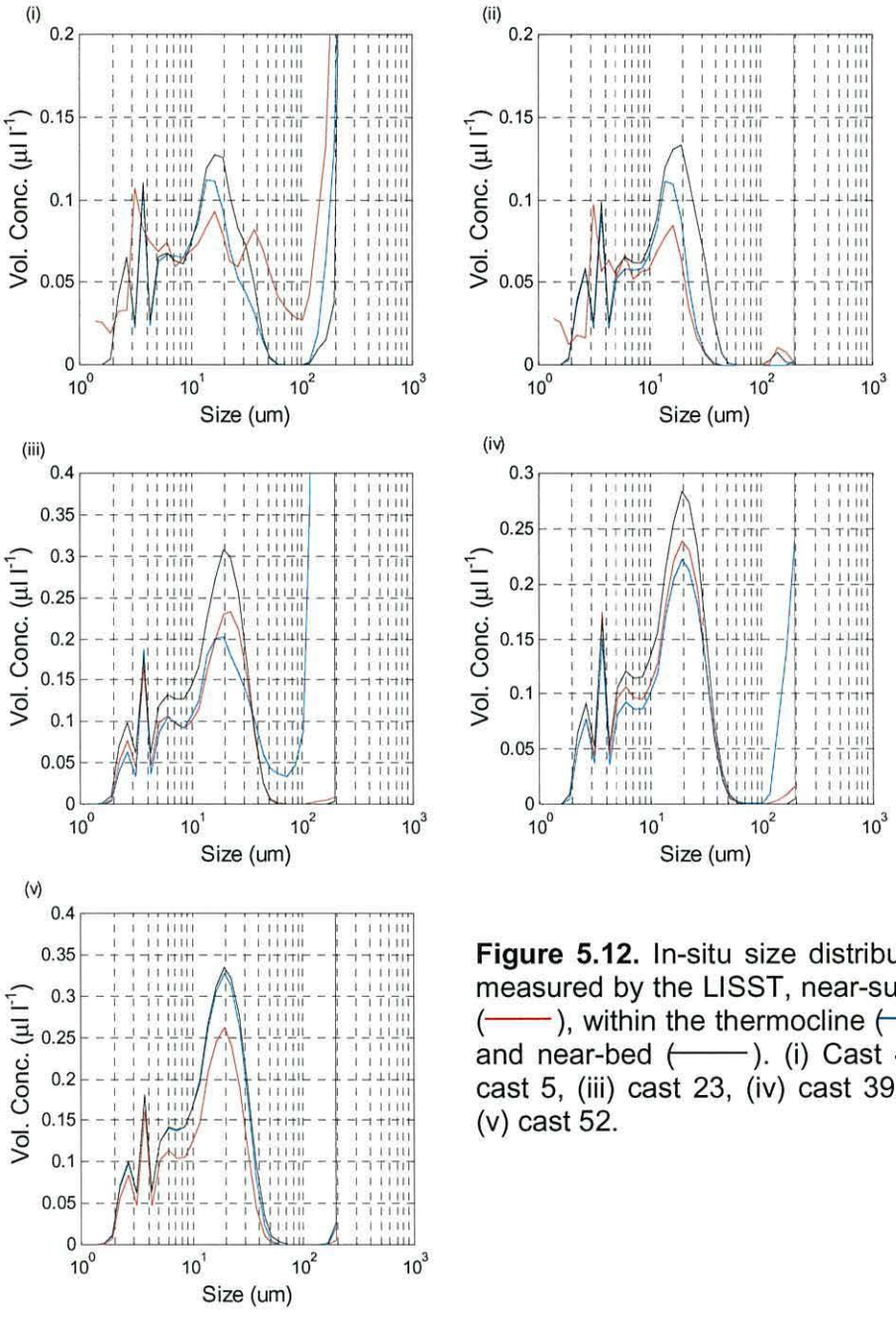

Figure 5.12. In-situ size distributions measured by the LISST, near-surface (——), within the thermocline (——), and near-bed (——). (i) Cast 4, (ii) cast 5, (iii) cast 23, (iv) cast 39, and (v) cast 52.

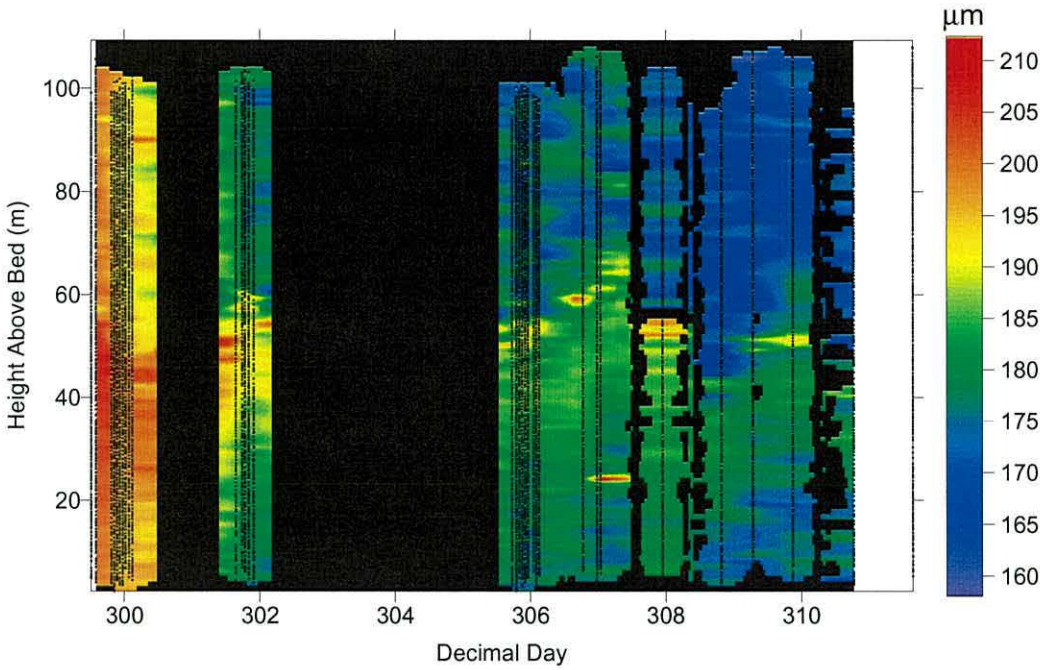

Figure 5.13. Mean particle size (µm) measured by the LISST at the northern North Sea site. Day 299 is 26/10/1998.

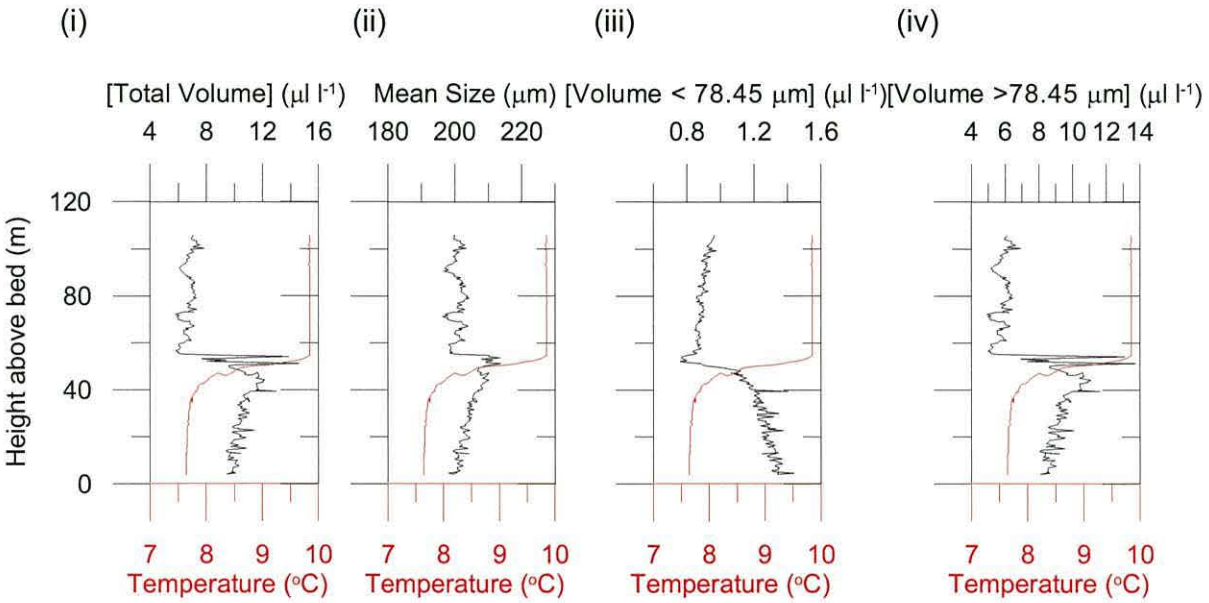

Figure 5.14. LISST profiles for day 299 (26/10/98 13:49). (i) Total volume concentration, (ii) mean size, (iii) volume concentration of particles less than 78.45 µm and (iv) volume concentration of particles greater than 78.45 µm.

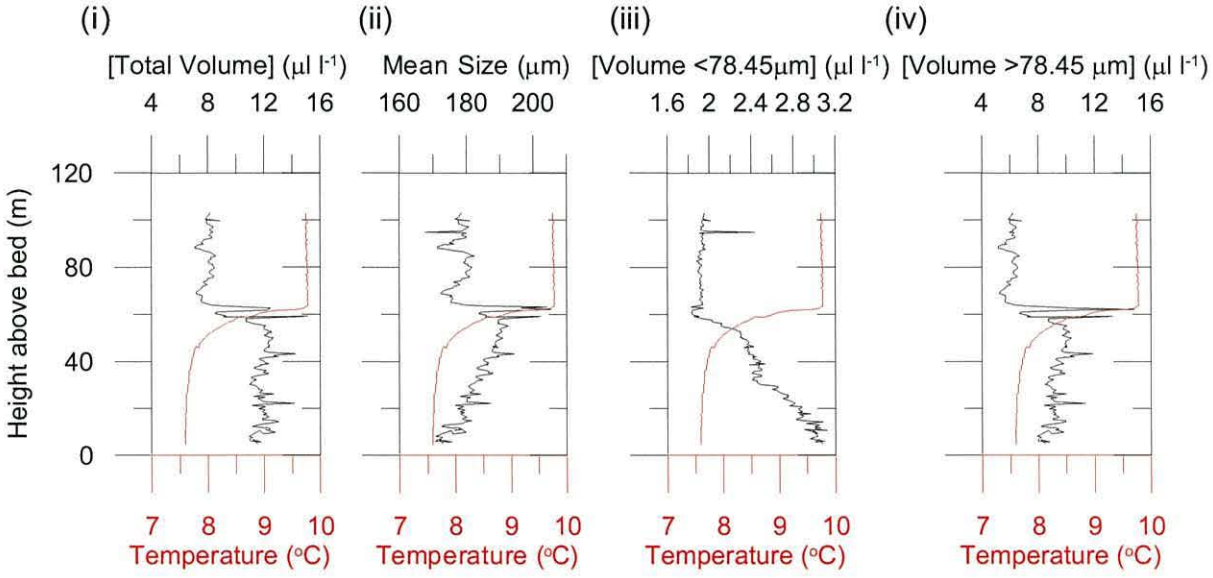

Figure 5.15. LISST profiles for day 301 (28/10/98 20:00). (i) Total volume concentration, (ii) mean size, (iii) volume concentration of particles less than 78.45 µm and (iv) volume concentration of particles greater than 78.45 µm.

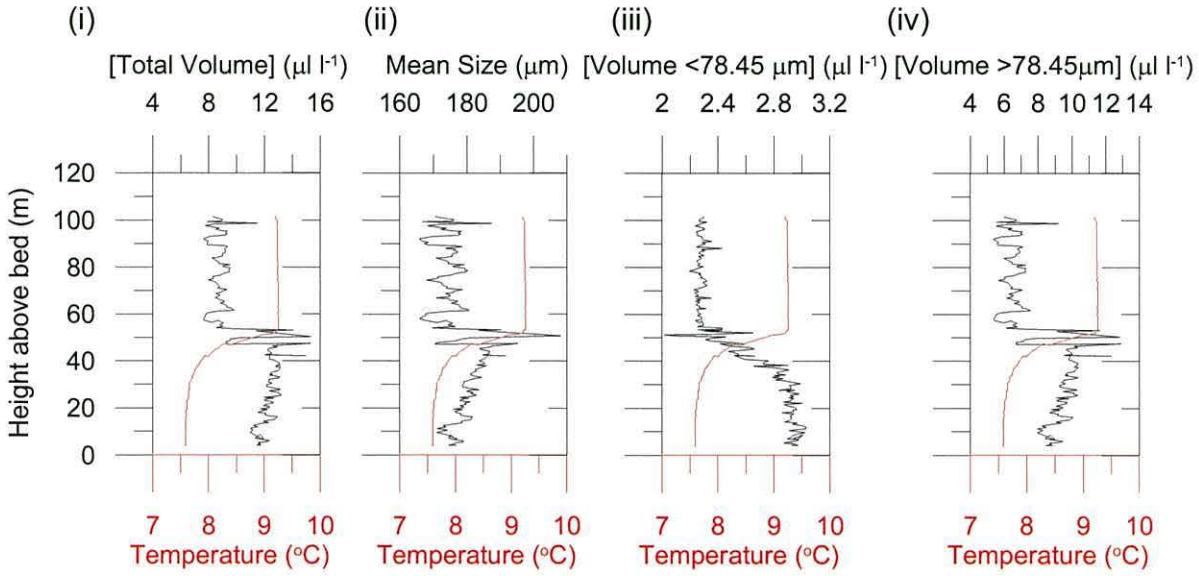

Figure 5.16. LISST profiles for day 305 (1/11/98 22:07). (i) Total volume concentration, (ii) mean size, (iii) volume concentration of particles less than 78.45 µm and (iv) volume concentration of particles greater than 78.45 µm.

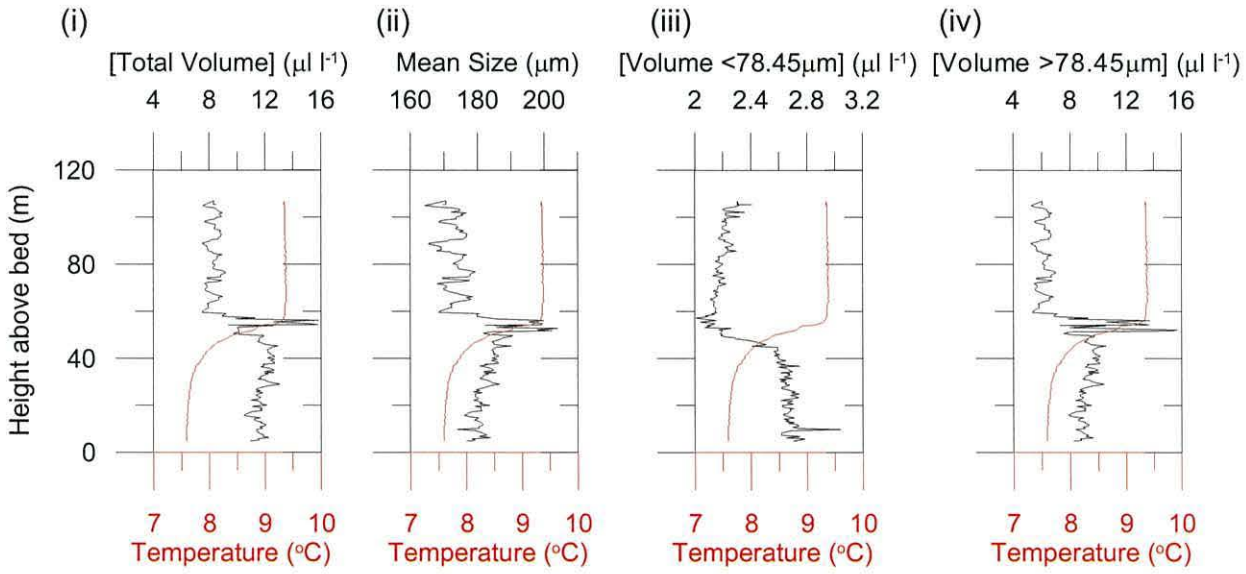

Figure 5.17. LISST profiles for day 307 (3/11/98 22:48). (i) Total volume concentration, (ii) mean size, (iii) volume concentration of particles less than 78.45 µm and (iv) volume concentration of particles greater than 78.45 µm.

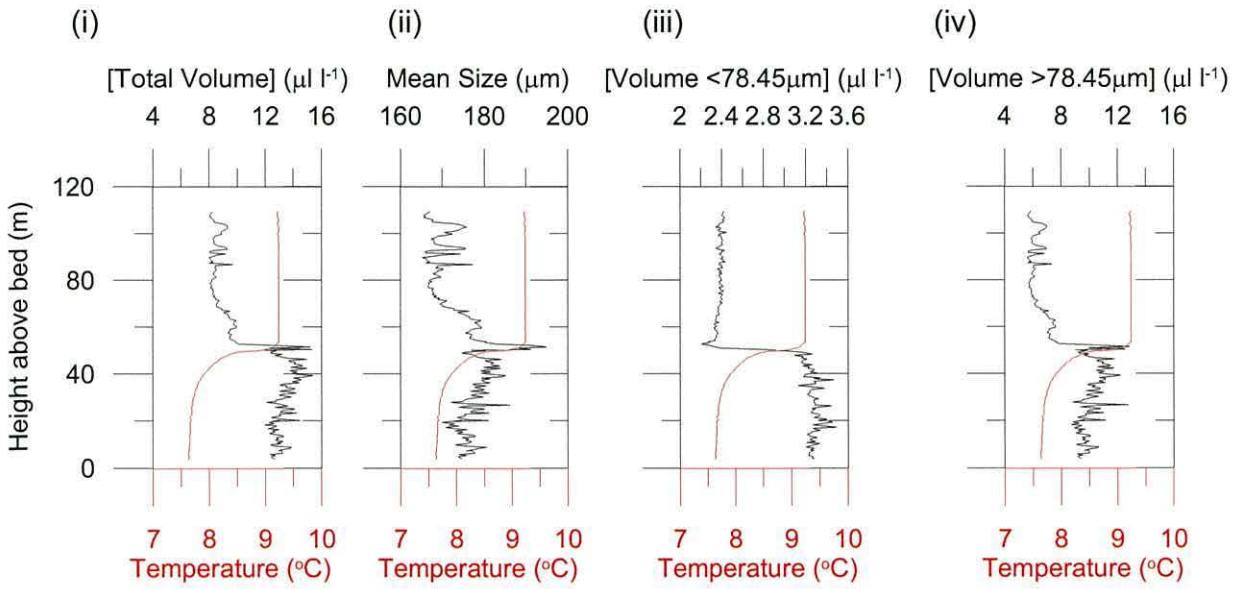

Figure 5.18. LISST profiles for day 309 (5/11/98 21:00). (i) Total volume concentration, (ii) mean size, (iii) volume concentration of particles less than 78.45 µm and (iv) volume concentration of particles greater than 78.45 µm.

Chapter 6

Clyde Sea

6.1. Introduction to the Study Site

The Clyde Sea (Figure 6.1) is a deep, partially enclosed basin on the west coast of Scotland, with a restricted exchange channel with the adjacent shelf sea only over a relatively shallow sill (~45 m depth). Within the basin the water depth reaches a maximum of 185 m. The basin receives large freshwater inputs from the River Clyde and other river sources which enter mainly through the sealoch system in the north of the region (Poodle, 1986).

Because of the constraint on exchange at the sill, the freshwater inflow produces a typical fjordic regime in which the salinity of the outflow water is up to 1.5 less than the inflow water resulting in the maintenance of a stable stratified system which is not eroded by tidal stirring (Simpson and Rippeth, 1993). This stratification persists year round, maintained by heating and freshwater inflow in the summer and freshwater inflow during the winter (Edwards *et al.*, 1986). The extent of stratification follows a well defined seasonal cycle with high levels in the summer and reduced levels during the winter (Simpson and Rippeth, 1993). Thermal stratification is stable throughout the summer (from May to September), becoming unstable with temperature inversions occurring during November and December. The instability observed in the temperature structure during the winter is compensated by the salinity structure which maintains a weak positive stability in density.

Outside of the sill in the North Channel tidal stirring is vigorous and promotes complete vertical mixing throughout the water column (Edwards *et al.*, 1986). The strong tidal currents in this region flow predominantly parallel to the sill ensuring rapid removal of waters leaving the Clyde in the exchange flow over the sill (Simpson and Rippeth, 1993). Inside the sill the Clyde is a well-defined ROFI (Region of Freshwater Influence) in which the input of freshwater buoyancy is of the same order as that due to seasonal heating.

The origin of SPM was found by Balls (1990) to be predominantly resuspension from the seabed, a process which was evident in their profiles of SPM concentration. Due to the strong stratification present Balls concluded that the upper layer of the water column was isolated from the deep water, thus no exchange of resuspended material with the upper part of the water column occurred.

6.2. Observation Programme

Observations were made at a station in the Clyde Sea from the *RRS Charles Darwin* (cruise CD122) over the period from 21/05/00 (day number 142) to 22/05/00 (day number 143) (referred to as the Clyde anchor site). LISST, CTD, transmissometer and fluorometer (see Chapter 3) data were collected at the site (Figure 6.1) during the survey period.

The LISST was mounted horizontally to the CTD frame and manually switched on before each deployment. The frame was lowered to a depth of approximately 10 m where it was left for a few minutes before being brought back to just below the surface. The CTD frame was then lowered continuously at 0.5 to 1 m s^{-1} to the closest comfortable proximity to the sea floor. The upcast was performed in stages between bottle firing depths which varied between profiles.

Water samples were taken for gravimetric analysis and subsequent gravimetric calibration of the transmissometer (Section 3.3.2). Two litres of water sample were filtered through each GF-C filter before rinsing with approximately 150 ml of distilled water.

6.3. Data Processing

For the LISST a running mean of beam attenuation over 8 scans (i.e. over a 2 second period which is over approximately 1 to 2 m) was calculated. Any points with values outside two standard deviations either side of this mean were

flagged as spikes. Any other obvious spikes which were not automatically removed by this method were removed manually afterwards. The data was then depth averaged into one meter bins as a further smoothing procedure.

Data from the transmissometer was delivered as raw voltages and were therefore converted to beam attenuation using

Equation 6.1. $$c = \frac{1}{pathlength} \log_e \left(\frac{volts}{5.0} \right).$$

The pressure sensor was found to have a constant offset of –2.5943 m which was added to all pressure readings before further analysis.

6.4. Results

6.4.1. Tides

Figure 6.2 shows sea level measurements made at Millport and Figure 6.3 shows the M_2 component in the east-west direction of current velocities measured at the ADCP mooring site (unfortunately the North-South component was not available). The study took place (on 21st / 22nd May 2000, day 142/143) just after a spring tide with a tidal range at Millport of approximately 3 m (1.5m +/- mean sea level) and maximum M_2 tidal velocities of 0.4 m s^{-1}, although the ADCP record stops as the sampling period begins.

6.4.2. Temperature

Figure 6.4 shows the temperature throughout the water column measured at the Clyde anchor site during the study period. A two layer water column is evident with a thermocline fluctuating between 28 m above the bed to 50 m above the bed, separating the warmer surface water (c. 11°C) and the cooler bottom waters (c. 8°C). The times when the base of the thermocline is the least height above the bed are at 6 hourly intervals, at both low and high water. This is

consistent with an M_2 internal oscillation and has been observed previously at this site (Inall & Rippeth, 2002).

Figure 6.5 shows a typical temperature profile from this study site. The thermocline region is broad, extending over 15 m with two distinct gradient changes, the first at 50 m above the bed and the second between 42 m and 34 m above the bed.

6.4.3. Salinity

Salinity shows a similar pattern to temperature with the location of the halocline sinking through the water column at both high and low water (Figure 6.6). The e halocline is centred around the base of the thermocline and separates the less saline surface waters (c. 32.9) from the more saline bottom waters (c. 33.35).

6.4.4. Turbulence

A turbulence profile measured by the FLY two hours after high tide, just prior to the 24 hour study period is presented in Figure 6.8. Unfortunately there are no turbulence measurements during the study period due to instrument failure. However, this profile is representative of the profiles made prior to the failure. A clear minimum in turbulent dissipation can be seen in the thermocline region, similar to that seen in the northern North Sea. As expected the turbulent dissipation rate increased towards the bed, a result of the friction caused by the sea bed.

6.4.5. Fluorometry

Figure 6.9 shows the fluorometry ($\mu g\ l^{-1}$) (conversion from volts to $\mu l\ l^{-1}$ is described in Chapter 3, section 3.5.2) measured at the Clyde anchor site at the same time as all other measurements. The highest chlorophyll concentrations are in the surface waters, with lower concentrations near-bed. Like both temperature and salinity the base of the higher concentrations fluctuates between 39 m and 45 m, the top of the pycnocline, above the bed on a 6 hourly

cycle. At the base of the thermocline region a minimum in chlorophyll concentration is observed.

6.4.6. Suspended Particulate Matter Concentration

A linear regression analysis was performed using the beam attenuation measured by the transmissometer and gravimetric concentrations measured during the study period (Figure 6.10) which produced a regression of

Equation 6.2 $\quad SPM\ (mg\ l^{-1}) = 2.13(\text{beam attenuation}) - 0.375$

with a r^2 equal to 0.314, p-value of 1.58×10^{-10} and n = 114. Therefore this regression is significant although the fit is poor.

Figure 6.11 shows the SPM concentration calculated using Equation 6.2 over the whole time series. Highest concentrations of between 2.8 mg l^{-1} and 4 mg l^{-1} occur between the bed and 20 m above the bed. The maximum height of this higher concentration fluctuated in a similar fashion to density (and temperature and salinity) with the maximum concentration extending higher in the water column at mid-flow, between high and low tides, indicating resuspension. The top of the high concentration region corresponds with the base of the thermocline.

Above the high concentration region, within the thermocline and pycnocline regions, is a region of minimum SPM concentration with values of c. 1.5 mg l^{-1}. This region extends to the top of the pycnocline before a slight increase in concentration is observed in the surface layer.

Figure 6.5 shows more clearly the presence of a concentration minimum within the thermocline and is a much broader feature than that measured in the northern North Sea, reflecting the less sharp thermocline at the Clyde anchor site compared to the northern North Sea. The transition to the minimum from the surface waters is rapid, occurring at the top of the second large gradient in

temperature. The increase in concentration towards the bed from this minimum begins at the base of the thermocline and is not as rapid as the decrease observed at the surface. Concentrations near-bed are approximately 1.5 times greater than those in the surface region and two times greater than the minimum region.

However, this mass concentration minimum is not reflected in the total volumetric concentration measured by the LISST (Figure 6.12). Instead, a gradual increase in concentration from the surface to the near-bed occurs throughout the water column with the minimum volumetric concentrations occurring near the surface. The gravimetric and volumetric concentrations are correlated in the near-bed region with impulses of higher concentrations occurring periodically. They are also correlated above the thermocline with a lessening in concentration towards the surface.

6.4.7. Particle Size

The particle size measured by the LISST was found to be very noisy, a result of statistically patchy large particles being present. Typical particle size distributions measured by the LISST in the near-surface, thermocline and near-bed regions are shown in Figure 6.13. Figure 6.13a and b are the same distributions but with different y-axis maximum values to allow examination of different parts of the distribution. From Figure 6.13a the main difference between the three regions is the volumetric concentration in each size class. Figure 6.12 shows that the greatest volumetric concentration throughout the water column is near-bed and this is reflected in the distribution with most of the size classes containing the most in the near-bed distribution.

Differences between each region also exist in the shape of the distributions (Figure 6.13a). All three regions have a mode around 4 μm, but as discussed in Chapter 5 (section 5.4.6), this is not likely to be real. Excluding this mode, both the near-surface and near-bed distributions are bimodal, whereas the thermocline distribution is trimodal. All three regions have a fine mode but this is different in the surface and thermocline (~15 μm and ~16 μm respectively)

compared to the near-bed region where it is ~24 μm. All three regions display evidence of a coarse mode greater than 250 μm, indicated by a "tail" in the largest size classes. The size class between this large mode and the finer part of the distribution for all three regions is 109.07 μm. Therefore, this has been chosen as the cut-off between the fine and coarse parts of the distribution. It is also the upper size class that gives the best estimate of the particle densities for the smaller size mode (section 6.4.8). The thermocline region has a third mode, not seen in the other two regions, in the 34.28 – 40.45 μm size class.

In the fine part of the distribution (between 1 μm and 109 μm) the concentration throughout all the size classes for the thermocline is consistently lower than both the surface and near-bed. However, Figure 6.12 indicates that the total volumetric concentration in the thermocline region is greater than in the surface region, less than the near-bed. In Figure 6.13b the largest size class in the thermocline distribution has the greatest volumetric concentration. As this contributes to nearly 75% of the total volume concentration, particularly in the near-surface and thermocline regions, differences in values in these size classes will be reflected in the total volume concentration.

Also, Figure 6.14 shows that the mean size in the thermocline region is much greater than that in the near-bed and surface regions. The increase in mean particle size is due to an increase in the volume of particles greater than 109.07 μm, a decrease in the volume of particles less than 109.07 μm or a combination of both. Figure 6.15 shows a clear decrease in the volume concentration of particles less than 109.07 μm in the thermocline. However, as already mentioned (section 6.4.5) there is no overall decrease in volumetric concentration in the region (Figure 6.12).

6.4.8. Dry Particle Densities

Dry particle densities were calculated in the near-surface, thermocline and near-bed regions over the whole sediment population using equation 3.5. The results are summarised in Table 6.1.

As the distributions show a large proportion of the volume of particles in the largest size classes, it is evident that particles larger than 250 μm are present resulting in the maximum total volume concentration being an underestimate of the actual total volume concentration. This will result in an inaccurate measure of the particle density. If these large particles are mainly organics then they will not contribute much to the gravimetric concentration. Therefore, by recalculating the particle density by removing the larger size classes a more satisfactory particle density maybe attained. The results of this are shown in Table 6.2. These results will be nearer the true particle densities for the smaller sized fraction of the particle population as they eliminate the contaminated larger LISST size classes. For this smaller sized fraction of the population the particle density is approximately the same between the three different regions of the water column.

	Average depth (m)	Mass Concentration (g l^{-1})	Particle Density (g cm^{-3})
Near-Surface	3.0 ± 0	$1.60 \times 10^{-3} \pm 0.75 \times 10^{-3}$	0.1625 ± 0.094
Thermocline	17.0 ± 3.3	$8.97 \times 10^{-4} \pm 2.06 \times 10^{-4}$	0.1294 ± 0.046
Near-Bed	77.5 ± 35.9	$3.60 \times 10^{-3} \pm 0.97 \times 10^{-3}$	0.2044 ± 0.057

Table 6.1. Dry particle densities for the whole particle distribution measured by the LISST in the near-surface, thermocline and near-bed regions.

LISST size classes included	Mid point of the upper size class included (μm)	Correlation co-efficient	Particle density (g cm^{-3})
SURFACE			
1 to 32	230.14	0.16	$0.163 \pm 0.94x10^{-1}$
1 to 31	195.02	0.35	$0.331 \pm 0.16x10^{-1}$
1 to 30	165.26	0.29	$0.540 \pm 2.7x10^{-1}$
1 to 29	140.04	0.39	$0.779 \pm 3.8x10^{-1}$
1 to 28	118.67	0.44	$0.937 \pm 4.7x10^{-1}$
1 to 27	**100.57**	**0.45**	**$0.964 \pm 4.9x10^{-1}$**
1 to 26	85.22	0.45	$0.973 \pm 4.9x10^{-1}$
THERMOCLINE			
1 to 32	230.14	-0.22	$0.129 \pm 0.46x10^{-1}$
1 to 31	195.02	0.44	$0.210 \pm 0.48x10^{-1}$
1 to 30	165.26	0.55	$0.332 \pm 0.76x10^{-1}$
1 to 29	140.04	0.56	$0.612 \pm 1.5x10^{-1}$
1 to 28	**118.67**	**0.63**	**$0.957 \pm 2.7x10^{-1}$**
1 to 27	100.57	0.63	$0.993 \pm 2.8x10^{-1}$
1 to 26	85.22	0.63	$1.001 \pm 2.7x10^{-1}$
NEAR-BED			
1 to 32	230.14	0.10	$0.204 \pm 0.57x10^{-1}$
1 to 31	195.02	0.21	$0.459 \pm 1.7x10^{-1}$
1 to 30	165.26	0.24	$0.670 \pm 2.5x10^{-1}$
1 to 29	**140.04**	**0.24**	**$0.829 \pm 3.0x10^{-1}$**
1 to 28	118.67	0.23	$0.946 \pm 3.4x10^{-1}$
1 to 27	100.57	0.23	$0.986 \pm 3.4x10^{-1}$
1 to 26	85.22	0.20	$1.006 \pm 3.4x10^{-1}$

Table 6.2. Results of density calculations when LISST size classes are removed. The values in bold indicate the point where removing any more classes does not significantly improve the results.

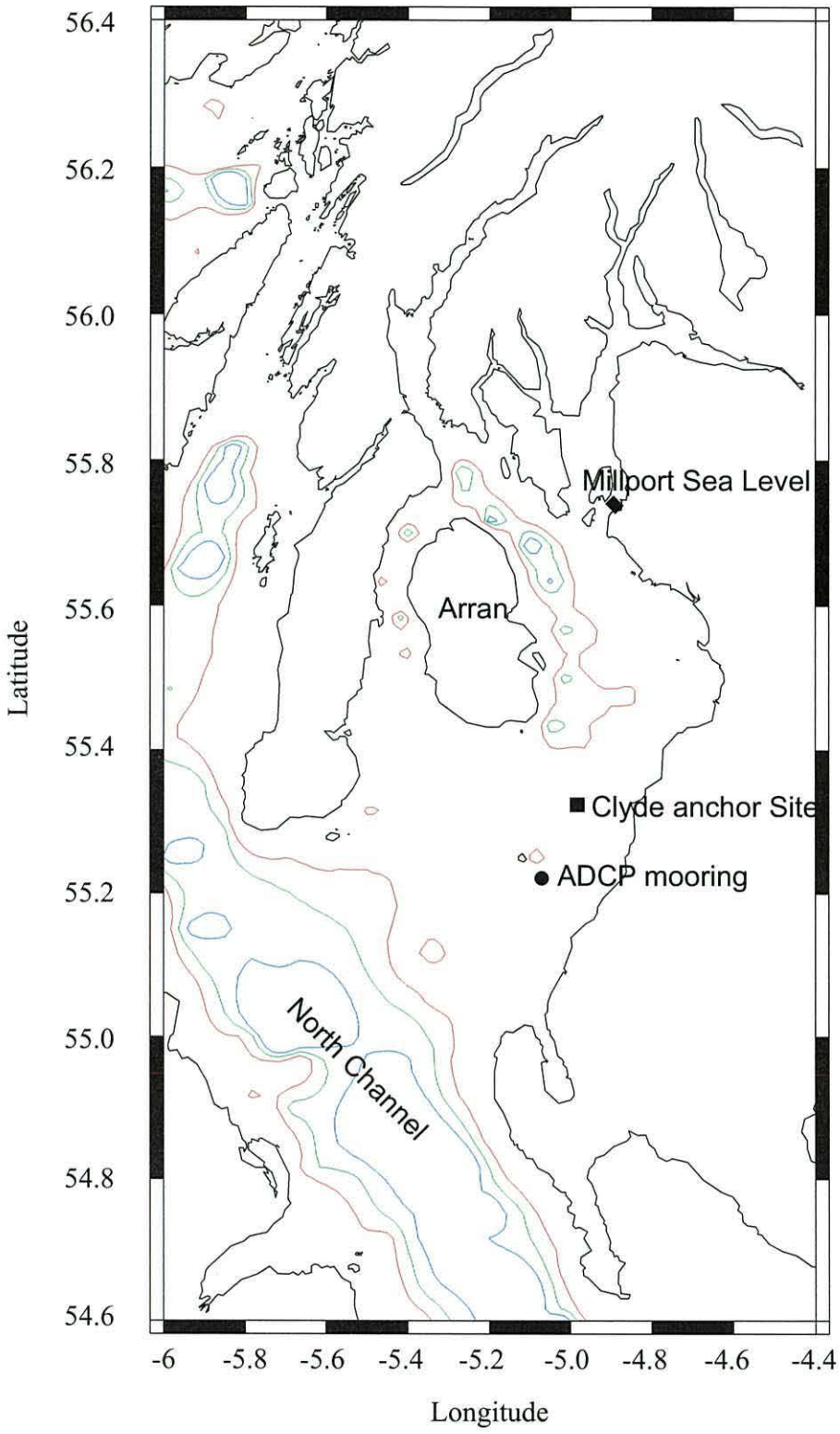

Figure 6.1. A map of the Clyde Sea and North Channel showing the study area and location of ADCP and sea level stations.

60m contour, 90m contour, 120m contour.

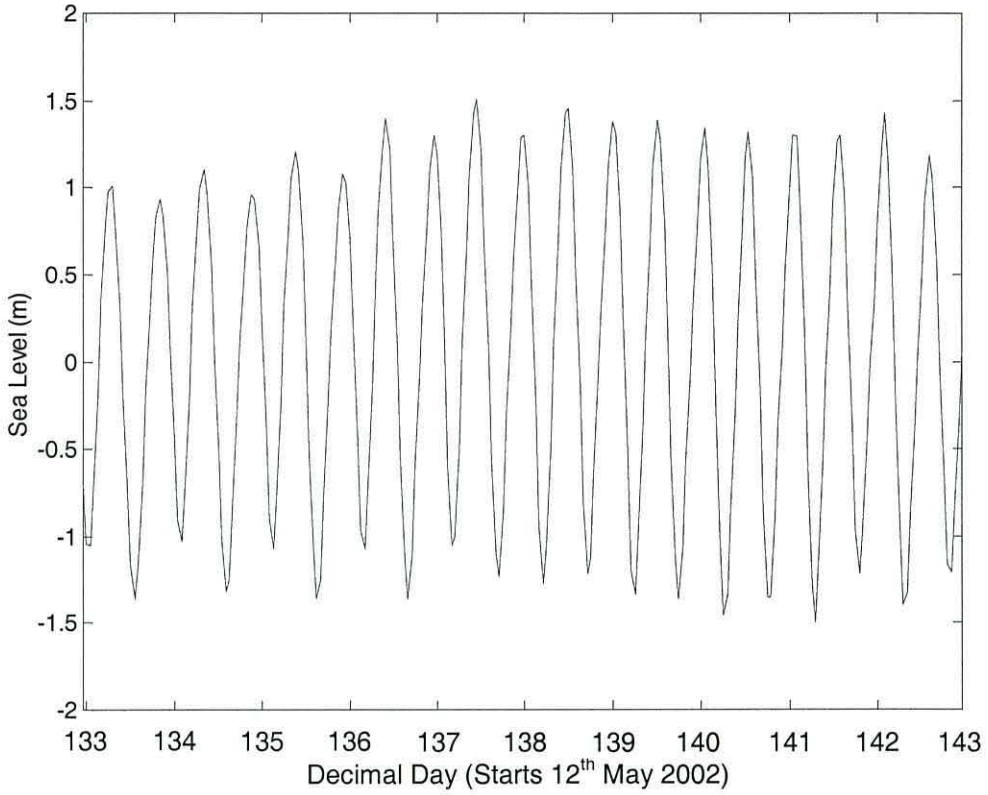

Figure 6.2. Sea level (minus mean sea level at Millport).

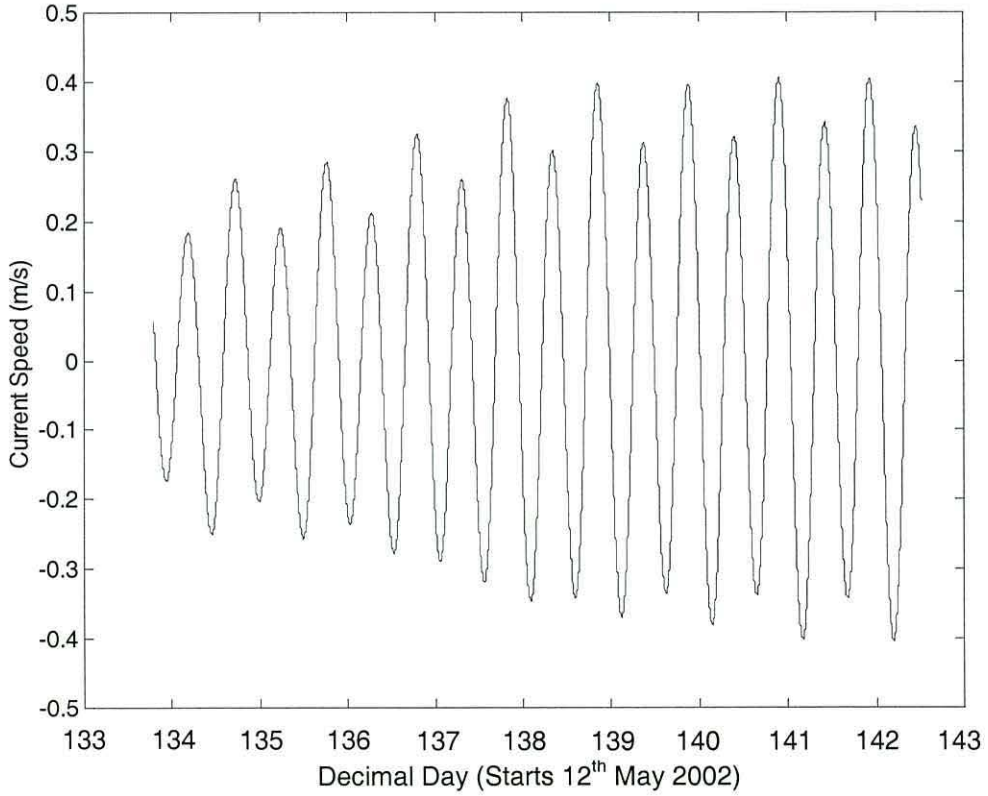

Figure 6.3. M_2 east-west component measured at ADCP mooring.

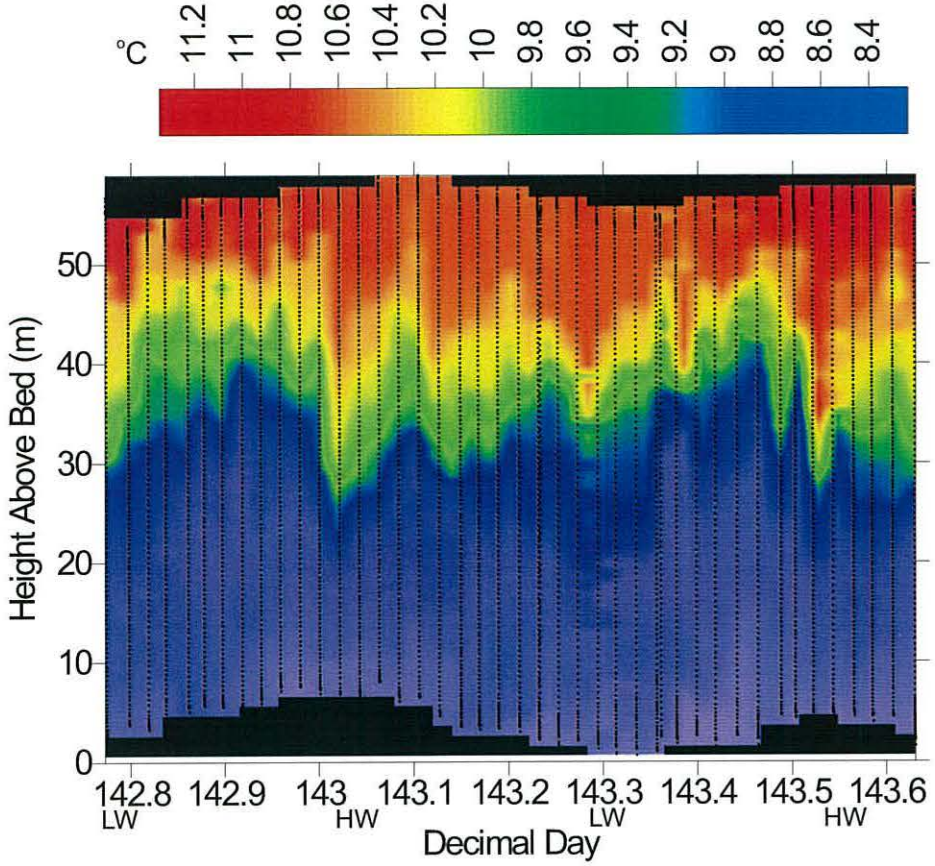

Figure 6.4. Temperature at the Clyde anchor site. HW indicates high water and LW indicates low water.

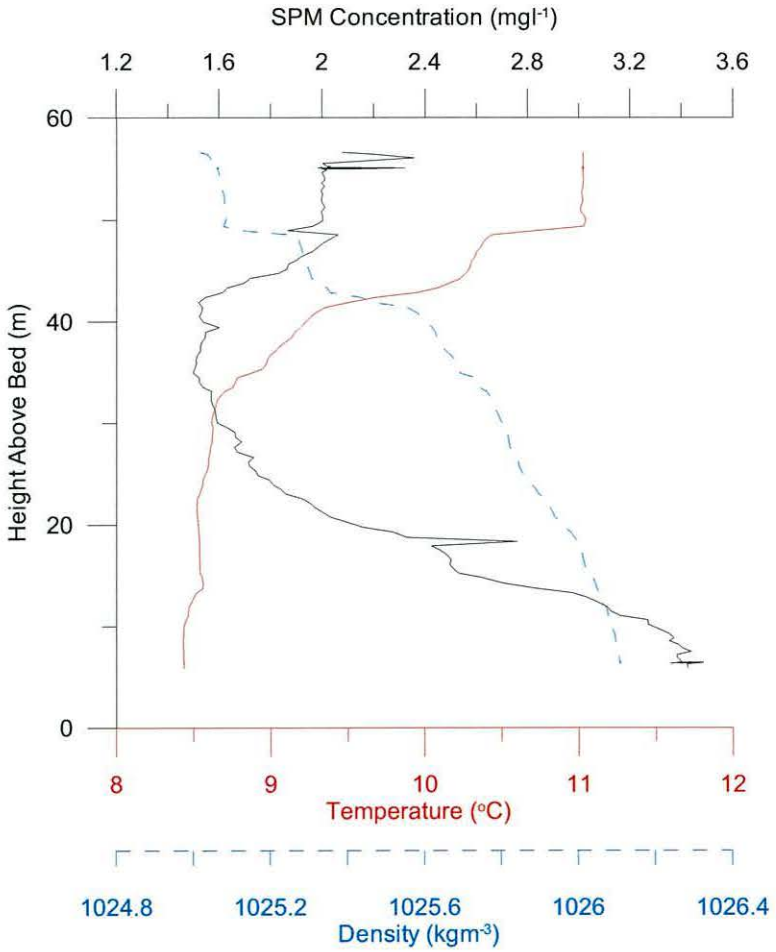

Figure 6.5. Typical profiles of temperature, density and SPM concentration.Profile from ~ day 143: *21/05/00 at 22:30.*

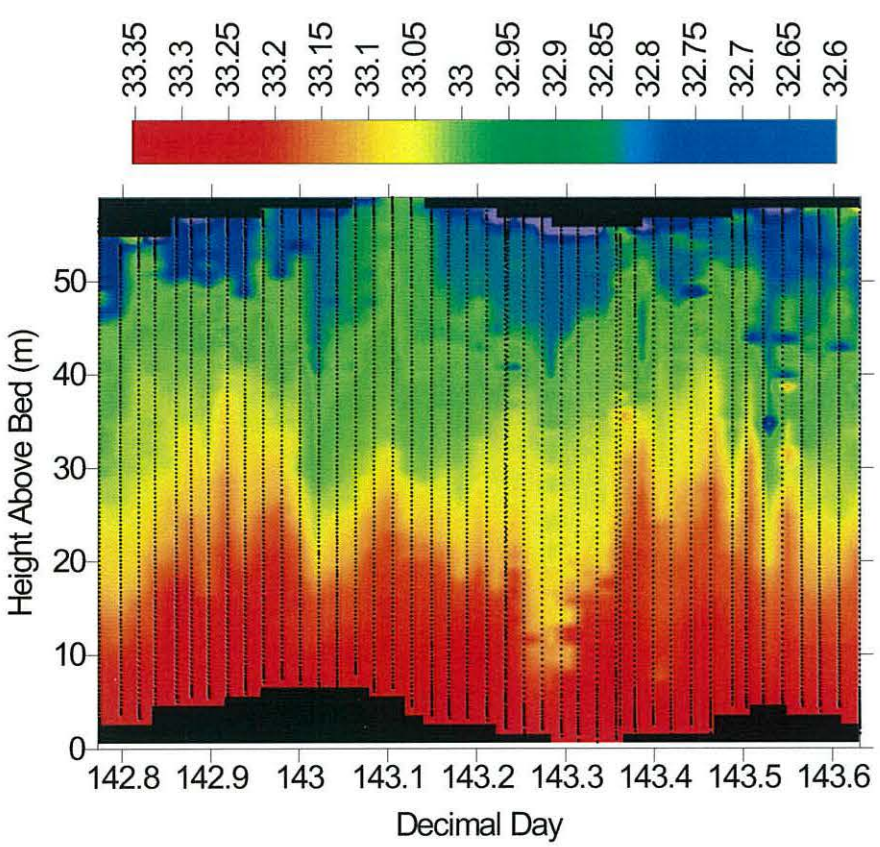

Figure 6.6. Salinity at the Clyde anchor site.

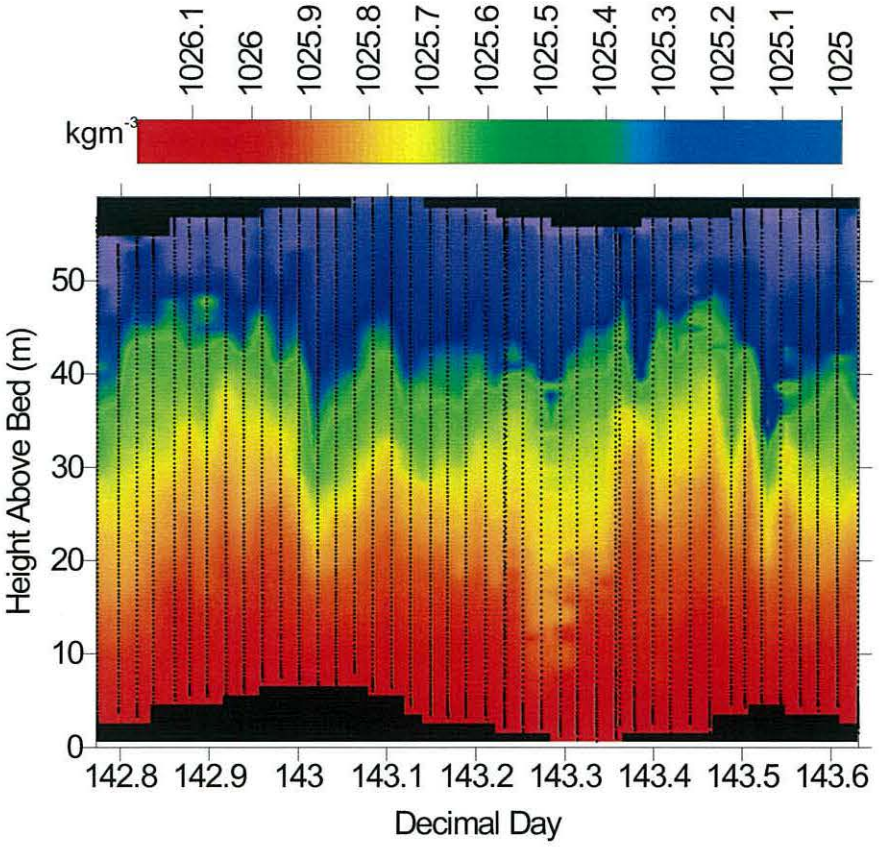

Figure 6.7. Density at the Clyde anchor site.

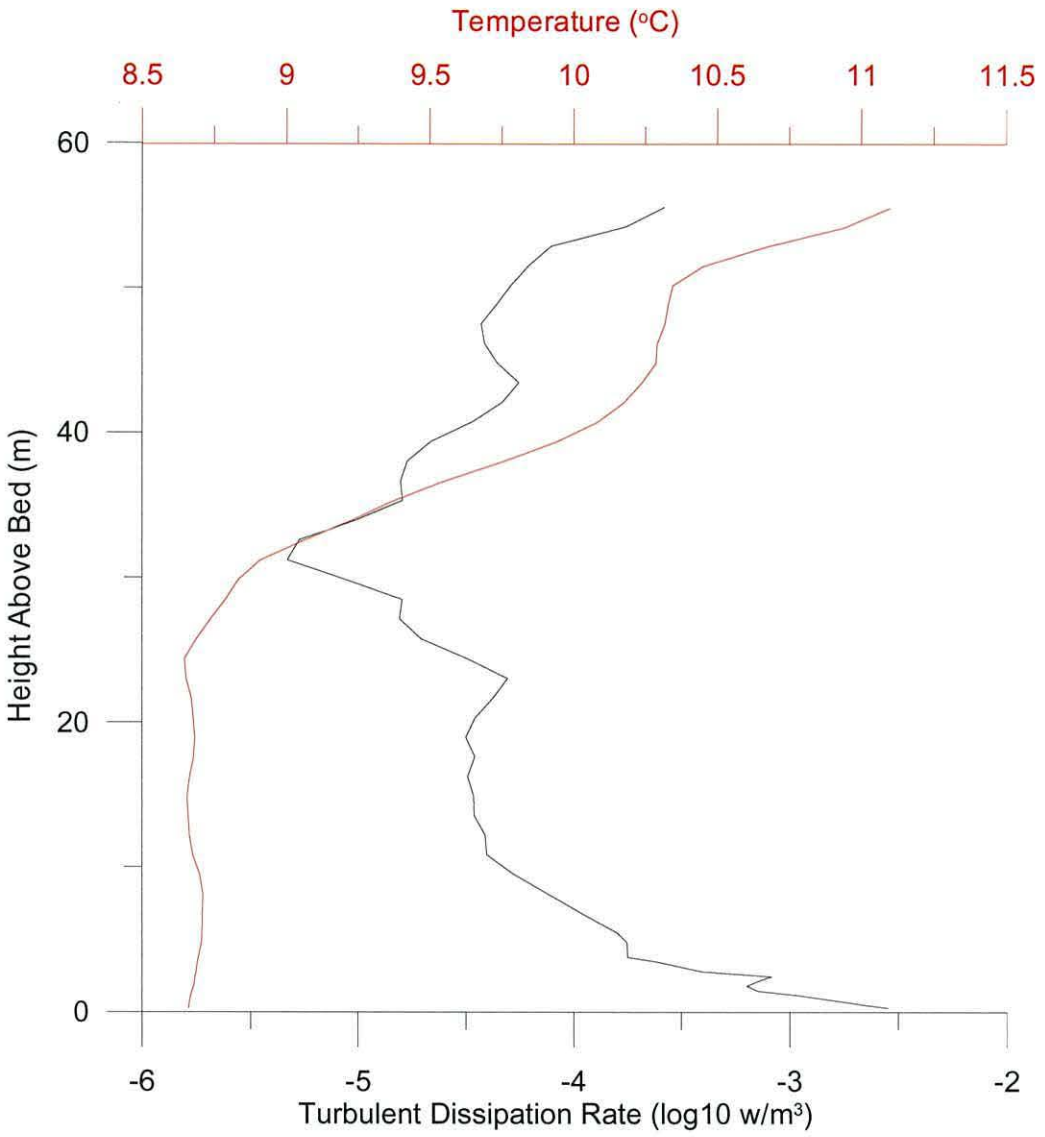

Figure 6.8. Typical profile of the turbulent dissipation rate measured by the FLY at the Clyde anchor site.

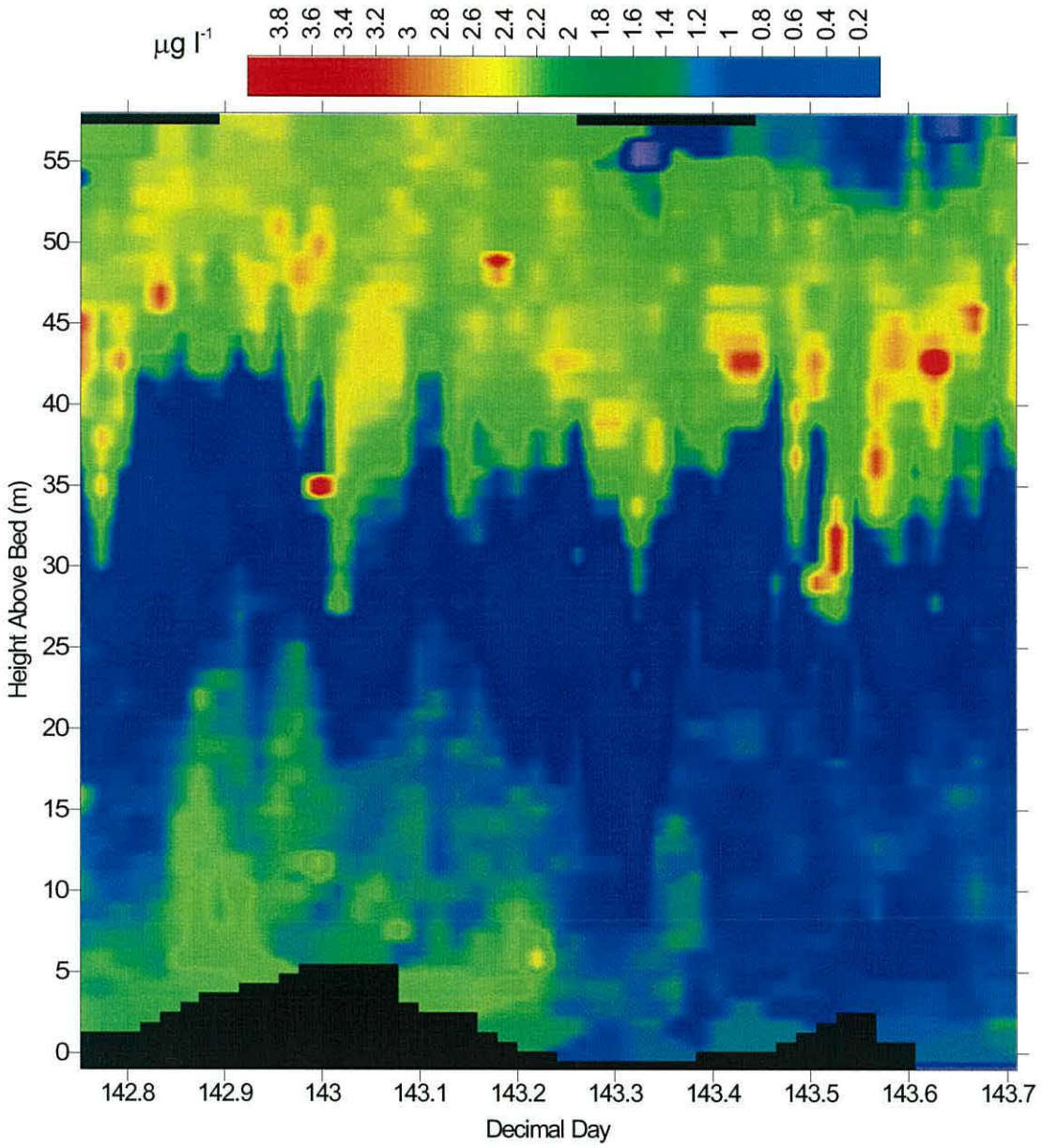

Figure 6.9. Chlorophyll concentration at the Clyde anchor site.

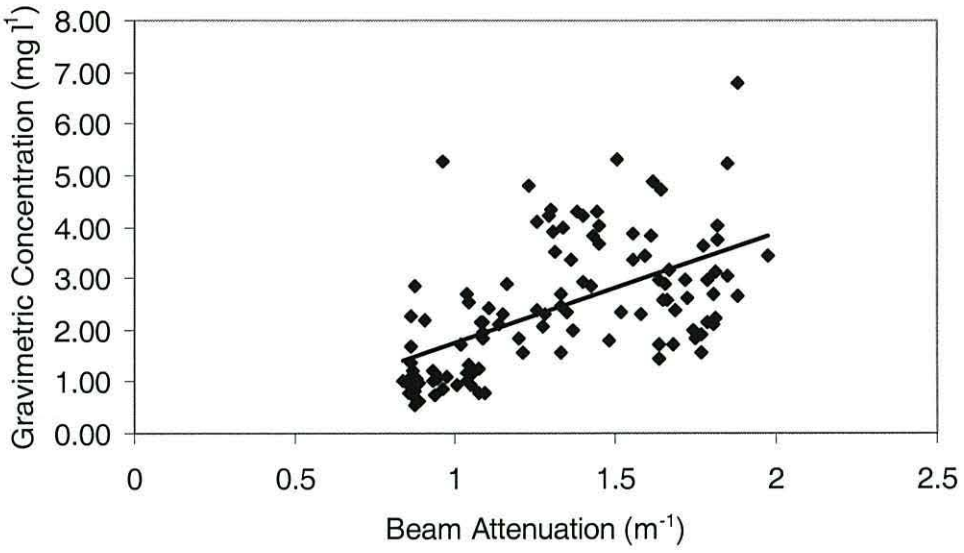

Figure 6.10. Linear regression plot of gravimetric concentration against beam attenuation. Observed values (♦) and regression line (———).

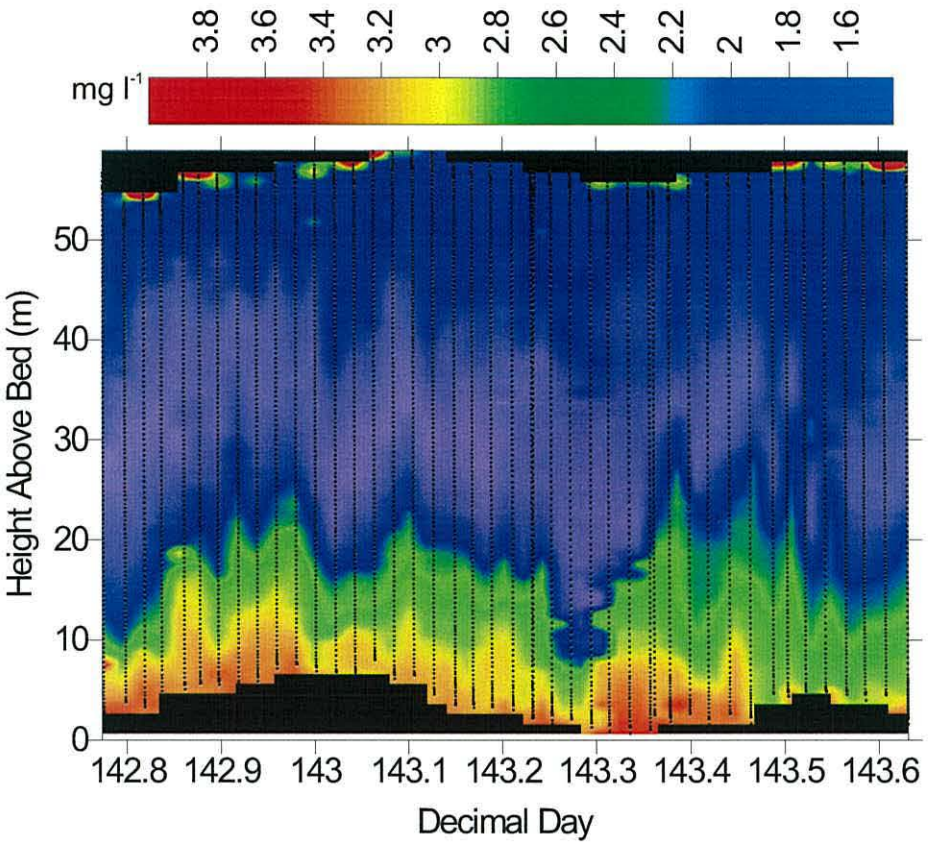

Figure 6.11. SPM mass concentration at the Clyde anchor site.

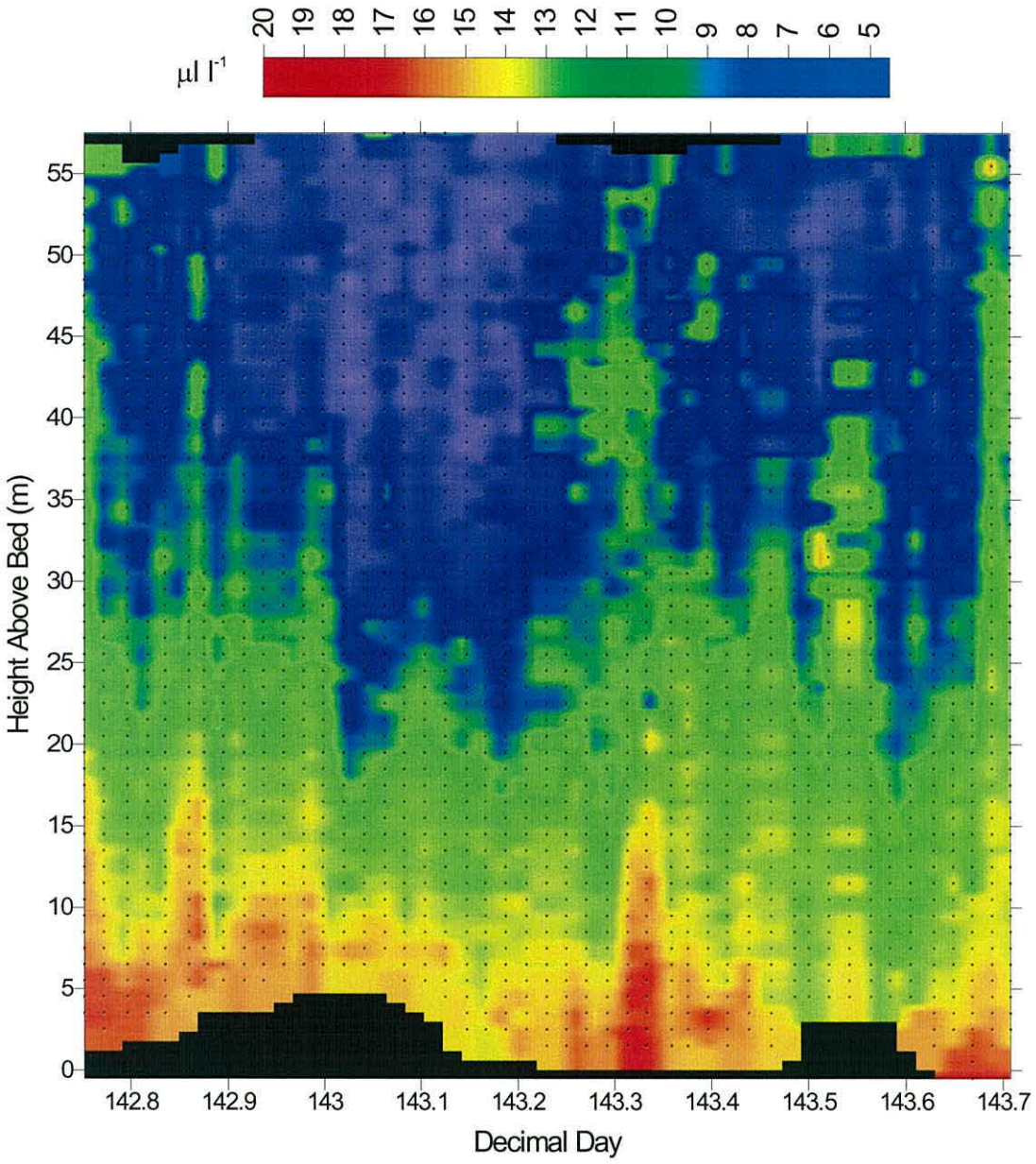

Figure 6.12. Total volume concentration of SPM (μl l^{-1}) (measured by the LISST) at the Clyde anchor site.

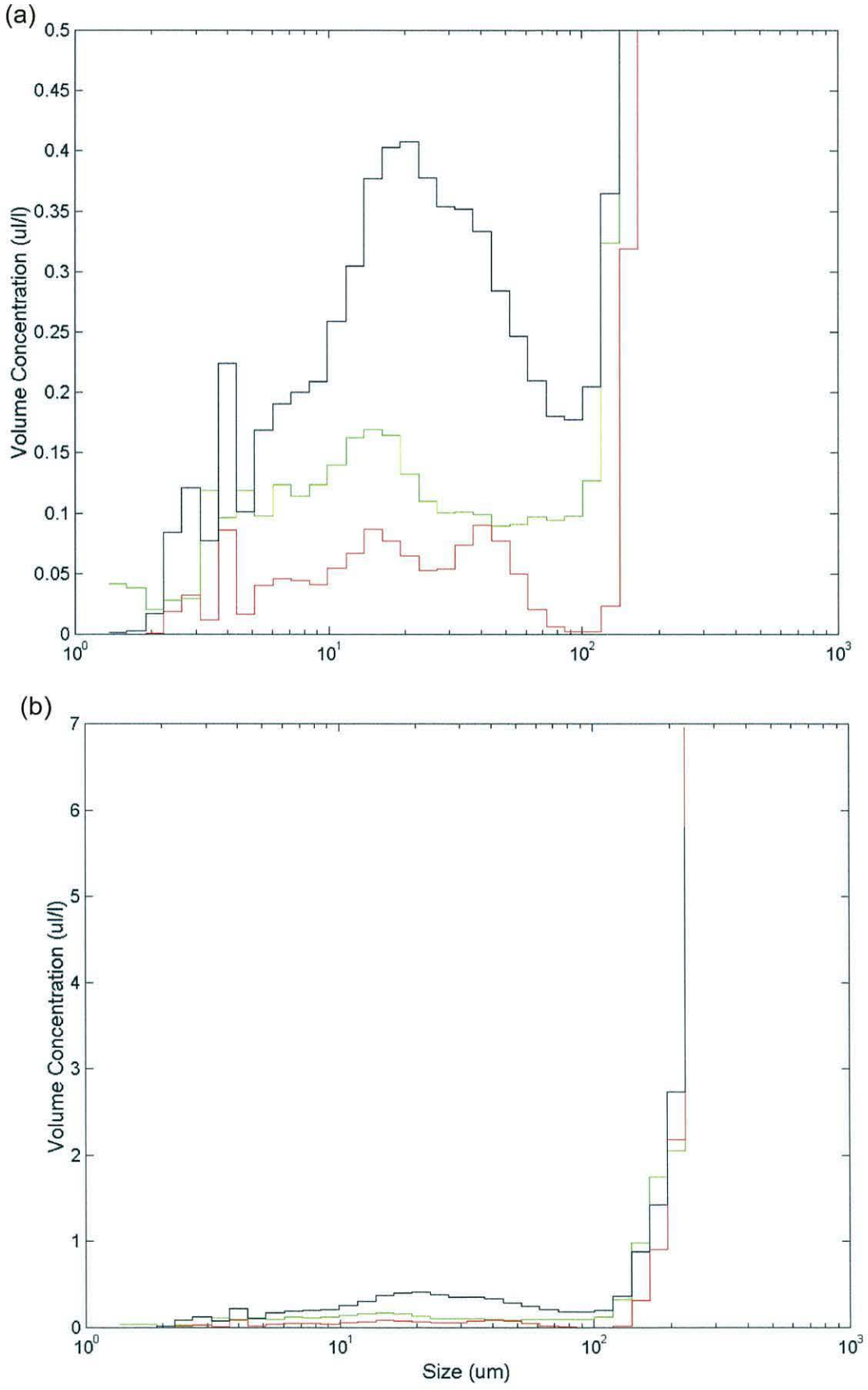

Figure 6.13. Typical particle size distributions at the Clyde anchor site measured by the LISST. Near-surface (——), thermocline (——) and near-bed (——).

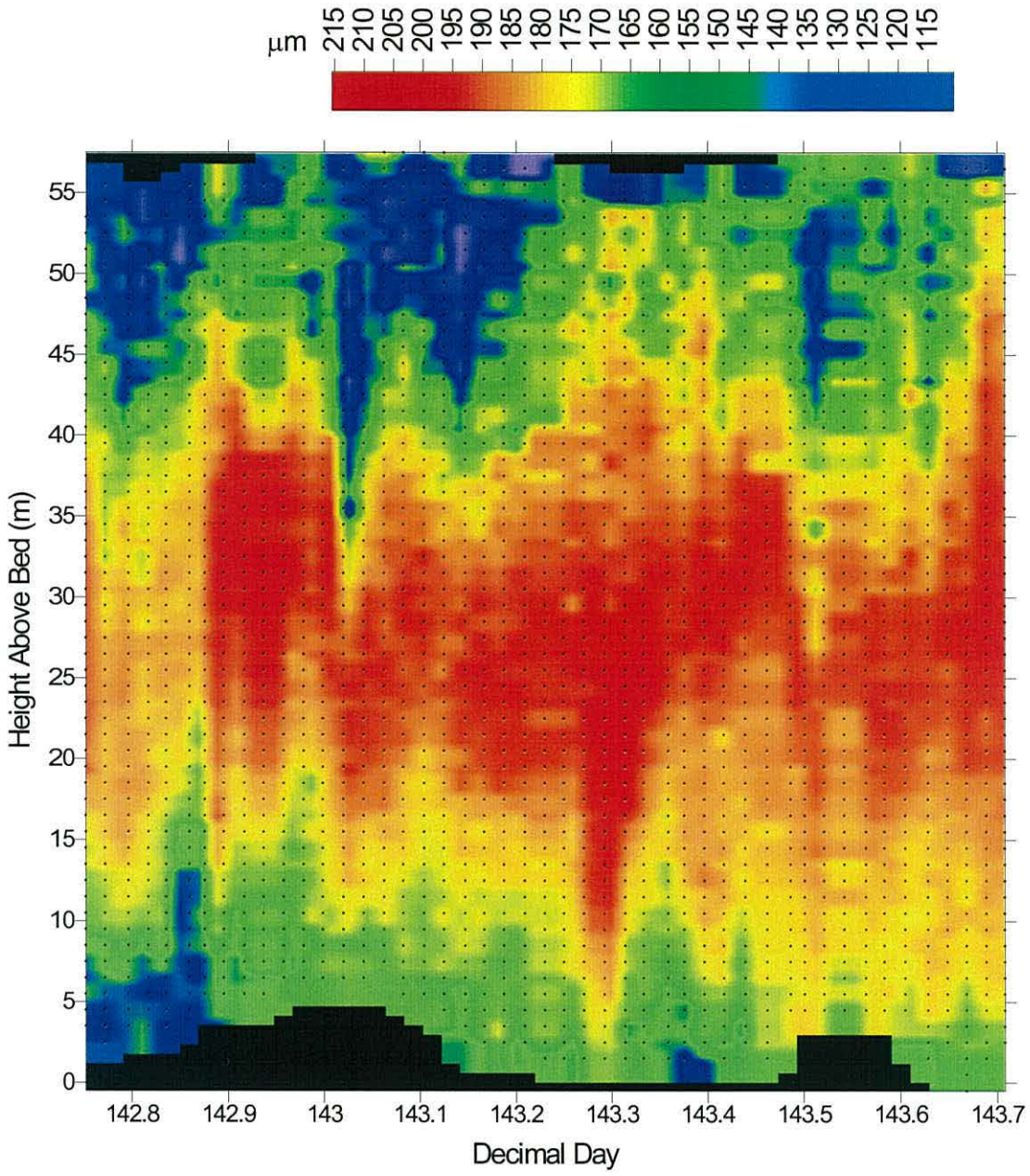

Figure 6.14. Mean size of SPM at the Clyde anchor site (measured by the LISST).

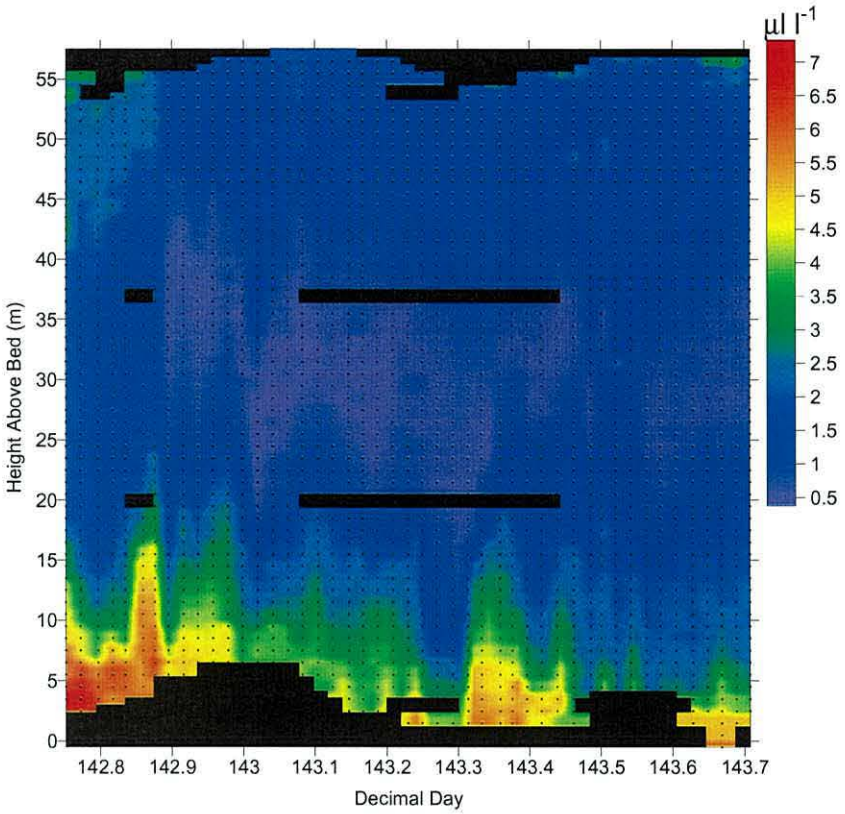

Figure 6.15. Volume concentration of particles less than 109.07 µm (measured by the LISST) at the Clyde anchor site.

Chapter 7

Discussion

7.1. Introduction

This is a discussion primarily of the results presented in Chapters 5 and 6 although results presented and discussed in Chapter 4 will be referred to. Two field experiments were performed, one in the northern North Sea and one in the Clyde Sea. Preliminary discussion of the approach used to interpret the observations will be followed by an individual discussion of each site. Finally the two sites will be compared.

7.2. Use of the LISST-100B to measure natural particle size distributions

The LISST-100B applies an inversion algorithm to the diffraction pattern measured by its detection rings to determine volume concentrations in 32 logarithmically spaced size classes from 1 - 250 μm. This procedure has been shown to produce an accurate representation for normal distributions of spherical particles but, as discussed in Chapter 4, does not reflect the true distribution for populations containing particles larger than 250 μm. In these cases some of the scattered signal from larger particles is incorporated into the light intensity received on the first detection ring and the algorithm interprets this as a large volume concentration in the largest size classes.

Data collected at all experimental sites indicate large and increasing concentrations in the largest two size classes, which is confirmed by video-microscope observations of large particles as discussed in Chapter 4. It is not possible to quantify the effect that these large particles have, nor is it possible using the data collected to conclude what size range beyond 250 μm has an influence on the measured distributions. Nevertheless the fact that systematic variation in mean grain size and coarse particle volume distributions has been observed at all experimental sites indicates that the measured distributions are

at least representative of variation over a somewhat wider size range than the stated limit.

The approach in interpreting these distributions can be formalised as follows. It is first assumed that for any given set of measurements the variation in particle population over depth and time is relatively small. The measured size distribution is then split into two, using the shape of the distribution to decide the cut-off point between coarse and fine populations. The observed fine particle volume concentrations can then be assumed to represent the actual fine particle distribution. Provided that the true variation in the coarse population is relatively small, the observed variation in coarse particle volume concentration can be assumed to be proportional to the true variation (with an unknown constant of proportionality). It is not possible to specify a size distribution of this coarse population as the observations cannot resolve the true size of the particles contributing to it.

It can then further be assumed that the observed mean grain diameter is proportional to the true mean grain diameter. Some authors prefer to use median, rather than mean grain diameter, as this is less sensitive to variation at the extreme ends of the distribution (e.g. McCandliss *et al.*, 2002). However in general mean and median grain diameter will be correlated. Mean grain diameter has been used here because it is easier to calculate. Observed variations in mean diameter will only be representative, and in general will be an underestimate, of the true variation in either mean or median diameter. It should be noted that the assumption that the relationship between observed and true mean diameter is linear cannot be tested directly using the data collected here and should be borne in mind when drawing conclusions.

There is a further consideration which must be allowed for in interpreting the LISST observations. For N particles per unit volume of diameter D the corresponding volume concentration is proportional to ND^3. Therefore a relatively small number of large particles will have a very large effect on the volume concentration. The effective instantaneous sampling volume of the LISST is ~ 0.01 litres, although this can be increased by averaging over

repeated measurements (during CTD profiling ~ 5 - 10 measurements are made per metre of water depth). A small number concentration of large particles will result in occasional large spikes in the LISST data corresponding to those times when large particles happen to be within the sampling volume. These will not be statistically representative of the true concentrations unless the data can be averaged over much longer averaging periods than are possible during routine CTD profiling. Large spikes were observed during all sampling periods described here, and many were removed by data processing described in Chapter 3. However at the northern North Sea site they occurred regularly and at a particular location in the water column. Therefore they have been retained as providing qualitative evidence of a real feature of the particle population (e.g. zooplankton scavenging).

7.3. Interpretation of transmissometer measurements.

Beam attenuations measured by the SeaTech transmissometer have been converted to mass concentrations using site specific calibrations obtained from gravimetric analysis of water samples obtained during the experiments. As indicated in Chapters 5 and 6 both calibrations involved a high degree of scatter. There are several possible reasons for this. At both sites concentrations were persistently low, so errors in gravimetric analysis will be high. Concentration ranges were also relatively low, which results in the errors having a larger effect on the regression analysis. The calibration is also known to be size dependent, and since significant variation in particle size was observed this is likely to have introduced further scatter. Finally, the calibration is dependent on optical characteristics of particles, and at the Clyde anchor site there was significant variation in chlorophyll concentration, and hence composition of the particle population.

These factors will all contribute to random errors in the calibration equation. There is a further issue that needs to be considered in interpreting the beam attenuation measurements in the presence of coarse particles. As discussed in Chapter 2 transmissometers are designed to measure the beam attenuation caused by relatively fine particles. If coarse particles are added to a population

of fine particles then forward scattering at small angles by the coarse particles will effectively render the instrument "blind" to the resulting increase in mass concentration. Figure 2.5 shows that for particles with a diameter of 80 μm approximately 91% of the total scattered light falls within a 1° angle. As the SeaTech transmissometers have an acceptance angle of 1° and a significant and varying proportion of the size distribution was coarser than 80 μm then observed transmissometer profiles will almost certainly have been influenced by this forward scattering effect.

Figure 7.1 shows the relationship between beam attenuation measured by transmissometer and the volume concentration of particles finer than 78.45 μm for the northern North Sea and 109.07 μm for the Clyde anchor site. It is clear that beam attenuation correlates well with volume concentration of fine particles at both sites.

In general, in low energy shelf sea environments the coarse particle population will have a low settling velocity and hence low density (otherwise they could not be maintained in suspension). The fine part of the population will have the highest density and therefore be the dominant component of the mass concentration. Provided that coarse particle volume concentrations are relatively low, the transmissometer measurements will then be representative of actual mass concentrations. If there is a significant coarse particle component which remains in constant proportion to the fine particle component then this component will have a systematic influence on the calibration coefficient for the transmissometer by reducing the measured beam attenuation for a given mass concentration, but calibrated concentrations will still be representative of actual mass concentrations. However if the proportion of large particles varies significantly then the transmissometer will measure an apparent variation in mass concentration which is not representative of the actual concentration: moreover further scatter will be introduced into the calibration. For example, if fine particles are converted to coarse particles by aggregation then the instrument will record a reduction in mass concentration when in fact it remains constant. All data discussed here indicate significant, and significantly varying,

concentrations of large particles, therefore variation in mass concentrations indicated by the transmissometer should be treated with caution. The transmissometer calibrations presented in Chapters 5 and 6 can thus only be used to estimate average mass concentrations at any site.

7.4. A simple aggregation model.

Before discussing the observed variations in particle diameter at the two sites a theoretical framework will be described which will allow some quantitative analysis of the results. However it should be noted that as observed mean particle diameters and volume concentrations are only, at best, proportional to the true values, it will not be possible to generalise quantitative results or apply them to other areas.

Recent developments in flocculation theory have allowed models of floc formation and break up to be formulated. Kranenburg (1994) proposed that flocs can be treated as self-similar fractal entities produced by sticking together a number of primary particles, which may be single mineral grains or stable microflocs. The fractal dimension, n_f, is obtained from the description of a growing object with diameter $D = LD_p$ and volume $V(LD_p)$, where D_p is the diameter of the primary particle (Vicsek, 1992). Assuming that $D_p = 1$, $V(L) \alpha N(L)$, where N is the number of primary particles. The fractal dimension n_f is defined as:

Equation 7.1.
$$n_f = \lim_{L \to \infty} \frac{\ln(N(L))}{\ln(L)}$$

From this approach it follows that the differential (or excess) density $\Delta\rho_f$ of mud flocs is given by (Kranenburg, 1994):

Equation 7.2.
$$\Delta\rho_f = \rho_f - \rho_w = (\rho_s - \rho_w)\left[\frac{D_p}{D}\right]^{3-n_f}$$

where ρ_f, ρ_w and ρ_s are the densities of the mud flocs, the (interstitial) water and the sediment (primary particles), and D and D_p are the diameters of the flocs and of the primary particles. Typical values of n_f for flocs of cohesive sediment in the water column of estuarine and shelf environments are in the range $1.4 < n_f < 2.2$, with an average value $n_f = 2$ (Kranenburg, 1994; Winterwerp, 1998). From Equation 7.2 it follows that the relation between the mass concentration c, the volumetric concentration ϕ and the number concentration of flocs N_v of the suspended sediment is:

Equation 7.3.
$$\phi = \left(\frac{\rho_s - \rho_w}{\rho_f - \rho_w}\right)\frac{c}{\rho_s} = \frac{c}{\rho_s}\left[\frac{D}{D_p}\right]^{3-n_f} = f_s N_V D^3$$

where f_s is a shape factor (= $\pi/6$ for spherical particles). The settling velocity W_s for flocs with a fractal structure can be obtained from a balance between gravitational and drag forces as (assuming spherical particles):

Equation 7.4a.
$$W_s = \frac{(\rho_s - \rho_w)g}{18\mu} D_p^{\,3-n_f} \frac{D^{n_f-1}}{1+0.15\mathrm{Re}^{0.687}}$$

For massive, single spherical grains ($n_f = 3$) with $R_e << 1$ this equation simplifies to the well known Stokes' Law:

Equation 7.4b.
$$w_s = \frac{(\rho_s - \rho_w)gD^2}{18\mu}$$

Using this approach, and applying a number of simplifying assumptions, a simple flocculation model has been proposed by Winterwerp (1998) based on aggregation via a collision frequency function and disaggregation via a floc breakup formulation. Collision frequency is controlled by particle concentration and one of three possible mechanisms: Brownian motion, differential settling of larger particles relative to smaller ones and turbulent motion (van Leussen, 1997). One of the major assumptions in the model is that Brownian motion and differential settling are much less important than turbulence. It is widely

accepted that flocculation due to Brownian motion is negligible in estuaries and shelf seas. It has been argued that aggregation by differential settling may be important during phytoplankton blooms in the open ocean, however recent theoretical analysis indicates that the effect of differential settling in the marine environment is much smaller than that due to turbulent motions as small particles tend to be deflected around larger particles as they settle (Stolzenbach & Elimelich, 1994). Floc breakup can be caused by turbulent shear or by self generated shear as the particle settles through the water column (Hill, 1998). This model assumes a simple break up formulation based on turbulent shear alone.

Both the floc breakup and the aggregation processes can be related to the dissipation parameter *G*, defined as:

Equation 7.5.
$$G = \sqrt{\frac{\varepsilon}{\nu}} = \frac{\nu}{\lambda_o^{\,2}}$$

in which ε is the turbulent dissipation rate per unit mass, ν is the kinematic viscosity of the suspension, and λ_0 is the Kolmogorov micro-scale of turbulence: $\lambda_0=(\nu/\varepsilon)^{1/4}$. *G* is a measure of the turbulent shear of the flow, and ε is calculated from the turbulent dissipation rate measured by the FLY profiler (E, Wm^{-3}) as $\varepsilon = E/\rho_w$. Using established flocculation formulations and a new simplified floc break up function, Winterwerp proposed that the differential equation for the diameter of cohesive particles under the influence of turbulent shear is:

Equation 7.6.
$$\frac{dD}{dt} = k_A c G D^{4-n_f} - k_B G^{q+1}(D - D_p)D^{2q+1}$$

where:

Equation 7.7.
$$k_A = \frac{3e_c \pi e_d}{2f_s}\frac{D_p^{n_f-3}}{n_f \rho_s}\ ,\quad k_B = \frac{ae_b}{n_f}D_p^{-p}\left(\frac{\mu}{F_y}\right)^q$$

where e_c is an efficiency parameter accounting for the fact that not all collisions will result in coagulation, e_d is an (efficiency) parameter for diffusion, e_b is an (efficiency) parameter for floc breakup, μ is the dynamic viscosity of the

suspension, F_y is the floc strength and a, p and q are parameters to be established empirically. The first and second terms on the right hand of Equation 7.6 are floc growth and break-up terms, respectively: it is assumed that both processes can be combined linearly and occur simultaneously. The parameter k_B is dimensional as it includes the primary particle size D_p, the suspension viscosity μ and the floc strength F_y; however, these are known so poorly that they are lumped into one empirical parameter. Winterwerp argued, using evidence from several experimental studies, that it was reasonable to assume $n_f = 2$, $p = 1$ and $q = 0.5$, which allows an analytical solution to Equation 7.6. Setting dD/dt = 0 and rearranging, an equilibrium floc size, D_e, is obtained:

Equation 7.8. $$D_e = D_p + \frac{k_A c}{k_B \sqrt{G}}$$

Characteristic time scales for particles to reach their equilibrium diameter can also be determined. In estuaries these range from a few minutes at maximum tidal flow to several hours at slack water (Winterwerp, 2002), in low concentrations on the shelf they may be much longer.

It should be noted that the aggregation process produces a distribution of particle sizes, rather than a single diameter D used in the model. However, it is reasonable to consider D as a characteristic floc size, which can be taken as the median or mean size of the distribution. Also the model describes processes in a Lagrangean reference frame. It has also been translated into a Eulerian coordinate system and applied in a numerical model of estuarine sediment transport (Winterwerp, 2002).

7.5. Northern North Sea

7.5.1 Overview

Temperature, salinity, transmission and particle size measurements were made at a site in the northern North Sea during autumn 1998 (Figure 5.1). The water column was stratified into two layers, a warmer, less saline and lower SPM

concentration surface mixed layer (SML) over a cooler, more saline and higher SPM concentration bottom mixed layer (BML). The layers were well defined with a small transitional region of approximately 10 to 20 m thick. This transitional region occurs in the same place in the water column for all parameters.

As Figure 5.2 shows, during the study period a number of storms passed over the study site resulting in wind speeds in excess of 15 m s^{-1}. During the calmer periods between these storm events the wind speed rarely dropped below 10 m s^{-1}. As a result of this constant wind forcing waves with large heights and long periods were present on several occasions (Figure 5.3). Maximum spring tide occurred on Day 293 and neap tide occurred on Day 300.

Figure 5.5 shows that the depth of the thermocline increased by 15 m from day 290 to 294 when it began to reduce again. At the beginning of the sediment sampling period (day 299) the thermocline was approximately 50 m above the bed, 10 m below where it had been 10 days previously. Between days 290 and 302 the temperature of the surface layer decreased by 2.5°C, a result of the wind and wave induced mixing and reduced air temperatures.

7.5.2 Suspended Particulate Matter

Both the SPM concentration measured by the transmissometer (Figure 5.10) and the total volume concentration of SPM as measured by the LISST (Figures 5.11 & 5.14(i) – 5.18(i)) were higher below the thermocline than above it. Prior to the measurements made with the LISST, which began on day 299, an apparent minimum in the SPM concentration was observed between 40 and 60 metres above the seabed (Figure 5.10). From day 299 this decrease in SPM concentration was not as pronounced but it can still be seen in the SPM concentration profiles in Figure 7.2.

This minimum in mass concentration of SPM towards the top of the thermocline region was not, however, accompanied by a minimum in total volume concentration of SPM (Figures 5.14(i) - 5.18(i)). In all cases the total volume

concentration of SPM actually increased throughout the thermocline with a broad maximum within the thermocline and large spikes occurring towards the top of the thermocline region. The spikes indicate the presence of a layer of very large particles concentrated at the top of the thermocline which are superimposed on a more gradually varying population. As these spikes may not be statistically representative of actual concentrations (section 7.2) they will not be considered in the following interpretation.

There was also a marked vertical variation in the size distribution of the SPM. The mean size, as measured by the LISST, showed a two layer structure with smaller mean sizes occurring above the thermocline. Towards the top of the thermocline the mean size increased by c. 20 μm in a majority of casts with a broad maximum in mean size within the thermocline. From the base of the thermocline towards the seabed mean size decreased gradually becoming similar to that observed in the surface layer or slightly larger than it. Note that, as discussed in section 7.2, the variations in mean size presented here must not be treated as absolute quantitative values but rather as a quantitative indication of relative changes in the size distributions.

Splitting the total volume concentration measured by the LISST into particles less than 78.45 μm and particles greater than 78.45 μm (Figure 7.3 & Figure 7.4) it can be seen that the minimum observed in the mass concentration of SPM is also observed in the volume concentration of particles less than 78.45 overall. This is because the change in the fine particle volume concentration is swamped by an increase in the coarse particle (> 78.45 μm) volume concentration.

To summarise, there is evidence of a reduction in small particle concentrations and an increase in large particle concentrations, and hence an increase in mean particle size, in the thermocline region. As discussed in Chapter 2 and section 7.4 turbulence can stimulate both floc growth and floc break-up with the final size of the aggregate being governed by the destructive properties of the turbulence field and the mass concentration of the suspension (van Leussen,

1997; Winterwerp, 1998). Thus, suspended particles in the surface layer attain an equilibrium floc diameter determined by mass concentration and turbulence levels. As they settle into the top of the thermocline they enter a region of reduced turbulence (Burchard *et al.*, 2002; Knight *et al.*, 2002; Figure 5.5). As energy dissipation is low within the thermocline region, i.e. mixing within the thermocline is less than mixing outside of the thermocline, larger flocs are able to form as they will not be broken up by the weaker turbulent eddies. As turbulence increases again in the near bed region (Burchard *et al.*, 2002; Figure 5.5) the large flocs formed within the thermocline are broken up, producing a reduction in mean diameter and the corresponding variations in coarse and fine particle volume concentrations shown in Figure 7.3 and Figure 7.4.

The formation of larger flocs within the thermocline would result in an increase in the total volume concentration as well as an increase in the mean particle size. Total volume concentration would be expected to increase, if mass concentration remained constant, because flocs consist of a certain proportion of water resulting in a larger volume than the total volume of all their constituent particles. Similarly floc break up in the near bed region would be expected to produce a reduction in total volume concentration towards the sea bed. Both of these changes are observed in the data.

Although an average dry particle density could not be determined for the thermocline region, it was estimated for the surface and near-bed regions (Table 5.2) using the total volume concentration measured by the LISST. The results are consistent with the presence of flocculated particles (i.e. densities are much lower than typical values for single mineral grains) and indicate no significant difference between the surface and near-bed populations. As the distributions and total volume concentrations are also similar between the surface and near-bed regions (Figure 5.11 & Figure 5.12) it is reasonable to assume that there was little vertical variation in particle composition. If it is further assumed that the observed variation in particle diameter was due to aggregation and disaggregation of the same population of particles, then the simple model described in section 7.3 can be applied. Mass concentration can then be estimated from the total volume concentration and mean grain diameter

using Equation 7.3. It is important to stress that the absolute values calculated may not correspond to true concentrations, as both measured mean diameter and volume concentrations are only proportional to their true values and moreover it is not known what the primary particle diameter D_p, density ρ_s or fractal dimension n_f, should be. However, if we assume $n_f = 2$ then we can use mass concentrations determined by gravimetric analysis to estimate the average product ($\rho_s D_p$, calculated by using Equation 7.3 and then obtaining an average over all samples, Table 7.1). Figure 7.5 shows mass concentrations calculated using the average of $\rho_s D_p = 0.0168$ kg m^{-2} plotted against gravimetric concentrations from surface and near bed. There is clearly a very high degree of scatter associated with this estimate, however calculating mass concentration should at least indicate relative variation around an approximate average through the water column. Figure 7.6 shows mass concentration profiles calculated for each of the observation periods. It is clear that total mass concentrations indicated by the LISST do not exhibit a minimum at the thermocline during this part of the study period, and appear to be more or less uniform in the upper and bottom mixed layers respectively (disregarding the influence of large spikes in the coarse particle volume concentration), with significantly higher mass concentrations in the bottom mixed layer. Varying n_f between accepted limits of 1.4 - 2.2 (the only parameter in Equation 7.3 which may affect the relative variation) does not contradict these conclusions. The mean mass concentrations determined by gravimetric analysis (Table 7.1) show the same difference between surface and bottom layers, but this difference is not statistically significant, probably because of the small sample size and the high errors associated with gravimetric analysis.

Although the mass concentration of SPM is significantly greater in the bottom layer compared with the surface layer it is not a gradual increase, rather a sudden change that occurs at the base of the thermocline. This, with the energy dissipation measurements, confirms that there is little mixing between the surface and bottom layers through the thermocline and therefore most of the particles within the thermocline will have originated from the surface layer.

Profiles of turbulent dissipation rate were measured at the site over a 24 hour period on day 299, enabling further analysis of the particle size variation observed on that day in terms of the aggregation model described in section 7.4. Figure 5.5 shows profiles of average turbulent dissipation rate and temperature for the 12.5 hour period centred on 299.3.

Figure 7.7 shows mean grain diameter plotted as a function of the turbulent dissipation rate E. It is clear that diameter is, in general, lower at high E and higher at low E but there are differences in the relationship above and below the thermocline. This could be because of the differences in mass concentration in the two layers, as concentration also influences equilibrium particle size (Equation 7.8). To include this, Figure 7.8 shows mean diameter plotted against $c/\sqrt{(G)}$ where c = mass concentration estimated using Equation 7.3 and G is the turbulent dissipation parameter, calculated from E using Equation 7.5.

It is clear that a good linear relationship ($R^2 = 0.90$) is obtained, which provides strong evidence to support the assumptions underlying the aggregation model. In other words, turbulence is the primary control of mean grain diameter during this observational period. Moreover, grain diameter was in equilibrium with local values of both turbulence and mass concentration, which suggests either short time scales for flocculation or relatively stable physical conditions within the water column at this time. For equilibrium to be maintained settling velocities must be relatively slow, or flocculated particles will settle rapidly out of their equilibrium positions.

A schematic of the process described above is shown in Figure 7.9. If this model is correct, then settling velocities of particles in the thermocline will be faster than those in the surface (SML) and near bed (BML) mixed layers. If the supply from the SML remains constant then this will eventually produce a mass concentration minimum in the thermocline. Although Figure 7.6 does not indicate that this is the case for days 299 – 310 when the apparent mass concentration minimum observed by transmissometer was relatively small, it may have been the case during the period before day 299. The longest time

series was obtained using a transmissometer, and it has been established that this instrument measures variation in fine particle concentrations. Figure 5.10 indicates a pronounced minimum in fine particle concentrations in the thermocline between day 289 – 299.

There are some other interesting features in the transmissometer data. In the SML high fine particle concentrations were observed on days 289.5, 291, 294.5 and 301.5. These correspond with periods of high wind, high wave height and long wave period (Figures 5.2 & 5.3). There are two possible explanations for a localised increase in fine particle concentrations in the SML: entrainment from beneath the thermocline, and increase of fine particle concentrations due to floc break-up. The thermocline did deepen between days 298.5 and 292 but there were very low fine particle concentrations within the thermocline at this time. Therefore it must be concluded either that large particles were entrained from the thermocline and then broken up or that flocs present in the SML were broken up, the mechanism being increased turbulence levels due to surface waves during these times.

In the BML high near bed concentrations were observed on day 289.5, day 294-298 and day 301.5 (Figure 5.10). Maximum wave heights of 4.5 m and wave periods of 6.5 seconds were observed during these times, but this produces a wavelength of 56m (using $\lambda = gT^2/2\pi$, where λ is the wavelength and T is the period, Soulsby (1997)). Since the water depth is significantly greater than half this wavelength, it is unlikely that surface waves would have influenced particles in the BML.

Lowest fine particle concentrations were observed around the spring tide (day 293), but Figure 5.4 indicates that current velocities in the BML were dominated by inertial currents at this time rather than the spring/neap cycle. From day 294 - 299 the largest inertial currents measured during the PROVESS campaign in the northern North Sea were present (Knight *et al.*, 2002), resulting in high current velocities in the BML (Figure 5.4). High BML current velocities were also observed on days 289.5 - 291, part of day 299, and 301.5. On all of these

occasions (except the first part of day 299 when transmissometer data were unavailable) higher fine particle concentrations were observed in the BML.

It seems that higher fine particle concentrations in the BML were associated with higher turbulence in the BML due to higher velocities. Except on day 301.5, when particle size data were available, it is not possible to state to what extent these were obtained by local resuspension due to increased bed shear stress or by enhanced break up of flocs in the BML. On day 301.5 mass concentrations calculated from LISST data were higher than on day 299.5, but slightly lower than on day 305.9 when current velocities were relatively low (Figure 7.6). Also the profile does not show an increase in mass concentration towards the bed, which would be expected for resuspension of rapidly settling particles. Therefore there is no consistent evidence for local resuspension during the study.

From day 299 it is possible to interpret further changes in mass concentration calculated using Equation 7.3. Lowest mass concentrations and largest mean sizes were observed on day 299.5 (Figure 5.13), coinciding with neap tide and much reduced wind conditions. In the SML mass concentrations increased from 0.6 mg l^{-1} on day 299.5 to 0.8 mg l^{-1} on day 306 (Figure 7.6), and continued to increase, to a maximum of 0.9 mg l^{-1} on day 310. In the BML mass concentrations were lowest (0.8 mg l^{-1}) on day 299.5 and then generally increased to a maximum of 1.25 mg l^{-1} on day 310. This general trend in mass concentrations contrasts with the more episodic changes in fine volume concentrations recorded by the transmissometer. The increase in the SML could be due to entrainment from the BML as the thermocline weakened: the increase in the BML is not apparently related to local variation in physical conditions and implies a gradual increase due to advection of material resuspended from shallower water.

7.5.3 Summary

Observations of particle size distribution, volume concentrations and turbulent dissipation rate at a stratified site in the northern North Sea have provided direct evidence, for the first time, that turbulence controls equilibrium floc diameter in the marine environment. The observations appear to be well explained by a simple aggregation model which predicts equilibrium diameter as a simple function of turbulent dissipation rate and total mass concentration, with diameter increasing either as turbulent dissipation reduces or as mass concentration increases. However there are several reasons why this good agreement is surprising. First, the model was developed for application to high concentration estuarine suspensions, whereas this data set exhibits very low concentrations. Second, the instrument used to measure volume concentrations and mean particle diameter is constrained within a particle size range which was almost certainly exceeded by the actual population measured, and therefore both volume concentration and mean diameter can only be considered as proportional to the true values. Finally the results indicate that particles were at their equilibrium diameter throughout the water column during the 24 hour period for which turbulence and particle size measurements were available, yet transmissometer and current meter observations over longer time scales indicate considerable variation, and therefore potential for time lags between turbulence and diameter if, as is likely in this low concentration environment, long time scales for flocculation are involved.

Another somewhat surprising conclusion is that mass concentrations remained relatively uniform in the near bed region (Figure 7.6) even though transmissometer data indicated increasing mass concentrations towards the sea bed (Figure 7.2). The discrepancy is explained by the fact that the transmissometer is most sensitive to fine particles, and therefore records a reduction in particle diameter, due to increased turbulence in the near bed region, as an increase in mass concentration. For the period where particle size data were available, there was no evidence of local resuspension (which should produce increasing mass concentrations towards the source) at the site.

Transmissometer data indicated that there were increased fine particle concentrations in the SML during periods of high winds, wave heights and wave periods, due to break up of flocs by enhanced levels of turbulence at these times. They also indicated increased fine particle concentrations in the BML during periods of high BML current velocity which could have been due to break up of flocs.

7.6. Clyde Sea

7.6.1 Overview

Measurements were taken at one station (Clyde anchor site) inside the sill within the Clyde Sea system over a period of 24 hours. The water column was well stratified with the top of the thermocline occurring at approximately 50 m above the seabed and the base occurring at 30 m above the bed. The surface layer consisted of warmer, less saline water compared to the bottom where the temperature was 2.5°C cooler and the salinity was slightly greater.

Measurements were taken at half-hourly intervals and consisted of temperature, salinity, fluorometry, turbulent dissipation rate, transmittance and suspended particle size distributions. Turbulence measurements were made prior to and over the full 24 hours but all data collected during the 24 hour study were rejected due to problems with the FLY probe.

Prior to the 24 hour study period an ADCP moored close by (Figure 6.1) showed that the current speeds, which are tidally dominated, were beginning to decrease towards neap tides. During the previous neap tide the ADCP measured current speeds of approximately 0.2 m s^{-1} (Figure 6.3).

7.6.2 Fluorometry

The fluorometry measurements (Figure 6.9) show higher chlorophyll concentrations above the thermocline than below it with a chlorophyll maximum at the base of the SML. This indicates that the SML may have become nutrient depleted so that phytoplankton are exploiting the higher nutrient levels, and

sufficient light levels, just within the thermocline (e.g. Fransz & Gieskes, 1984). Beneath this, however, there was a pronounced minimum in chlorophyll concentration within the thermocline region, with moderate concentrations in the near bed region. This feature will be discussed further in section 7.8.

7.6.3 Suspended Particulate Matter

Mass concentration of SPM measured by the transmissometer, which is indicative of fine particle concentration, (Figures 6.5 & 6.11) clearly shows a three layered structure with the surface mixed layer (SML) extending to the top of the thermocline, the middle layer occurring within the thermocline and the bottom mixed layer (BML) occurring from the base of the thermocline to the seabed.

The BML exhibits the key characteristics of tidal resuspension with maximum mass and volumetric concentrations (Figures 6.11 & 6.12) occurring near bed approximately every six hours. During the periods of maximum resuspension the SPM is mixed throughout the whole of the bottom layer. These incursions of increased SPM concentration higher into the water column coincide with the movement of the base of the thermocline, halocline and pycnocline to higher positions in the water column.

Throughout the whole 24 hour period fine particle concentrations in the SML remained approximately constant and low in comparison with the BML (Figure 6.15). The few high concentration spikes at the surface are likely to be air bubbles.

A marked minimum in fine particle concentration measured by the transmissometer and the LISST persisted at the base of the thermocline throughout the full 24 hour cycle (Figures 6.11, 6.15 & 7.10). This is similar to that observed in the northern North Sea, especially for the period before day 299. At the Clyde anchor site there was a corresponding minimum in chlorophyll concentration (Figure 6.9). There was also a maximum in mean particle size (Figure 6.14) and an increase in total volume concentration which began

abruptly at the top of the thermocline and continued throughout the bottom layer (Figure 6.12). As some of these features are similar to those observed in the northern North Sea it is possible that they are caused by the same process which is described in Figure 7.9.

From the increase in mean particle size (Figure 6.14), the observed decrease in volume concentration of particles less than 109.07 μm (Figure 6.15) and the effective dry particle densities presented in Table 6.1 it can be concluded that particles settling into the thermocline region form larger flocs. The densities calculated in Table 6.1 are likely to be incorrect as the larger particles are not measured by the LISST, however the values calculated are within the range measured by Fennessy *et al.* (1994) and other investigators (Gibbs, 1985; McCave, 1975; McCave, 1984; Alldredge & Gotschalk, 1988) who have calculated effective densities ranging between 0.1 kg m^{-3} to 1000 kg m^{-3}. The calculated densities show significant differences, with maximum density in the BML and minimum density in the thermocline.

If, as for the North Sea site, it is assumed that the vertical variations in mean diameter and volume concentration can be explained by flocculation/break-up of the same SPM population then Equation 7.3 can be used to estimate mass concentration from the LISST data and gravimetric samples. For the Clyde study samples for gravimetric analysis were obtained from surface, near bed and within the thermocline (Table 6.1): lowest concentrations were obtained within the thermocline and highest concentrations were obtained near bed. Table 7.1 shows the results of calculating the average product ($\rho_s D_p$) from these mass concentrations for SML, thermocline and BML respectively. It is clear that rather different estimates are obtained for the BML: Figure 7.11 shows mass concentrations calculated from Equation 7.3 using the average value of $\rho_s D_p$ over both the SML and thermocline (0.0235 kg m^{-2}) (Table 7.1) plotted against gravimetrically determined concentrations. Reasonable agreement is obtained for the upper part of the water column but in the BML the calculated concentration is clearly less than that measured directly, especially during periods of high concentration associated with tidal resuspension. This indicates

that there is a different, higher density, component of SPM in the BML which must be considered separately from the flocculated population settling from the surface layers. This observation is consistent with a predominantly inorganic population subject to local resuspension from the sea bed. This is further supported by examination of the size distribution of near bed samples (Figure 6.13): in the BML the mean size of the fine part of the population was considerably larger (~24 μm) than in the upper part of the water column (~15 and 16 μm respectively).

It is clear that applying Equation 7.3 to the Clyde data will underestimate mass concentrations calculated in the near bed region. However Figure 7.11 indicates that variation occurring in the surface and thermocline regions, and at certain times in the BML, can be adequately described using this approach. Figure 7.12 shows mass concentrations estimated over the study period from mean diameter and total volume concentration profiles using $\rho_s D_p = 0.0235$ kg m^{-2}. In contrast to the profiles calculated for the latter part of the northern North Sea site, a mass concentration minimum is indicated by the LISST data as well as by the transmissometer and gravimetric samples, although it is not as pronounced. There is also a clear increase in mass concentration towards the bed, despite the fact that this is an underestimate of the true near bed values, which confirms the presence of local resuspension at this site and again contrasts with the North Sea data.

Given the preceding discussion the simple flocculation model described in section 7.2 would not be expected to fully explain the observed variation in mean diameter throughout the water column at the Clyde anchor Site. There was a further problem: only one good turbulence profile was obtained just before the 24 hour LISST profiling period commenced. Since considerable tidal variation in turbulent dissipation would be expected (and considerable variation in LISST data was found) it was important to match this data with an appropriate LISST profile, rather than use a tide average. This was done by matching the time relative to high water and the temperature profile measured by the LISST and the FLY: the best correspondence was found for the cast deployed 11 hours after the FLY data was obtained (at 1 hour after high water).

Figure 7.13 shows mean grain diameter plotted against turbulent dissipation rate for this cast. As for the North Sea site, high mean grain diameter is found at low dissipation and vice versa, but there is a marked hysteresis in the profile. Figure 7.14 shows mean grain diameter plotted against $c/\sqrt{(G)}$ where c = mass concentration estimated using Equation 7.3 and G is the turbulent dissipation parameter, calculated from E using Equation 7.5. There is a reasonable straight line relationship for the SML and thermocline data with slightly more scatter than that obtained in the North Sea (R^2 = 0.85). However in the BML mean diameter is much smaller than the flocculation model predicts. In fact, since the value of c used has been shown to be an underestimate the data points should lie even further away from the trend line.

Therefore it can be concluded that the simple aggregation model can be applied to explain the variations in concentrations and size of SPM in the SML and thermocline at this site, but that in the BML the model breaks down as the flocculated population is joined by a higher density resuspension population. There are other reasons why the model may not be expected to work at this site. First, significant tidal variation in turbulent parameters would be expected (Inall & Rippeth, 2002) and significant variation in mass concentration was observed in the BML. Therefore the changing particle population would need time to respond to changes in the turbulence field and may well not reach its' equilibrium diameter. A time series of both turbulent dissipation rate and SPM volume concentration/size profiles would be required in order to investigate this problem.

7.6.4 Summary

Observations of particle size distribution, volume concentrations and turbulent dissipation rate at a stratified site in the Clyde Sea have provided further evidence to support the finding at the northern North Sea site that turbulence controls equilibrium floc diameter. Observations made in the surface mixed layer and thermocline regions appear to be well explained by a simple aggregation model which predicts equilibrium diameter as a simple function of

turbulent dissipation rate and total mass concentration, with diameter increasing either as turbulent dissipation reduces or as mass concentration increases.

Once these particles settle into the BML the larger flocs are broken up as turbulence increases towards the bed. The observations also indicate that the settling population is combined with another population resuspended locally from the sea bed which has higher density than the population originating in the SML and which produces increasing mass concentrations towards the bed.

7.7 Comparison of the northern North Sea and Clyde Sea

In Sections 7.5 and 7.6 it has been concluded that enhanced aggregation occurred within the thermocline at both the North Sea and Clyde Sea sites, producing larger flocs. As these settled into the BML the larger flocs broke up, producing an increase in fine particle concentrations and decrease mean grain diameter towards the bed. Fine particle concentration was defined as the volume concentration of particles less than 78.45 μm for the North Sea and 109.07 μm for the Clyde.

The observations discussed in Sections 7.5 and 7.6 indicate that particle size is controlled by a combination of turbulence and mass concentration at the two sites. The relationship is particularly well defined at the northern North Sea site and this represents the first direct evidence for such a control. For example Hill *et al.* (2001) propose that flocs are rarely broken by turbulence. Their argument is that observations fail to identify turbulence as the primary determinant of particle size: the results presented here therefore represent an important contribution to the field. At the Clyde anchor site there was evidence of an additional higher density SPM population in the BML which could not be accounted for using a simple equilibrium model. It has not been possible to conclude from this data set whether turbulence controls particle size in the benthic boundary layer when resuspension is occurring.

This model first assumes that mass concentration can be calculated from volume concentration and mean grain diameter (Equation 7.3). The product ($\rho_s D_p$) was estimated from gravimetric samples obtained at each site (Table 7.1). Although these estimates are almost certainly in error as the total volume concentration and mean grain diameter are underestimates, it is worth checking that they are reasonable. First a minimum value of D_p can be estimated by assuming that ρ_s will not exceed that of a single mineral grain (2650 kg m^{-3}). However, in shelf sea environments it is unlikely that the primary particles will be single mineral grains: generally it has been found that SPM populations comprise stable "microflocs" of modal diameter 5 - 15 μm which form the building blocks of organo-mineral aggregates (Eisma & Kalf, 1987; Jago & Jones, 1998; Jones *et al.*, 1998). If a value of D_p based on the modal diameter (15 μm) of the fine particle size distribution at both sites is assumed then the density of these microflocs can be estimated. Table 7.2 presents the results of this analysis for each site, including single grain and modal microfloc values of D_p. Winterwerp (1998) used a single grain D_p = 4 μm, so the values estimated here for single grains are not unreasonable. The estimated microfloc densities also fall within the published range (ρ_f lies between 1001 – 2000 kg m^{-3}, e.g Gibbs, 1985; McCave, 1974, 1984; Alldredge & Gotschalk, 1988; Fennessy *et al.*, 1994). The product (ρ_s D_p) is about 40% larger for the Clyde Sea than for the North Sea, even in the upper part of the water column, which suggests either larger primary particle diameter or larger microfloc density at this site, or both. Given that it is shallower, closer to the coast and higher energy this is not surprising. In the BML the product is 50% larger again than in the upper part of the water column: the "microfloc" density here is quite close to that of single mineral grains which supports the argument that there are significant proportions of an additional high density resuspended population in the BML at this site which does not conform to the simple aggregation model.

The model, where it applies, predicts a straight line relationship between equilibrium mean grain diameter and the product ($c/\sqrt{G}$), Equation 7.8. Regression parameters obtained for the North Sea and Clyde sites have been presented in Table 7.3. It is not possible to apply the regression constants

generally because of the uncertainties in measuring D and ϕ. For the North Sea site the slope, which corresponds to the ratio k_A/k_B (Equation 7.8) is 0.003 m^4 kg^{-1} $s^{-0.5}$, which is ~3 times higher than that calculated by Winterwerp (1998) from experiments using estuarine mud. This seems to be surprisingly good agreement, with the increase indicating perhaps that sticking efficiency (incorporated within k_A) is greater in the shelf environment. This seems reasonable considering that these particles are likely to have a higher organic component. For the Clyde Sea the slope is 0.046 m^4 kg^{-1} $s^{-0.5}$, about 15 times more than for the North Sea and ~50 times more than Winterwerp's value. There was more phytoplankton in the Clyde, but there is also more uncertainty in the turbulence data, so it is probably not worth speculating further on this difference.

The intercepts should represent the primary particle diameter D_p. Both intercepts are much higher than would be expected if the primary particles originated from the fine part of the SPM population. For the North Sea site the predicted D_p is 191 μm, which is ten times greater than would be expected if it is assumed that the primary particles involved in the aggregation process comprise the fine part of the observed distribution. For the Clyde it is 57 μm which is smaller than for the North Sea but still almost three times more than would be expected. However, D_p of sizes ranging up to 80μm have been observed using a camera assembly by Hill *et al.* (2001) and Agrawal & Traykovski (2001). These particles are not typical primary particles consisting of one particle but are very strong microflocs that have a n_f value of 3 (Agrawal & Traykovski, 2001). Therefore the primary particle size observed in the Clyde of 57μm may actually be a true representation of D_p at this site.

As already stated the uncertainties associated with calculating the parameters used in Equation 7.8 could well introduce uncertainty in the regression parameters, and the apparent overestimation in D_p may be a result of this. The model may also represent an oversimplification, neglecting processes which may effectively increase equilibrium particle size. It is just possible that the aggregation process being observed at these sites was occurring only in the

coarse part of the distribution, with large sticky organic particles forming the primary particles, a situation that has been observed on the North American shelf by other investigators (Agrawal & Traykovski, 2001). This would certainly explain the strongly bimodal nature of the size distributions obtained. However, more accurate determination of the coarse particle distribution would be needed to explore this further.

Further explanations for the apparent overestimation of D_p include the hypothesis that D_p may not be constant throughout the water column. This would result in the intercept and slope of the lines in Figure 7.8 and Figure 7.14 changing for each depth. Given the current data it is not possible however to comment on this further.

In the northern North Sea analysis of volume concentrations and mean particle diameter indicated there was no mass concentration minimum at the thermocline after day 299. Therefore the apparent mass concentration minimum recorded by the transmissometer is likely to be a response to the increase in size and the affect that size has on the beam attenuation. Agrawal & Traykovski (2001) observed a similar effect on the transmissometer during a storm event on the North American continental shelf where a decrease in particle size resulted in an apparent increase in mass concentration which did not actually occur.

In the Clyde Sea the pronounced mass concentration minimum indicated by the transmissometer data (approximately a factor of 4 times larger than that in the latter part of the North Sea data set) did appear to reflect a true mass concentration minimum, although it was exaggerated due to the sensitivity of the transmissometer to fine particles. A similarly pronounced minimum was observed in the North Sea during days 290 - 299.

It remains to explain the mass concentration minimum in the thermocline indicated by these observations. This can be explained if the larger floc diameter obtained in the thermocline results in a larger settling velocity. This will produce a net difference between mass flux of slow settling particles into the

thermocline and mass flux of fast settling particles into the BML. Provided that conditions are maintained this will eventually produce a minimum in mass concentration within the thermocline region.

If this process was occurring at the Clyde and North Sea sites then significant differences in settling velocity between the SML and thermocline region should be observed. There are two possible approaches in determining settling velocity. The first is to follow the approach adopted by Mikkelsen & Pejrup (2001) and use mean grain diameter and effective densities from Table 6.1, in conjunction with Stokes' Law (Equation 7.4b). The second is to adopt the fractal approach and use Equation 7.4a (neglecting the Reynolds term), using estimated values of ρ_s and D_p from Table 7.2. Once again it should be noted that all of these will only be estimates, due to uncertainties in the quantities used to calculate them. Table 7.4 shows the calculated characteristic settling velocity for surface, near bed and thermocline populations using these two different methods. Table 7.5 shows the corresponding settling velocities calculated using Stokes' Law just for the fine particle population at the Clyde site. These represent estimates of the settling velocity of the primary particles at this site, and indicate a clear increase in the BML which further supports the argument that there was an additional resuspended population at this site.

Table 7.4 indicates a range of possible settling velocities depending on the approach used. Maximum settling velocities, of between 1.4 - 3 mm s^{-1} were obtained using Stokes' Law and average effective floc density. This corresponds to between 120 – 250 m day^{-1}. However at this settling rate it is unlikely that flocs would remain in the thermocline for long enough to change their size significantly. The range estimated using the fractal approach and a 15 μm microfloc diameter produces the lowest values, 0.14 – 0.9 mm s^{-1} or 12 – 74 m day^{-1}. These seem to correspond better with shelf sea values quoted in the literature (e.g Hill, 1998; Jones *et al.*, 1998; Jago *et al.*, 2002) and those obtained using the Manning & Dyer (1999) multiple regression equation (Table 7.6), with much larger values obtained for the Clyde than for the North Sea site. The main conclusion is that, irrespective of approach used, for the Clyde site a

significant increase in settling velocity was observed at the thermocline, with the percentage increase ranging from 50% for the fractal approach to 80% for the Stokes approach. This provides good evidence of a mechanism to generate a mass concentration minimum within the thermocline at this site.

For the North Sea site it was not possible to apply the Stokes approach as there were no gravimetric samples from within the thermocline region, but the fractal approach indicated very little change in settling velocity between the SML and the thermocline. In other words, the vertical variation in mean diameter observed at this site after Day 299 was not enough to produce a significant change in settling velocity and therefore no mass concentration minimum was observed at the thermocline.

Further quantitative testing of the conceptualised model in Figure 7.9 would involve calculating the flocculation time and residence time in the thermocline to see whether De could be obtained in the correct time scales. Unfortunately it is not possible with the current data to calculate the flocculation time using the Winterwerp (1998) approach as only the ratio K_A/K_B is known and the calculation requires K_B to be known.

7.8 Biogeochemical significance

The biogeochemical/ecological impact of SPM is determined primarily by the size of the particles. Light scattering, adsorptive capacity and settling flux are controlled by particle size. SPM consists largely of flocs – complex particles, composed of inorganic matter, organic matter and water. The irregular shape of the flocs generates a large surface area for light scattering and chemical adsorption. Although they have low density they can grow to a large size and hence have relatively high settling velocity, hence much of the settling flux is accounted for by large flocs.

In the presence of the mechanism conceptualised in Figure 7.9 the effect on other mid-water column processes could be significant. In both cases presented here the water column was a decoupled, two layer structure with little interaction

between the surface and bottom layer other than the settling of particles from the surface to the bottom layer. In a system where this process is active, particles that settle into the thermocline are destined to form larger, fragile flocs while in the thermocline and then to settle out of it into the bottom layer, where the larger flocs will be broken up by increasing turbulence levels.

This clearly provides a mechanism for accelerating the transfer of SPM, and hence of particulate carbon, from SML to BML. During periods of primary production in the SML, phytoplankton cells incorporated into the surface flocs will also be transported into the BML. There is evidence of this occurring at the Clyde site, where chlorophyll concentration also displays a minimum in the thermocline region (Figure 6.9). This indicates that particles, including phytoplankton cells, settle slowly from the SML into the thermocline where larger flocs are created, resulting in increased settling velocities and hence a minimum in chlorophyll concentration. The fact that chlorophyll concentrations increase again in the BML indicates that the settling velocity must be relatively fast, as phytoplankton (and hence chlorophyll concentrations) should not survive more than a few days once they sink below the photic zone. Typical settling velocities for single phytoplankton cells are of the order of 1m day^{-1} (Tett, 1999): at this rate they would be dead by the time they reached the BML. Table 7.4 indicates minimum estimates of settling velocity in the thermocline at ~74 m day^{-1}, which provides a mechanism for living phytoplankton to settle into the BML.

Once in the BML, break up of larger flocs by increased turbulence levels produces lower settling velocities. This tends to concentrate SPM in the BML, as smaller particles are more likely to remain in suspension. However the model applied here indicates that as concentration increases the equilibrium floc size also increases. So it can be assumed that, given constant supply from the SML and constant turbulent environment, BML concentrations will increase to the point where settling velocity increases enough to allow deposition to the sea bed. It is clear that observations of both particle size distribution and turbulent dissipation rate are required in a range of different environments over relatively long time scales in order to properly elucidate these processes.

North Sea								
	Mass concentration ($mg\ l^{-1}$)		**Volume concentration ($\mu l\ l^{-1}$)**		**Mean diameter (μm)**		**$\rho_s D_p$ ($kg\ m^{-2}$)**	
Near bed	1.11	(0.52)	11.3	(1.1)	181.3	(11.2)	16.6×10^{-3}	(7×10^{-3})
Surface	0.76	(0.42)	8.1	(0.8)	179.8	(11.4)	17.2×10^{-3}	(11×10^{-3})
All	0.94	(0.59)	9.9	(1.9)	180.6	(11.3)	16.8×10^{-3}	(9×10^{-3})
Clyde Sea								
	Mass concentration ($mg\ l^{-1}$)		**Volume concentration ($\mu l\ l^{-1}$)**		**Mean diameter (μm)**		**$\rho_s D_p$ ($kg\ m^{-2}$)**	
Near bed	3.62	(0.95)	17.8	(1.7)	172.3	(14.1)	35.1×10^{-3}	(8×10^{-3})
Thermocline	0.82	(0.31)	7.3	(1.4)	174.5	(15.6)	22.0×10^{-3}	(6×10^{-3})
Surface	1.45	(0.75)	11.7	(5.0)	173.9	(23.9)	24.7×10^{-3}	(11×10^{-3})
Surface & Thermocline	1.13	(0.70)	9.8	(4.4)	174.2	(20.8)	23.5×10^{-3}	(9×10^{-3})

Table 7.1. Estimated values of $\rho_s D_p$ using Equation 7.3. Values in brackets are standard deviations.

North Sea			
	$\rho_s D_p$ ($kg\ m^{-2}$)	**ρ_s ($kg\ m^{-3}$)**	**D_p (μm)**
All	16.8×10^{-3}	2650	6
	16.8×10^{-3}	1124	15
Clyde Sea			
	$\rho_s D_p$ ($kg\ m^{-2}$)	**ρ_s($kg\ m^{-3}$)**	**D_p (μm)**
Surface & thermocline	23.5×10^{-3}	2650	9
	23.5×10^{-3}	1568	15
Near bed	35.1×10^{-3}	2650	13
	35.1×10^{-3}	2340	15

Table 7.2. Estimated values of primary particle diameter D_p and density ρ_s using values for $\rho_s D_p$ given in Table 7.1.

	Coefficient	Confidence limits	
		Lower 95%	Upper 95%
North Sea (R^2 = 0.901)			
Slope $m^4 kg^{-1} s^{-0.5}$	0.0033	0.0031	0.0035
Intercept μm	190.6	190.0	191.1
Clyde Sea (R^2 = 0.853)			
Slope $m^4 kg^{-1} s^{-0.5}$	0.0460	0.0394	0.0527
Intercept μm	57.3	40.7	73.8

Table 7.3. Regression parameters for the relationship between mean grain diameter and the expression $c/\sqrt{(G)}$.

Stokes' method (Equation 7.4b)						
	North Sea			**Clyde Sea**		
	D (μm)	$(\rho_f - \rho_w)$ (kg m^{-3})	W_s (m s^{-1})	D (μm)	$(\rho_f - \rho_w)$ (kg m^{-3})	W_s (m s^{-1})
Surface	180	90	0.0015	140	162.5	0.0016
Thermocline	-	-	-	210	129.4	0.0029
Near-Bed	178	88	0.0014	160	204.4	0.0027

Fractal method (Equation 7.4a)								
	D (μm)	D_p (μm)	ρ_s (kg m^{-3})	W_s (m s^{-1})	D (μm)	D_p (μm)	ρ_s (kg m^{-3})	W_s (m s^{-1})
Surface	193	6	2650	0.00095	140	9	2650	0.0010
	193	15	1124	0.00014	140	15	2650	0.0006
Thermocline	205	6	2650	0.00101	210	9	1568	0.0016
	205	15	1124	0.00015	210	15	1568	0.0009
Near bed	196	6	2650	0.00097	160	-	-	-
	196	15	1124	0.00014	160	-	-	-

Table 7.4. Settling velocities calculated using effective densities presented in Tables 5.2 & 6.1, typical mean diameters from LISST profiles and values of D_p and ρ_s given in Table 7.2.

	D (μm)	$(\rho_f - \rho_w)$ (kg m^{-3})	W_s (m s^{-1})
Surface	15	964.8	1.1×10^{-4}
Thermocline	16	993.2	1.3×10^{-4}
Near-Bed	24	1005.8	2.9×10^{-4}

Table 7.5. Settling velocities of the particles less than 109.07 μm calculated for the Clyde anchor site using the densities presented in Table 6.2.

	North Sea				Clyde Sea			
	D (μm)	G (s^{-1})	C (mg l^{-1})	W_S (m s^{-1})	D (μm)	G (s^{-1})	C (mg l^{-1})	W_S (m s^{-1})
Surface	180	0.226	0.76	0.0009	140	0.262	1.45	0.0008
Thermocline	-	-	-	-	210	0.133	0.82	0.001
Near-Bed	178	0.152	1.11	0.0009	160	0.224	3.62	0.0008

Table 7.6. Settling velocities calculated using the multiple regression by Manning & Dyer (1999). $W_S = 0.301 - 0.00337G - 0.000606C + 0.00335D$

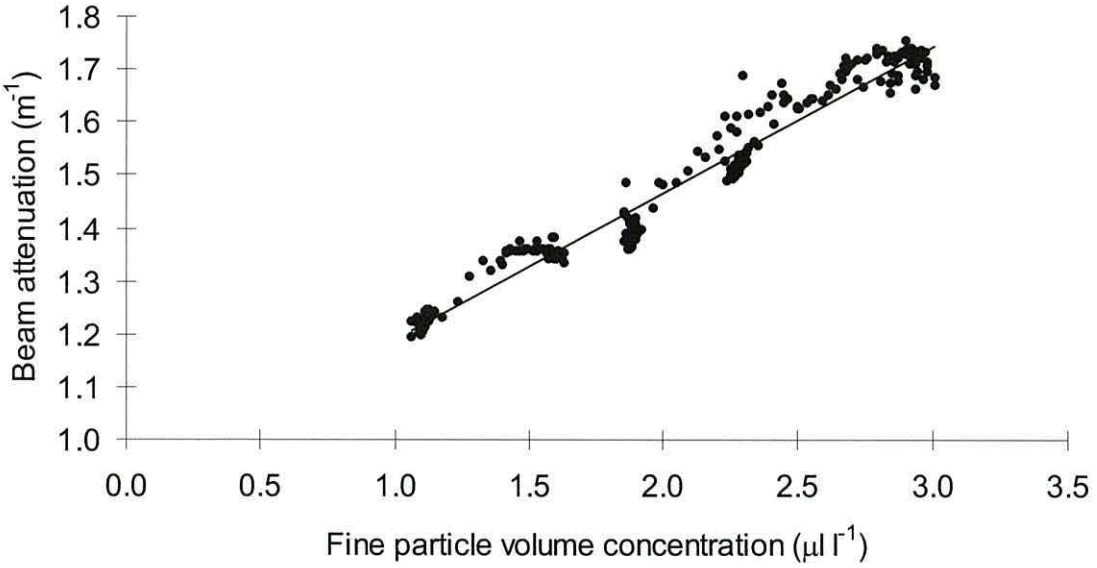

Figure 7.1a. Beam attenuation versus fine volume concentration (diameters less than 78.45 μm) at the northern North Sea site.

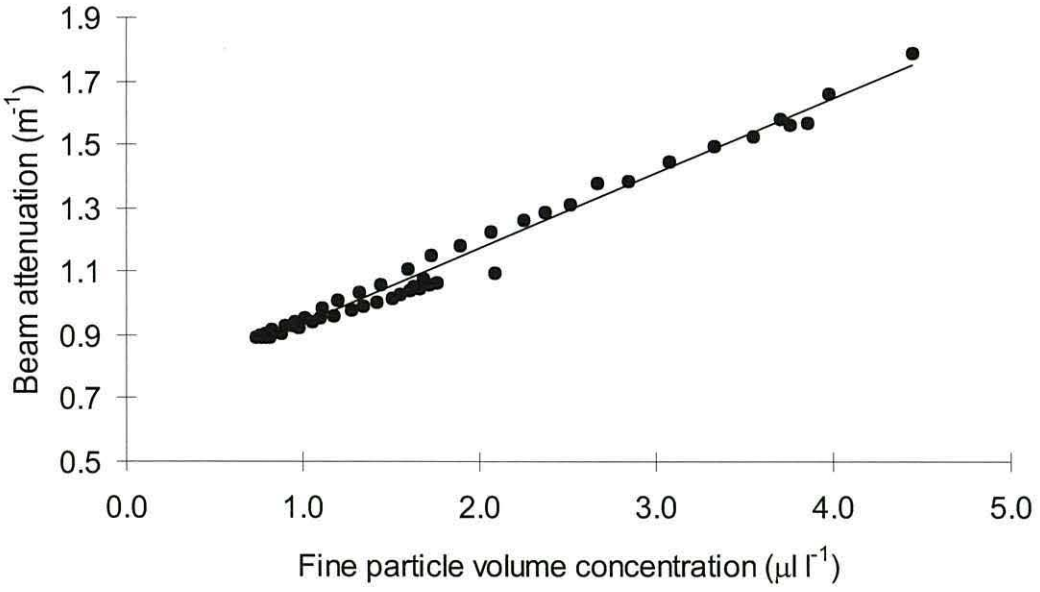

Figure 7.1b. Beam attenuation versus fine volume concentration (diameters less than 109.07 μm) at the Clyde anchor site.

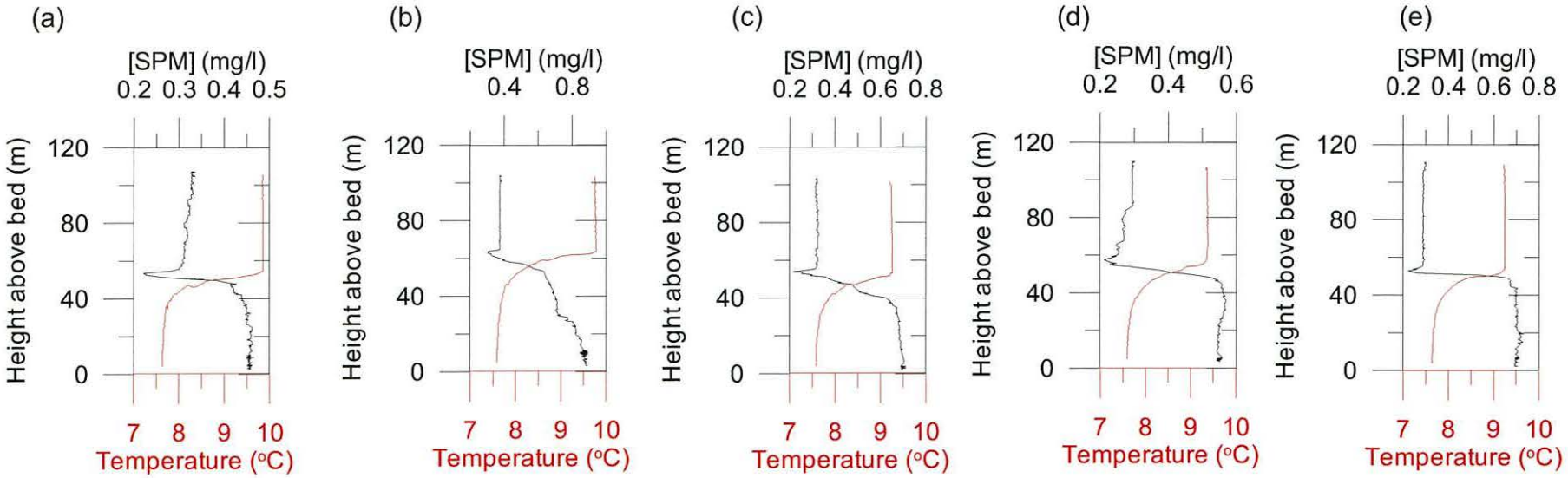

Figure 7.2. SPM concentration at the northern North Sea site (measure by the transmissometer). (a) Day 299.58, (b) day 301.83, (c) day 305.92, (d) day 307.95 and (e) day 309.88.

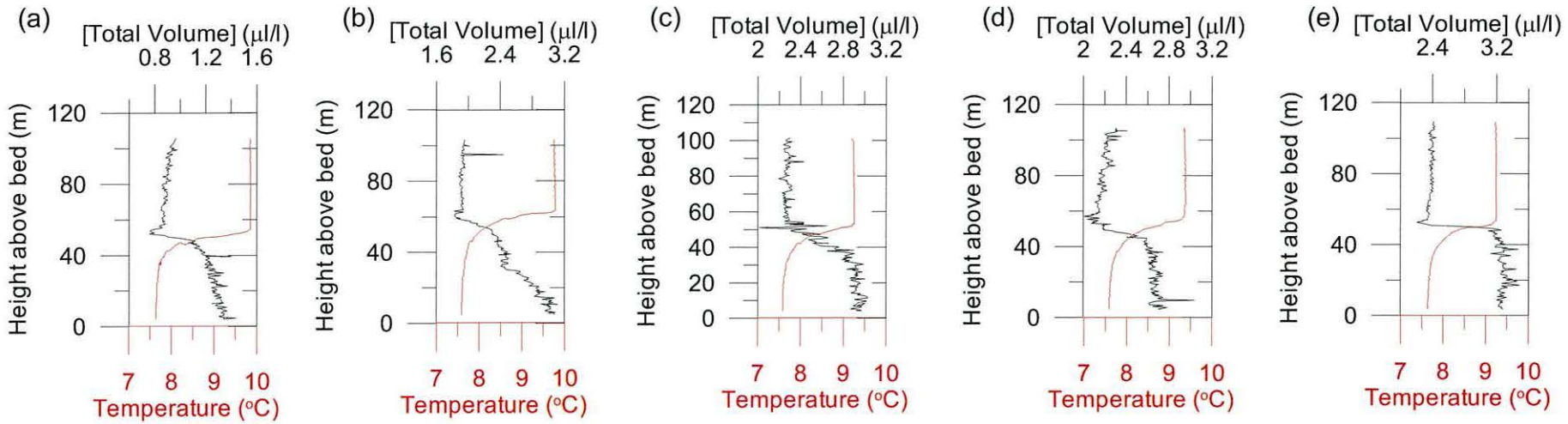

Figure 7.3. Volume concentration of particles with diameters less than 78.45 µm measured by the LISST at the northern North Sea site. (a) Day 290.57, (b) day 301.83, (c) day 305.92, (d) day 307.95 and (e) day 309.88.

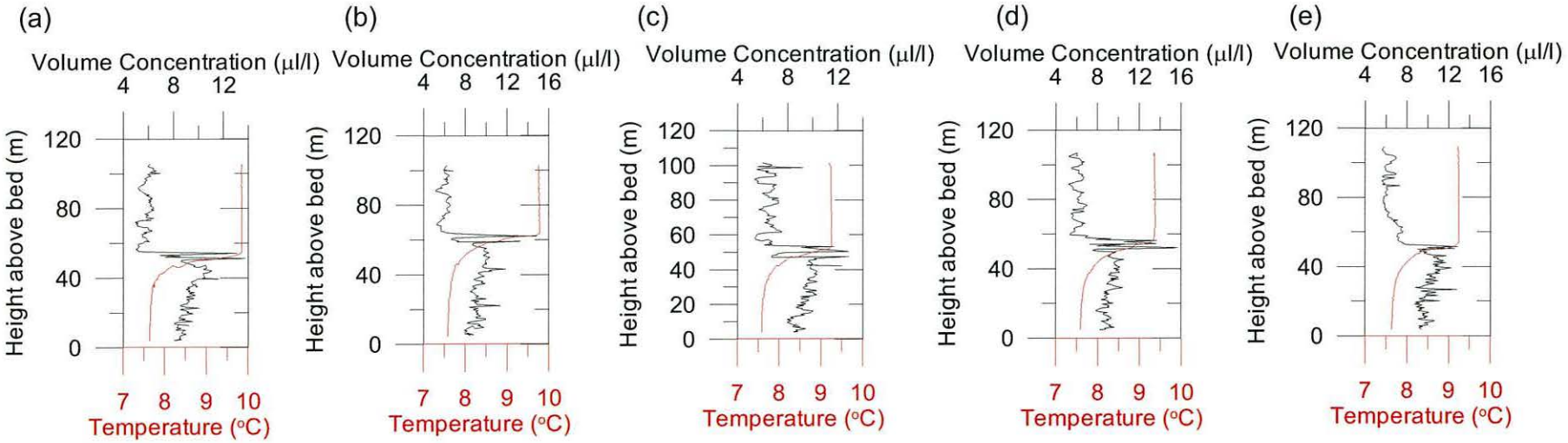

Figure 7.4. Volume concentration of particles with diameters greater than 78.45 µm measured by the LISST at the northern North Sea site. (a) Day 299.58, (b) day 301.83, (c) day 305.92, (d) day 307.95 and (e) day 309.88.

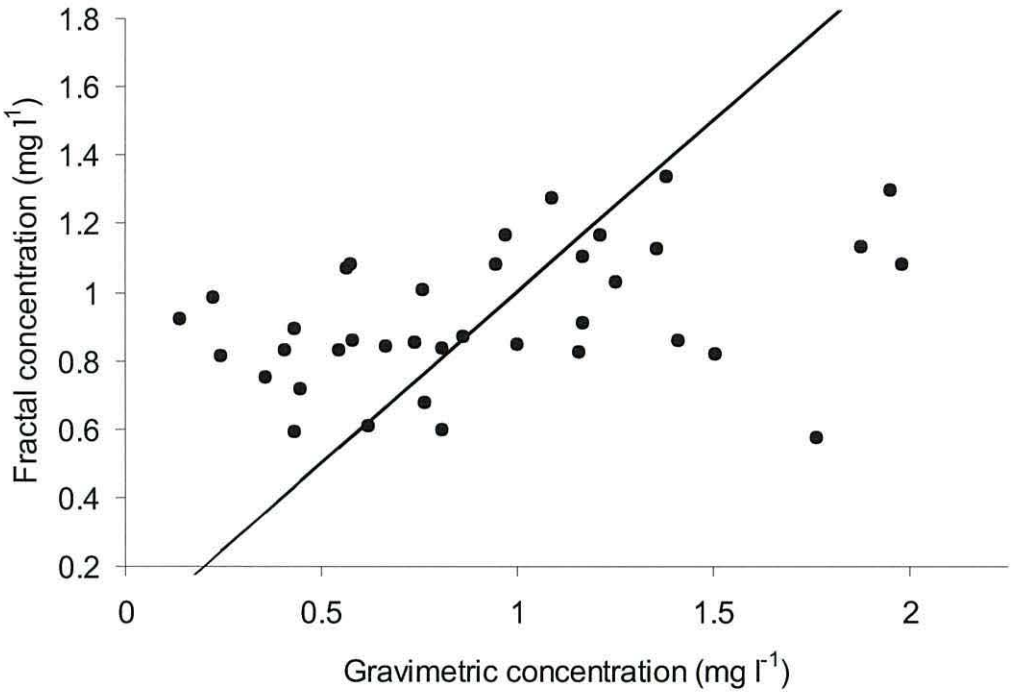

Figure 7.5. Mass concentrations calculated from LISST data versus gravimetric concentrations (northern North Sea). 1:1 relationship (———).

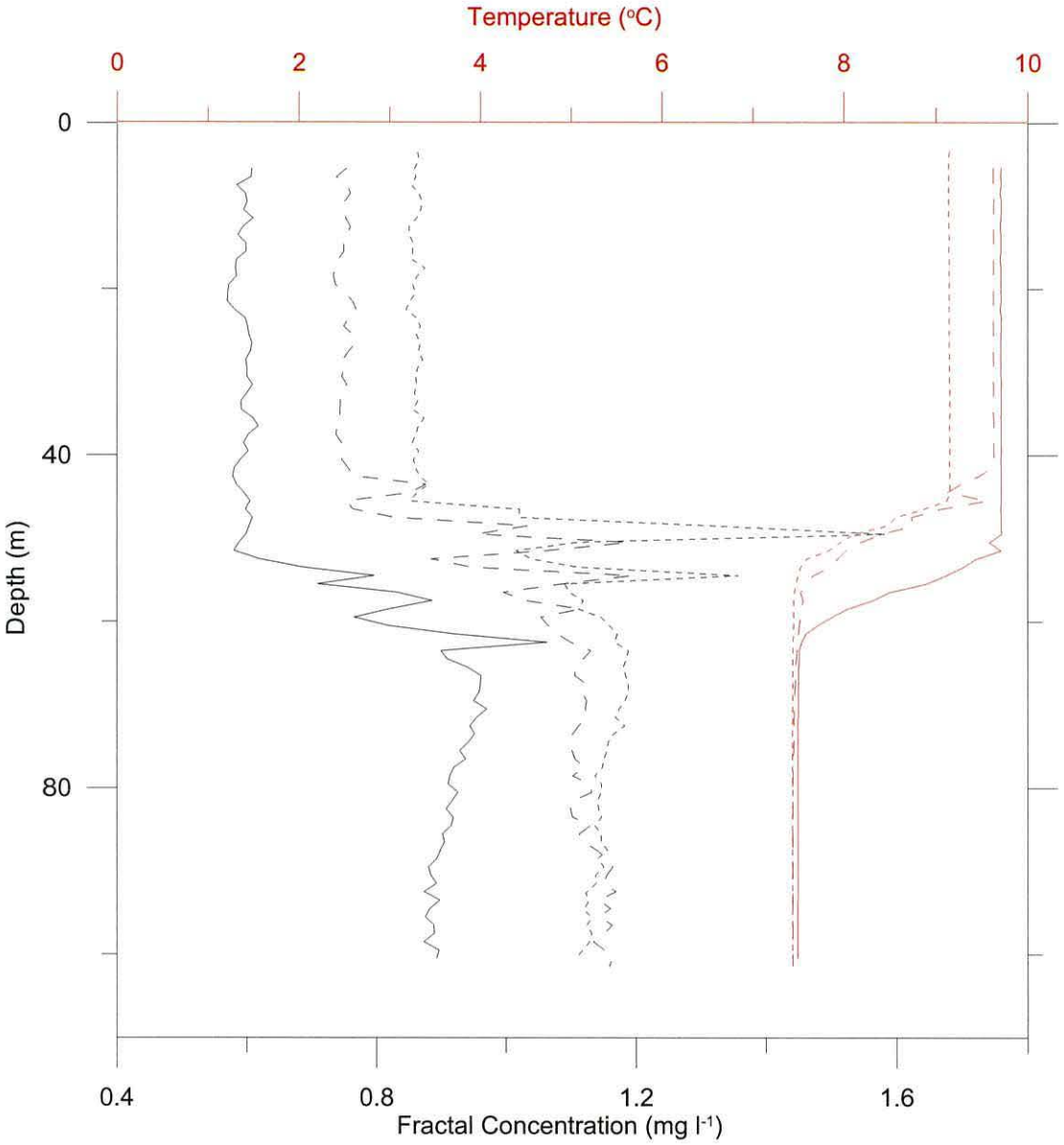

Figure 7.6. Mass concentration calculated from LISST data (black) and temperature (red) profiles (northern North Sea). Period 1 (————), period 2 (– – – – – –) and period 3 (----------)

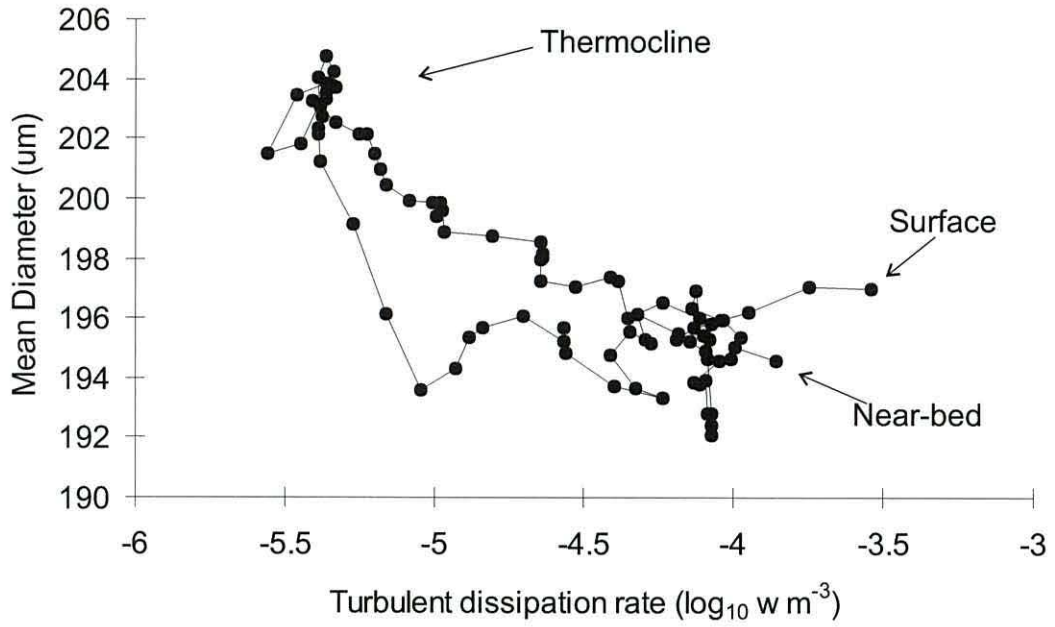

Figure 7.7. Mean diameter versus turbulent dissipation rate (northern North Sea).

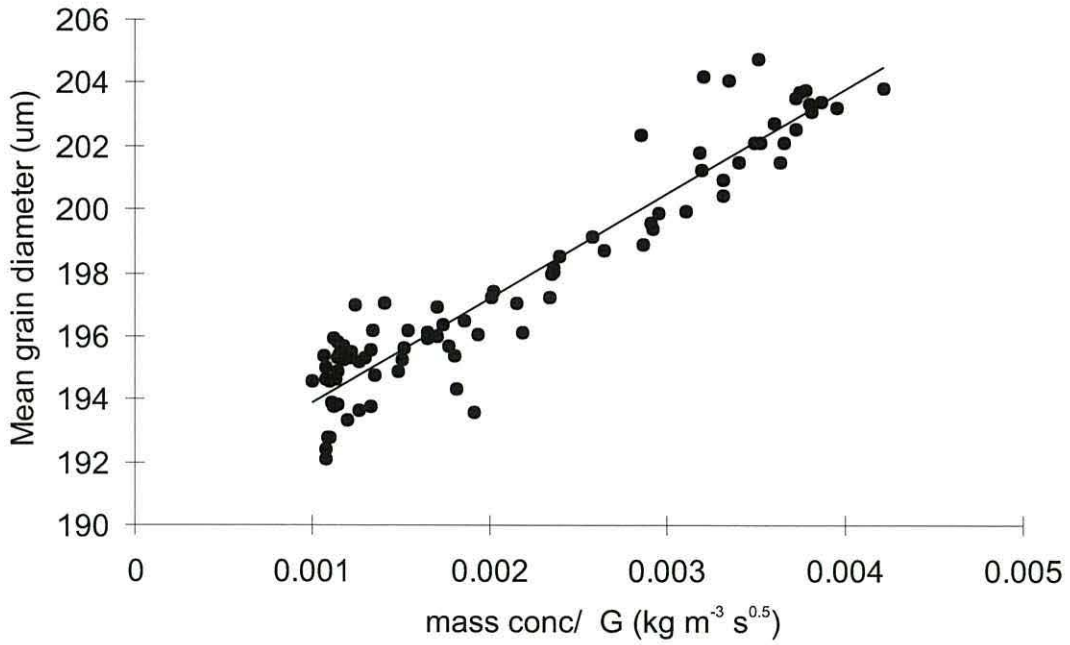

Figure 7.8. Mean grain diameter versus mass concentration/ G (northern North Sea).

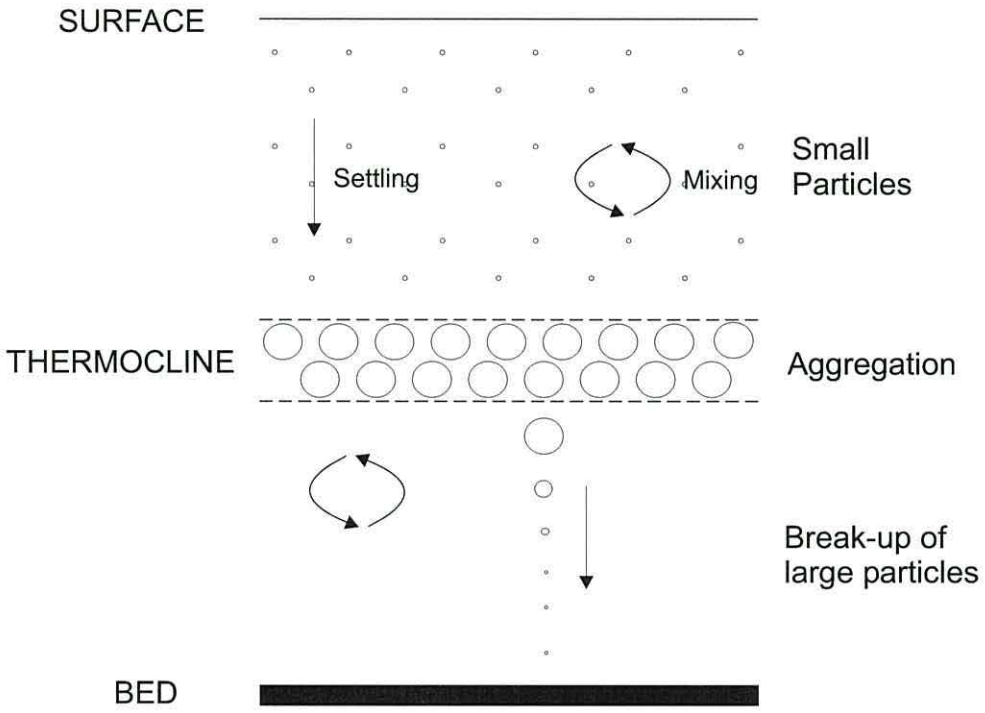

Figure 7.9. A conceptual model of the physical processes occurring within the thermocline.

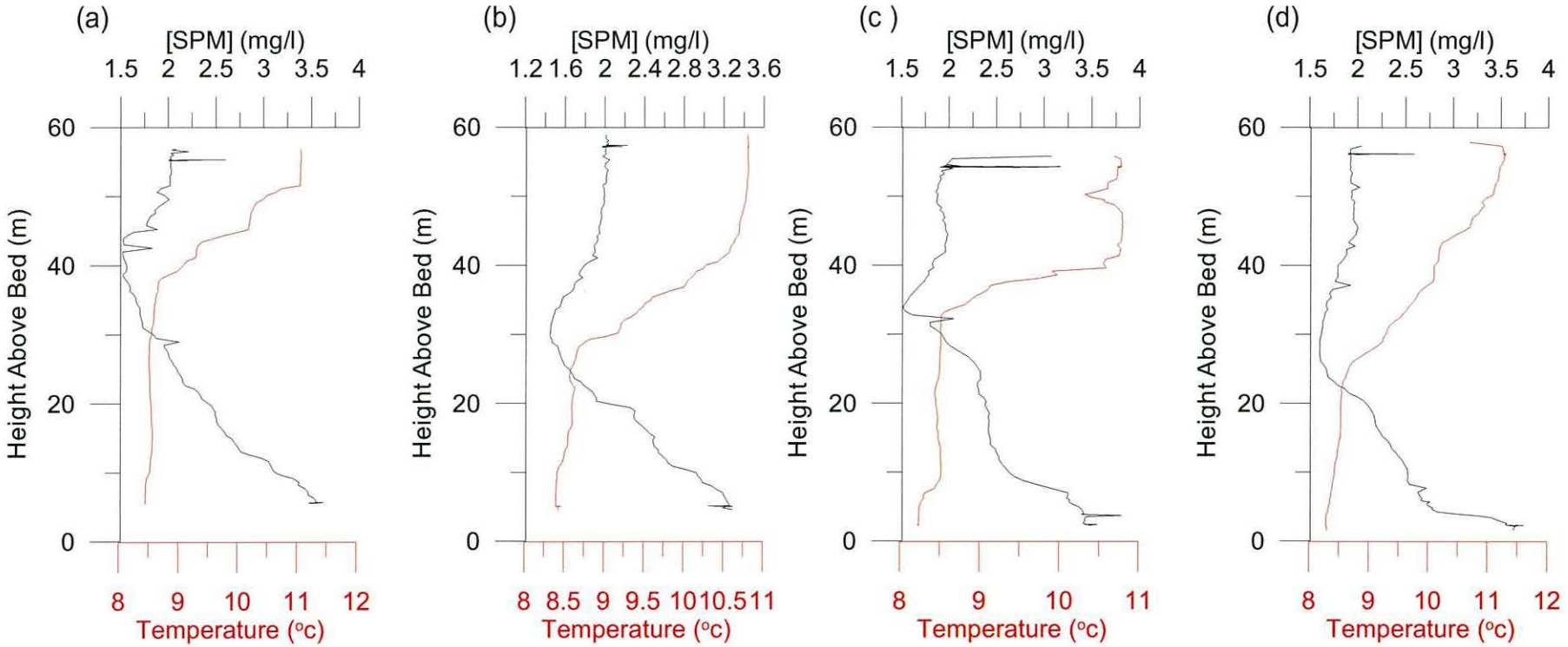

Figure 7.10. SPM concentration (mg l^{-1}) profiles at the Clyde anchor site measured by the transmissometer. (a) Day 142.92, (b) day 143.13, (c) day 143.38 and (d) day 143.63.

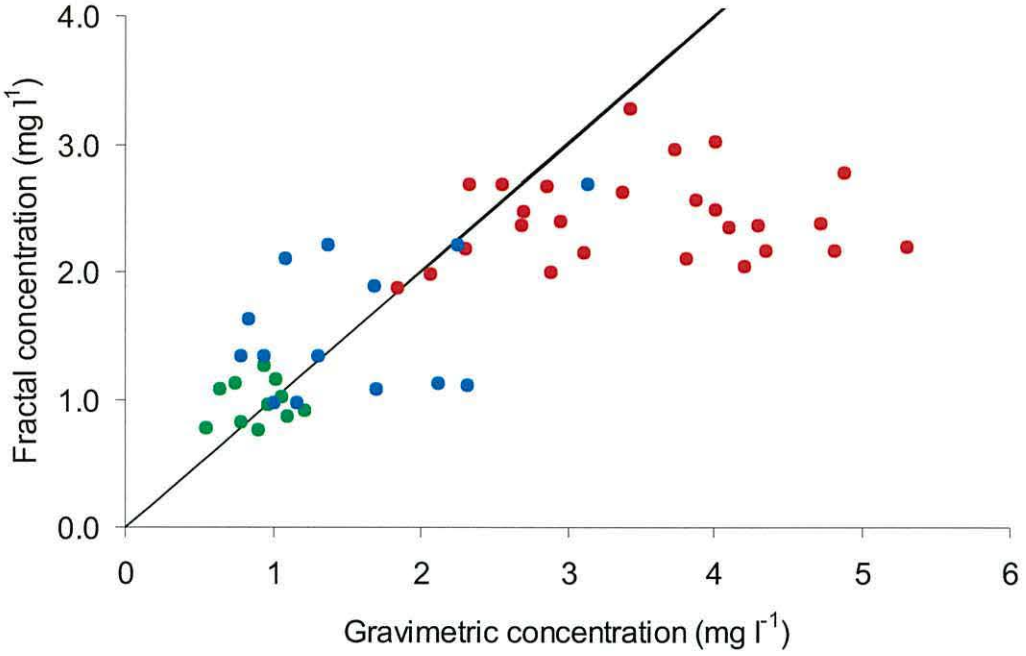

Figure 7.11. Fractal mass concentration calculated via Equation 7.3 versus gravimetric concentration. ● = thermocline, ● = surface, ● = near-bed and ——— = 1:1 relationship. (Clyde Sea).

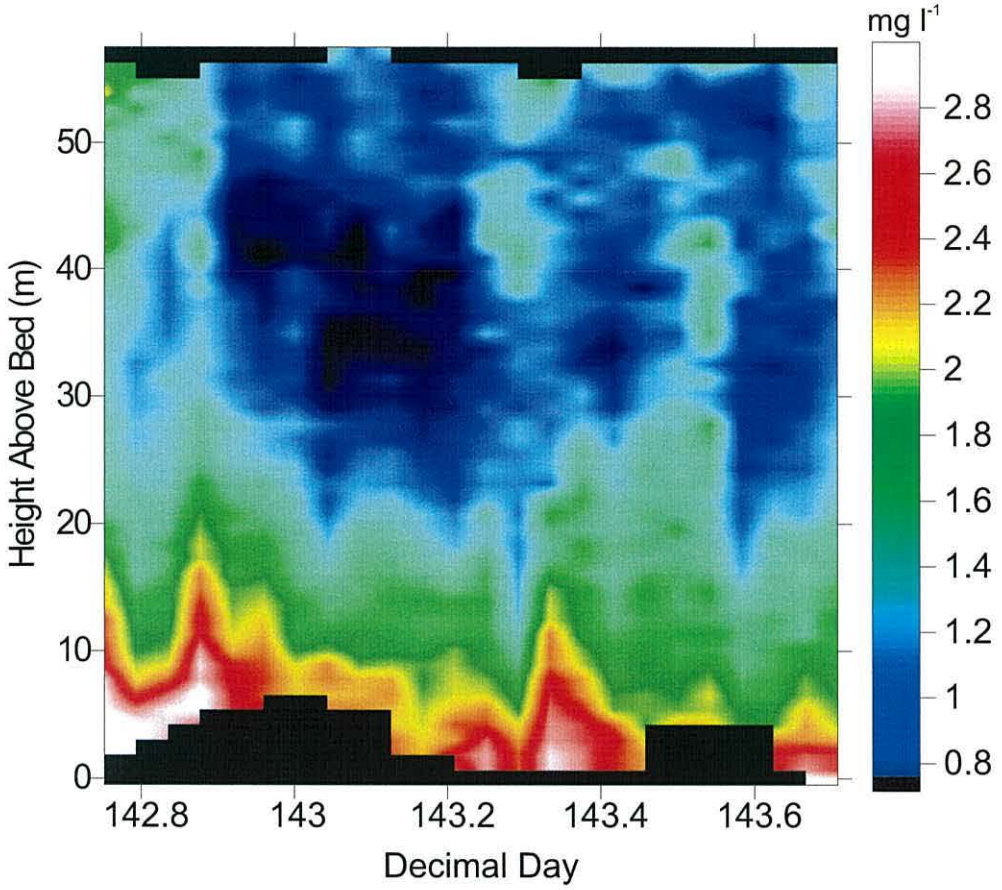

Figure 7.12. Mass concentration (calculated from LISST data) in the Clyde Sea.

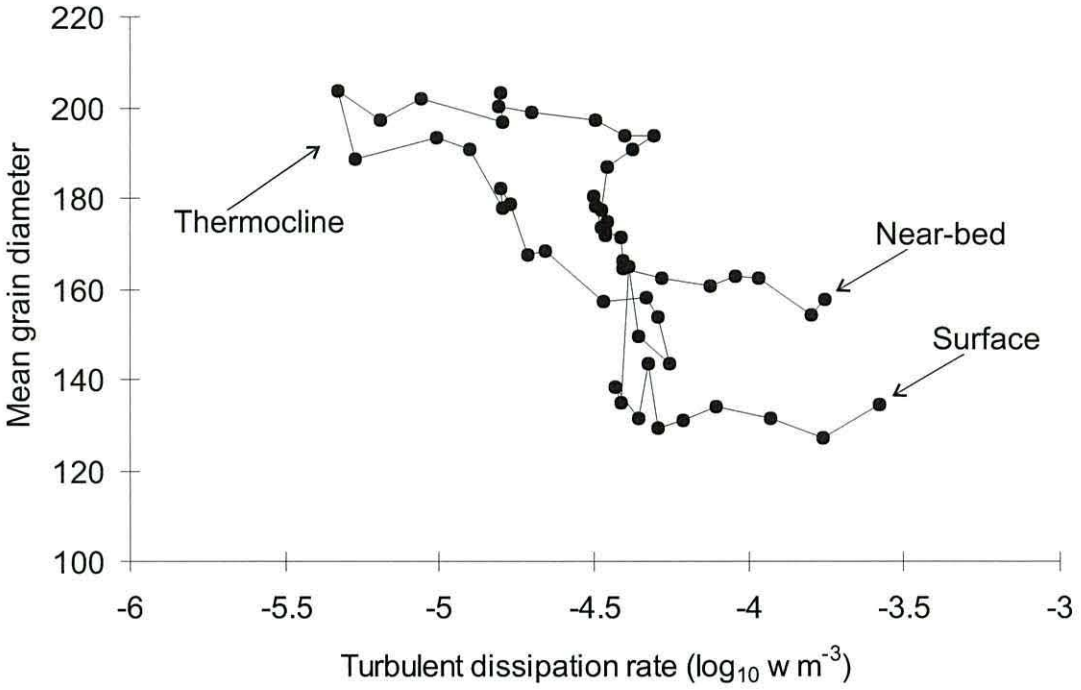

Figure 7.13. Mean diameter versus turbulent dissipation (Clyde Sea).

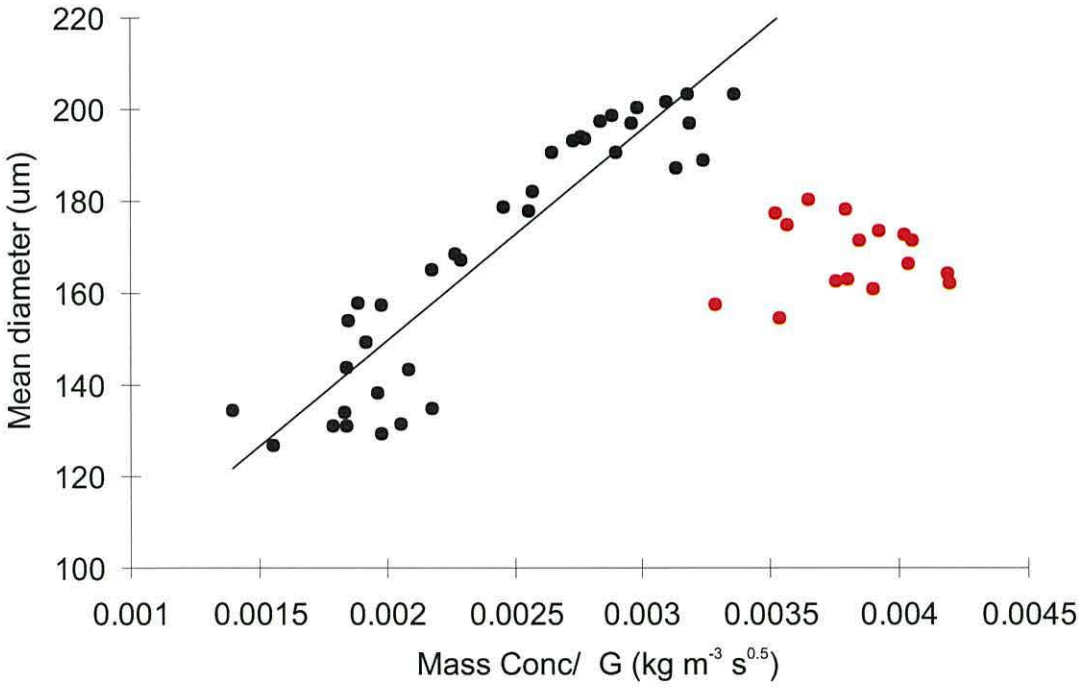

Figure 7.14. Mean diameter versus mass concentration/ G (Clyde Sea)

● = Surface and thermocline, ● = near-bed,

——— regression line (surface and thermocline only).

Chapter 8

Conclusions and Further Work

8.1. Conclusions

A LISST-100B laser diffraction analyser has been used to measure volume concentration and particle size distribution of suspended particulate matter (SPM) at two sites in the northern North Sea and Clyde Sea. Laboratory and field experiments comparing the performance of this instrument with other techniques established that this instrument was not able to measure absolute total volume concentrations or mean particle size at these sites, because of the presence of particles larger than the upper measuring limit of the instrument (250 μm). It was, however, sensitive to variation in the coarse part of the spectrum and measured systematic variation in both volume concentration and particle size distribution. Therefore relative changes over time and depth could be interpreted in terms of variation in suspended particle characteristics.

In addition to the LISST measurements, SPM mass concentrations were determined using a transmissometer calibrated by standard gravimetric techniques. There were also concurrent measurements of temperature, salinity, currents, chlorophyll concentrations and turbulent dissipation rates. At both sites the water column was well stratified with a warmer, less saline, well mixed surface layer above the thermocline (SML) and a cooler, more saline, well mixed layer below it (BML). Within the thermocline, a significant increase in the mean particle size was measured at both sites, accompanied by an apparent decrease in the mass concentration measured by the transmissometer and an increase in the total volumetric concentration. Beneath the thermocline the mean particle size reduced from its maximum within the thermocline towards the sea bed.

By splitting the size distribution data into fine and coarse components, it was shown that the transmissometer data correlated closely with volume concentrations of particles finer than 78.45 μm at the North Sea site and 109.07 μm in the Clyde. It is concluded that because of forward scattering effects the

transmissometer is highly biased towards particles smaller than ~ 75 μm and is effectively "blind" to particles greater than ~ 150 μm. In environments where the coarse particle volume concentrations are relatively low, transmissometer measurements will be representative of actual mass concentrations. Also, if there is a significant coarse particle component which remains in constant proportion to the fine particle component then this component will have a systematic influence on the calibration coefficient, but calibrated concentrations will still be representative of actual mass concentrations. However, if the proportion of coarse particles varies significantly then the transmissometer will measure an apparent variation in mass concentration which is not representative of the actual concentration. Therefore variation in mass concentration recorded by a transmissometer may, in certain circumstances, reflect either variation in true mass concentration or variation in mean particle size.

By assuming that SPM was in the form of aggregates which could be treated as fractal entities, mass concentrations could be estimated from LISST measurements of total volume concentration and mean particle diameter. Using this approach it was concluded that in the North Sea (for the period when particle size measurements were available) the minimum in apparent mass concentration measured by transmissometer was due to conversion of fine particles into large particles by enhanced aggregation in the thermocline, and did not reflect a true mass concentration minimum. However, in the Clyde Sea the minimum measured by the transmissometer was reflected both in gravimetric measurements and in mass concentrations calculated from the LISST data, although it was exaggerated due to the variation in mean grain diameter.

A mechanism to explain the observed variations in mean particle diameter and mass concentration was proposed (represented in Figure 7.9). Small particles settle slowly from the SML into the thermocline. Here, where turbulence is reduced, larger fragile flocs are formed. At both sites the formation of larger flocs is confirmed not only by the increase in mean particle size but also by the

increase in the volume concentration and decrease in particle density. These flocs, which are less dense than the surface and near-bed particles, settle faster than the surface particles. This is because increase in size counteracts the decrease in density. The result of the particles settling faster out of the thermocline than in from the SML is a negative mass flux and therefore eventually a mass concentration minimum. Once in the BML, larger flocs are broken up by increasing levels of turbulence towards the sea bed, producing a reduction in mean particle diameter.

A simple aggregation model which predicts equilibrium diameter of aggregates behaving as fractal entities as a function of turbulent dissipation rate and total mass concentration was applied to the observations. There was good agreement with observations throughout the water column at the North Sea site, and also in the SML and thermocline at the Clyde site. In the Clyde, observed particle sizes were finer, and densities were higher, than predicted by this simple equilibrium model in the BML.

Settling velocities (Table 7.4) were calculated for aggregates in SML, thermocline and BML, and were shown to be consistent with the proposed mechanism. Significantly higher settling velocities were obtained in the thermocline than the SML at the Clyde site, leading to a mass concentration minimum. There was a much smaller difference for the northern North Sea Site (and hence no mass concentration minimum), at least for the period where LISST data were available.

Apparent resuspension signals were observed in the transmissometer data at both sites. It was shown that some of the variation measured by the transmissometer at the North Sea site may have been indicative of dissaggregation, rather than resuspension, during periods of increased turbulent dissipation rates under surface waves or inertial currents. However, in the Clyde Sea it was concluded that an additional tidal resuspension population was present in the BML, which was relatively fine and had a higher density than the particles derived from the SML.

The observations of particle size distribution, volume concentration and turbulent dissipation rate made in this study have provided direct evidence, for the first time, that turbulence controls equilibrium floc diameter in the marine environment. The observations are well explained by a simple aggregation model which predicts equilibrium diameter as a function of turbulent dissipation rate and total mass concentration, with diameter increasing as either the fourth root of the turbulent dissipation rate reduces or the mass concentration increases.

8.2. Further and Work

Quantification of the problems associated with the transmissometer with regards to the presence of particles with diameters greater than 100 μm is required. This would involve establishing how much beam attenuation decreases with increased particle size whilst the mass concentration remained constant, as well as the effect of altering the concentration whilst the size distribution remained constant.

The work done would have been greatly helped by an in-situ video camera assembly and size distribution measurements of the coarse part of the sediment population. This would have enabled the quantification of the increase in particle size and how much both the LISST and the Galai have underestimated the size distribution and enable in-situ measurements of the settling velocity. Also, such an assembly would allow the identification of floc break-up by the sampling procedure for the Galai.

With such quantifications it would be possible to accurately calculate the particle densities. Combined with simultaneous turbulent dissipation measurements further support of the settling velocities calculated in this study and the conclusion that enhanced aggregation occurred within the thermocline region at both study sites would be obtained.

References

Adams, C.E. and Weatherly, G.L. (1981). Some effects of suspended sediment stratification on an oceanic bottom boundary layer. *Journal of Geophysical Research*, 86(C5), 4161-4172.

Agrawal, Y.C., McCave, I.N., and Riley, J.B. (1991). Laser diffraction size analysis. In: Syvitski, J.P.M. (Ed.), *Principles, methods, and application of particle size analysis*, Cambridge University Press, 119-128.

Agrawal, Y.C. and Pottsmith, H.C. (2000). Instruments for particle size and settling velocity observations in sediment transport. *Marine Geology*, 168, 89-114.

Agrawal, Y.C. and Riley, J.B. (1984). Optical particle sizing for hydrodynamics based on near forward scattering, *Ocean Optics* VII, SPIE (489), 68-76.

Agrawal, Y.C. and Traykovski, P. (2001). Particles in the bottom boundary layer: Concentration and size dynamics through events. *Journal of Geophysical Research*, 106(C5), 9533-9542.

Alldredge, A.L. and Gotschalk, C.C. (1988). *In-situ* settling behaviour of marine snow. *Limnology and Oceanography*, 33, 399-351.

Allen, T. (1981). Microscopy. In: Particle size measurement. 3rd ed, Chapman & Hall, London. 678pp.

Allen, T. and Davies, R. (1988). An evaluation of the LAB-TEC 100 particle size analyser. In: Lloyd, P.J. (Ed.). Particle size analysis. John Wiley & Sons Ltd., 361pp.

Baker, E.T. and Lavelle, J.W. (1984). The effect of particle size on the light attenuation coefficient of natural suspensions. *Journal of Geophysical Research*, 89(C5), 8197-8203.

Bale, A.J. and Morris, A.W. (1987). In-situ measurement of particle size in estuarine waters. *Estuarine, Coastal and Shelf Science*, 24, 253-263.

Balls, P.W. (1990). Distribution and composition of suspended particulate material in the Clyde Estuary and associated sea lochs, *Estuarine, coastal and shelf science*, 30, 475-487.

Bartz, R., Zaneveld, J.R.V. and Pak, H. (1978). A transmissometer for profiling and moored observations in water. *SPIE Ocean Optics*, 160, 102-108.

Benns, E.J. and Pilgrim, D.A. (1994). The effect of particle characteristics on the beam attenuation coefficient and output from an optical backscatter sensor. *Netherlands Journal of Aquatic Ecology*, 28(3-4), 245-248.

Bishop, J.K.B. (1986). The correction and suspended particulate matter calibration of Sea Tech transmissometer data. *Deep-Sea Research*, 33(1), 121-134.

Braithwaite, C.J.R. (1973). Settling behaviour related to sieve analysis of skeletal sands. *Sedimentology*, 20, 251-262.

Bunt, J.A.C., Larcombe, P., Jago, C.F. (1999). quantifying the response of optical backscattering devices and transmissometers to variations in suspended particular matter. *Continental Shelf Research*, 19, 1199-1220.

Burban, P-Y., Lick, W. and Lick, J. (1989). The flocculation of fine-grained sediments in estuarial waters, *Journal of Geophysical Research*, 94, 8323-8330.

Burchard, H., Bolding, K., Rippeth, T.P., Stips, A., Simpson, J.H. and Sündermann, J. (2002). Microstructure of turbulence in the northern North Sea: a comparative study of observations and model simulations. *Journal of Sea Research*, 47(3-4), 223-238.

Cooper, L.R., Haverland, R.L., Hendricks, D.M. and Knisel, W.G. (1984). Microtrac particle-size analysis: An alternative particle-size determination method for sediment and soils. *Soil Science*, 138, 138-146.

de Boer, G.B.J., de Weerd, C., Thoenes, D. and Goossens, H.W.J. (1987). Laser diffraction spectrometry: Fraunhofer diffraction versus Mie Scattering. *Particle Characterisation*, 4, 14-19.

Dewey, R.K., Crawford, W.R., Garret, A.E., Oakey N.S. (1987). A microstructure instrument for profiling oceanic turbulence in coastal bottom boundary layers. *Journal of Atmospheric and Oceanic Technology*, 4(2), 288-297.

Dewey, R.K. and Crawford, W.R. (1988). Bottom stress estimates from vertical dissipation rate profiles on the continental shelf. *Journal of Physical Oceanography*, 18(8), 1167-1177.

Drake, D.E. and Cacchione, D.A. (1989). Estimates of the suspended sediment reference concentration of (C_a) and resuspension coefficient (γ_0) from near-

bottom observations on the Californian Shelf. *Continental Shelf Research*, 9 (1), 51-64.

Dyer, K.R. (1986). Coastal and estuarine sediment dynamics. John Wiley & Sons, Chichester, 342pp.
Dyer, K.R. and Manning, A.J. (1999). Observation of the size, settling velocity and effective density of flocs and their fractal dimensions. *Journal of Sea Research*, 41, 87-95.

Edwards, A., Baxter, M.S., Ellett, D.J., Martin, J.H.A., Meldrum, D.T. and Griffiths, C.R. (1986). Clyde Sea hydrography, *Proceedings of the Royal Society of Edinburgh*, 90B, 67-83.

Eisma, D. (1986). Flocculation and de-flocculation of suspended matter in estuaries, *Netherlands Journal of Sea Research*, 20, 183-199.

Eisma, D. (1990). Transport and deposition of suspend matter in the North Sea and the relation to coastal situation, pollution and bottom fauna distribution. *Aquatic Sciences*, 3(2-3), 181-216.

Eisma, D and Kalf, J. (1987). Distribution, organic content and particle size of suspended matter in the North Sea. *Netherlands Journal of Sea Research*, 21, 265-285.

Fennessy, M.J., Dyer, K.R. and Huntley, D.A. (1994). INSSEV: An instrument to measure the size and settling velocity of flocs in situ. *Marine Geology*, 117, 107-117.

Fransz H.G. and Gieskes, W.W.C., (1984). The imbalance of phytoplankton and copepods in the North Sea. *Rapp. P.-v Reun. Conc. Perm. Int. Explor. Mer*, 183, 218-225.

Gartner, J.W., Cheng, R.T., Wang, P-F. and Richter, K. (2001). Laboratory and field evaluations of the LISST-100 instrument for suspended particle size determinations. *Marine Geology*, 175, 199-219.

Gibbs, R.J. (1981). Floc breakage by pumps. *Journal of Sedimentary Petrology*, 51, 670-672.

Gibbs, R.J. (1982a). Floc stability during Coulter Counter analysis. *Journal of Sedimentary Petrology*, 52, 657–670.

Gibbs, R.J. (1982b). Coagulation rates of clay minerals and natural sediments. *Journal of Sedimentary Petrology*, 53, 1193-1203.

Gibbs, R.J. (1983). Coagulation rates of clay minerals and natural sediments. *Journal of Sedimentary Petrology*, 53, 1193-1203.

Gibbs, R.J. (1985). Estuarine flocs: Their size, settling velocity and density. *Journal of Geophysical Research*, 90(C2), 3249-3251.

Gibbs, R.J. and Konwar, L.N. (1982). Effect of pipetting on mineral flocs. *Environmental Science Technology*, 16(2), 119-121.

Gibbs, R.J. and Konwar, L.N. (1983). Sampling of mineral flocs using Niskin bottles. *Environmental Science Technology*, 17(6), 374-375.

Gibbs, R.J., Mathews, M.D. and Link, D.A. (1971). the relationship between sphere size and settling velocity. *Journal of Sedimentary Petrology*, 41, 7-18.

Glenn, S.M. and Grant, W.D. (1987). A suspended sediment stratification correction for combined wave and current flows. *Journal of Geophysical Research*, 92(C2), 8244-8264.

Hainbucher, D., Pohlmann, T. and Backhaus, J. (1987). Transport of conservative passive tracers in the North Sea: first results of a circulation and transport model. *Continental Shelf Research*, 7, 1161-1179.

Hallermeir, R.J. (1981). Terminal settling velocity of commonly occurring sand grains. *Sedimentology*, 28, 859-865.

Harfield, J.G. and Cowan, M.P. (1988). High resolution particle size analysis over an extended size range using a multichannel Coulter Counter instrument with a focussed flow aperture system. In: Lloyd, P.J. (Ed.). Particle Size Analysis, John Wiley & Sons Ltd. 361pp.

Hecht, E. and Zajac, A. (1974). Optics. 1st ed. Addison-Wesley Publishing Company, 565pp.

Hill, P.S. (1998). Controls on floc size in the sea. *Oceanography*, 11(2),13-18.

Hill, P.S., Sherwood, C.R., Sternburg, R.W. and Nowell, A.R.M (1994). In situ measurements of particle settling velocity on the northern California continental shelf. *Continental Shelf Research*, 14(10/11), 1123-1137.

Hill, P.S., Syvitski, J.P., Cowan, E.A. and Powell, R.D. (1998). In situ observations of floc settling velocities in Glacier Bay, Alaska. *Marine Geology*, 145, 85-94,

Hill, P.S., Voulgaris, G., Trowbridge, J. (2001). Controls on floc size in a continental shelf bottom boundary layer. *Journal of Geophysical Research*, 106(C5), 9543-9549.

Hillier, S. (1995). Erosion, sedimentation and sedimentary origin of clays. In: Velde, B. (Ed.), Origin of mineralogy of clays: Clays and the environment. Springer, Berlin, 334pp.

Howarth, M.J., Simpson, J.H., Sundermann, J. and van Haren, H. (2002). Processes of vertical exchange in shelf seas (PROVESS). *Journal of Sea Research*, 47, 199-208.

Inall, M.E and Rippeth, T.P. (2002). Dissipation of Tidal Energy and Associated Mixing in a Wide Fjord. *Environmental Fluid Mechanics*, 2, 219-240.

Jago, C.F., Bale, A.J., Green, M.O., Howarth, M.J., Jones, S.E., McCave, I.N., Millward, G.E., Morris, A.W., Rowden, A.A. and Williams, J.J. (1993). Resuspension processes and seston dynamics, southern North Sea. *Philosophical Transactions of the Royal Society, London*, A343, 475-491.

Jago, C.F and Jones, S.E. (1998). Observation and modelling of the dynamics of benthic fluff resuspended from a sandy bed in the southern North Sea. In: Morris, A.W., Jago, C.F., Howarth, M.J. and Bale, A.J. (Eds.). The North Sea Sediment Resuspension Experiment. *Continental Shelf Research*, 18(11), 1255-1282.

Jago, C.F., Jones, S.E., Latter, R.J., McCandliss, R.R., Hearn, M.R. and Howarth, M.J. (2002). Resuspension of benthic fluff by tidal currents in deep stratified waters, northern North Sea. *Journal of Sea Research*, 48(4), 259-269.

Jantschik, R., Nyffeler, F., and Donard, O.F.X. (1992). Marine particle size measurement with a stream-scanning laser system. *Marine Geology*, 106, 239-250.

Jerlov, N.G. (1976). Marine Optics. Elsevier, Amsterdam, 231pp.

Johansen, C. and Larsen, T. (1998). Measurement to settling velocity of fine sediment using a recirculated settling column. *Journal Coastal research*, 14 (1), 132-139.

Jones, S.E., Jago, C.F., Bale, A.J., Chapman, D., Howland, R., Jackson, J. (1998). Aggregation and resuspension of suspended particulate matter at a seasonally stratified site in the southern North Sea: physical and biological controls. In: Morris, A.W., Jago, C.F., Howarth, M.J. and Bale, A.J. (Eds.), The

North Sea Sediment Resuspension Experiment (SERE). *Continental Shelf Research*, 18(11), 1283-1309.

Karasikov, N., Krauss, M., Barazani, G., 1988. Measurement of particles in the range of 150-1200μm using a time-of-transition particle size analyzer. In: Lloyd, P.J. (Ed.), Particle Size Analysis. Wiley, New York, pp. 51-62.

Kautsky, H. (1987). Investigations on the distribution of ^{137}Cs, ^{134}Cs and ^{90}Sr and the water mass transport times in the Northern North Atlantic and the North Sea. *Dutch Hydrographic Journal*, 40, 49-69.

Kirk, J.T.O. (1983). Light and photosynthesis in aquatic ecosystems. Cambridge University Press.

Knight, P.J., Howarth, M.J. and Rippeth, T.P. (2002). Inertial current in the northern North Sea. *Journal of Sea Research*, 47(3-4), 269-284.

Knowles, S.C. and Well, S.J.T. (1998). In situ aggregate analysis camera (ISAAC): A quantitive tool for analyzing fine-grained suspended material. *Limnology Oceanography*, 43(8), 1954-1962.

Kranck, K. (1973). Flocculation of suspended sediment in the sea. *Nature*, 246, 348-350.

Kranck, K. (1980). Variability of particulate matter in a small coastal inlet. *Canadian Journal of Fishery and Aquatic Science*, 37(8), 1209-1215.

Kranck, K., Petticrew, E., Milligan, T.G. and Droppo, I.G. (1993). In situ particle size distributions resulting from flocculation as suspended sediment. In: Mehta, A. (Ed.), Coastal and estuarine studies, 42. Near shore and estuarine cohesive sediment transport, 60-74, American Geophysical Union.

Kranenburg, C. (1994). On the fractal structure of cohesive sediment aggregates. *Estuarine, Coastal and Shelf Science*, 39, 451-460.

Krone, R.B. (1978). Aggregation of suspended particles in estuaries. In: Kjerfve, R. (Ed.). Estuarine processes. University of South Carolina Press, Columbia, SC, 177-190.

Lavelle, J.W., Mofjeld, H.O. and Baker, E.T. (1984). An in situ erosion rate for a fine-grained marine sediment. *Journal of Geophysical Research*, 89(C4), 6543-6552.

Law, D.J. (2001). Optical characterisation of suspended particulate matter in estuaries and near coastal waters. PhD Thesis, University of Wales Bangor.

Law, D.J., Bale, A.J., and Jones, S.E. (1997). Adaptation of focused beam reflectance measurement to in-situ particle sizing in estuaries and coastal waters. *Marine Geology*, 140, 47-59.

Lee, A.J. (1980). North Sea: Physical Oceanography. In: Banner, F.T., Collins, M.B., and Massie, K.S. (Eds.). The North-West European Shelf Seas the seabed and the sea in motion. II. Physical and chemical oceanography, and physical resources. Elsevier Oceanography Series, 24b, Elsevier, Amsterdam, 467-493.

Leeder, M.R. (1982). Sedimentology. Process and product. Chapman & Hall, London, 344pp.

Lees, B.J. (1983). The relationship of sediment transport rates and paths to sandbanks in a tidally dominated area off the coast of East Anglia, U.K., *Sedimentology*, 30, 461-483.

Leuttich, R.A., Well, J.T. and Kim, S-Y. (1993). In situ variability of large aggregates: Preliminary results on the effects of shear. In: Mehta, A. (Ed.), Coastal and estuarine studies, 42. Nearshore and estuarine cohesive sediment transport. American Geophysical Union.

Lick, W. and Huang, H. (1993). Flocculation and the physical properties of flocs. In: Mehta, A.(Ed.), Coastal and estuarine Studies, 42. Near shore and estuarine cohesive sediment transport. American Geophysical Union.

Lick, W., Huang, H. and Jepsen, R. (1993). Flocculation of fine-grained sediments due to differential settling. *Journal of Geophysical Research*, 98(C6), 10279-10288.

Lick, W. and Lick, J. (1988). Aggregation and disaggregation of fine-grained lake sediments. *Journal of Great Lakes Research*, 14, 514-523.

Manning, A.J. and Dyer, K.R. (1999). A laboratory examination of floc characteristics with regard to turbulent shearing. *Marine Geology*, 160, 147-170.

McCandliss, R.R., Jones, S.E., Hearn, M., Latter, R. and Jago, C.F. (2002). Dynamics of suspended particles in coastal waters (southern North Sea) during a spring bloom. *Journal of Sea Reseach*, 47(3-4), 285-302.

McCave, I.N. (1975). Vertical flux of particles in the ocean. *Deep-Sea Research*, 22, 491-502.

McCave, I.N. (1983). Particulate size spectra, behaviour, and origin of nepheloid layers over the Nova Scotia continental rise. *Journal of Geophysical Research*, 88, 7647-7666.

McCave, I.N. (1984). Size spectra and aggregation of suspended particles in the deep ocean. *Deep-Sea Research*, 31(4), 329-352.

McCave I.N., Bryant, R.J., Cook, H.F., and Coughanowr, C.A. (1986). Evaluation of a laser diffraction size analyser for use with natural sediments. *Journal of Sedimentary Petrology*, 56, 561-564.

McCave, I.N. and Syvitski, J.P.M. (1991). Principles and methods of geological particle size analysis. In: Syvitski, J.P.M. (Ed.), Principles, methods and application of particle size analysis. Cambridge University Press, Cambridge.

Mikkelsen, O.A. and Pejrup, M. (2001). The use of a LISST-100 laser particle sizer for in-situ estimates of floc size, density and settling velocity. *Geo-Marine Letters*, 20, 187-195.

Milligan, T.G. and Hill, P.S. (1998). A laboratory assessment of the relative importance of turbulence, particle composition, and concentration in limiting maximal floc size and settling behaviour. *Journal of Sea Research*, 39, 227-241.

Moody, J.A., Butman, B. and Bothner, M.H. (1987). Near-bottom suspended matter concentration on the continental shelf during storms: estimates based on in situ observation of light transmission and a particle size dependent transmissometer calibration. *Continental Shelf Research*, 7(6), 609-628.

Nowell, A.R.M., Jumars, P.A. and Eckman, J.E. (1981). Effects of biological activity on the entrainment of marine sediments. *Marine Geology*, 5, 141-146.

Otto, L., Zimmerman, J.T.F., Furnes, G.K., Mork, M., Saetre, R., and Becker, G. (1990). Review of the physical oceanography of the North Sea. *Netherlands Journal of Sea Research*, 26(2-4), 161-238.

Paffenhőffer, G.A., Deibel, D., Atkinson, L.P. and Dunstan, W.M. (1980). The relation of concentration and size distribution of suspended particulate matter to hydrography in Onslow Bay, North Carolina. *Deep-Sea Research*, 27A, 435-447.

Partheniades, E. (1993). Turbulence, flocculation and cohesive sediment dynamics. In: Mehta, A. (Ed.), Coastal and estuarine studies, 42. Near shore and estuarine cohesive sediment transport. American Geophysical Union.

Poodle, T. (1986). Freshwater inflows to the Clyde Sea. *Proceedings of the Royal Society of Edinburgh*, 90B, 55-66.

Prandle, D. (1984). A modelling study of the mixing ^{137}Cs in the seas of the European Continental Shelf. *Phil. Trans. R. Soc. Lond.*, A244, 185-219.

Riley, J.B. and Agrawal, Y.C. (1991). Sampling and inversion of data in diffraction particle sizing. *Applied Optics*, 30(33), 4800-4817.

Rhoads, D.C. and Boyer, L.F. (1982). Effects of marine benthos on physical properties of sediments: A successional perspective. In: McCall, P.I. and Tevesz, M.J.S. (Eds.), Animal - sediment relations, Plenum, NewYork, 3-52.

Sequoia Scientific, Frequently asked questions, LISST-100, http://www.sequoiasci.com, accessed 1/7/2001a.

Simpson, J.H. (1997). Physical processes in the ROFI regime. *Journal of Marine Systems*, 12, 3-15.

Simpson, J.H. and Hunter, J.R. (1974). Fronts in the Irish Sea. *Nature*, 250, 404-406.

Simpson, J.H. and Rippeth, T.P. (1993). The Clyde Sea: a model of the seasonal cycle of stratification and mixing. *Estuarine, Coastal and Shelf Science*, 37, 129-144.

Soulsby, R. (1997). Dynamics of marine sands. Thomas Telford Publications, London, 1st Edition, 249pp.

Spicer, P.T. and Pratsinis, S.E. (1996). Shear induced flocculation: the evolution of floc structure and shape of the size distribution at steady state. *Water Research*, 50, 1049-1056.

Stolzenbach, K.D. and Elimelich, M. (1994). The effect of density on collisions between sinking particles: implications for particle aggregation in the ocean. *Journal of Deep Sea Research I*, 41(3), 469-483.

Syvitski, J.P.M. and Murray, J.W. (1981). Particle interaction in fjord suspended sediment. *Marine Geology*, 39, 215-242.

Tambo, N. and Hozumi, H. (1979). Physical characteristics of flocs –II. Strength of flocs. *Water Research*, 13, 421-427.

ten Brinke, W.B.M. (1994). Settling velocities of mud aggregates in the Oosterschelde tidal basin (the Netherlands), determined by a submersible video system. *Estuarine, Coastal Shelf Science*, 39, 549-564.

Tett, P. (1990). The photic zone. In: Herring, P.J., Campbell, A.K., Whitfield, M., Maddock, L. (Eds.), Light and Life in the sea, Cambridge University Press, 59-87.

Traykovski, P., Latter, R.J., Irish, J.D. (1999). A laboratory evaluation of the LISST instrument using natural sediments. *Marine Geology*, 159, 355-367.

Tritton, .J. (1988). Physical fluid dynamics. Oxford University Press, 2nd Edition, 519pp.

Tsai, C-H. (1996). An assessment of a time-of transition laser sizer in measuring suspended particles in the ocean. *Marine Geology*, 134, 95-112.

Tsai, C-H., Iacobellis, S., Lick, W. (1987). Flocculation of fine-grained lake sediments due to uniform shear stress. *Journal of Great Lakes Research*, 13, 135-146.

van Aken, H. (1986). The onset of seasonal stratification in shelf seas due to differential advection in the presence of a salinity gradient. *Continental Shelf Research*, 5(4), 475-485.

van de Hulst, H.C. (1957). Particles very large compared to the wavelength. In: Light scattering by small particles (1st edition). John Wiley & Sons Ltd., New York, 470pp.

van Leussen, W. (1997). The Kolmogorov scale as a limiting value for the floc sizes of suspended fine-grained sediments in estuaries. In:Burt, N., Parker, R. and Watts, J. (Eds.). Cohesive Sediments, John Wiley & Sons Ltd.

van Leussen, W. (1988). Aggregation of particles, settling velocity of mud flocs - a review. In: Dronkers, J. and van Leussen, W. (Eds.), physical processes in estuaries, Springer - Verlag, 347-403.

Vicsek, T. (1992). Fractal Growth Phenomena, World Scientific, Singapore.

Villaret, C and Trowbridge, J.H. (1991). Effects of stratification by suspended sediments on turbulent shear flows. *Journal of Geophysical Research*, 96(C6), 10659-10680.

Volten, H., Haan de, J.F., Hovenier, J.W., Schreurs, R., Vassen, W., Dekker, A.G., Hoogeonboom, H.J., Charlton, F., Wouts, R. (1998). Laboratory measurements of angular distributions of light scattered by phytoplankton and silt. *Limnology and oceanography*, 43 (6), 1180-1197.

Wells, J.T. and Shanks, A.L. (1987). Observations and geologic significance of marine snow in a shallow-water, partially enclosed marine embayment. *Journal of Geophysical Research*, 92,13185-13190.

Wheatcroft, R.A. and Butman, C.A. (1997). Spatial and temporal variability in aggregated grain - size distributions, with implications for sediment dynamics. *Continental Shelf Research*, 17 (40), 367-390.

Winterwerp, J.C. (1998). A simple model for turbulence induced flocculation of cohesive sediment. *Journal of Hydraulic Research*, 36(3), 309-326.

Winterwerp, J.C., 2002. On the flocculation and settling velocity of estuarine mud. *Continental Shelf Research*, 22(9),1339-1360.

Young, H.D. and Freedman, R.A. (1996). University Physics, Addison-Wesley, 1484pp., 9th edition.

Zaneveld, J.R.V., Sprinrad, R.W. and Bartz, R. (1982). An optical settling tube for the determination of particle size distribution. *Marine Geology*, 489, 357-376.

APPENDIX A

APPENDIX A

Technical Specifications of the LISST-100B

- An external analogue input (0-5V)
- Two external digital I/O ports (5V logic)
- Optical pathlength: 5cm
- Optical transmission: 12 bit resolution
- Particle size range: 1.2 - 250μm
- Resolution: 32 size classes, log spaced
- VSF angle range: 1.7 to 340 mrad
- Maximum sample speed: 4 size distributions per second
- Temperature sensor range: -10 to 45°C, resolution: 0.01°C
- Pressure sensor range: 0 to 300m of H_2O, resolution: 8cm of H_2O

Lower Limit	Median	Upper Limit
1.25	1.36	1.48 *+
1.48	1.60	1.74 *+
1.74	1.89	2.05 *+
2.05	2.23	2.42 *+
2.42	2.63	2.86 *+
2.86	3.11	3.38 *+
3.38	3.67	3.98 *+
3.98	4.33	4.70 *+
4.70	5.11	5.55 *+
5.55	6.03	6.55 *+
6.55	7.11	7.72 *+
7.72	8.39	9.12 *+
9.12	9.90	10.76 *+
10.76	11.69	12.69 *+
12.69	13.79	14.98 *+
14.98	16.27	17.68 *+
17.68	19.20	20.86 *+
20.86	22.66	24.62 *+
24.62	26.74	29.05 *+

Lower Limit	Median	Upper Limit
29.05	31.56	34.28 *+
34.28	37.24	40.45 *+
40.45	43.95	47.74 *+
47.74	51.86	56.33 *+
56.33	61.20	66.48 *+
66.48	72.22	78.45 *+
78.45	85.22	92.58 *+
92.58	100.57	109.25 *+
109.25	118.67	128.92 *+
128.92	140.04	152.13 *+
152.13	165.26	179.53 *+
179.53	195.02	211.85 *+
211.85	230.14	250.00 *+
250.00	271.58	295.02 +
295.02	320.48	348.14 +
348.14	378.19	410.83 +
410.83	446.29	484.81 +
484.81	526.65	572.11 +
572.11	585.89	600.00 +

Table A1.1. Logarithmic size classes for LISST (*) and Galai (+).

Elements	Parameter
1:32	Volume concentration (in μl/l) for size classes 1 through 32
33	Laser transmission sensor
34	Battery voltage in calibrated units
35	External auxiliary input 1 in calibrated units
36	Laser reference sensor in calibrated units
37	Pressure in calibrated units
38	Temperature in calibrated units of °C
39	Time stamp 1 (either hours or minutes)
40	Time stamp 2 (either minutes or seconds)
41	Computed % Optical transmission over path
42	Computed Beam-C in units of 1/m
(Optional) 43-75	Volume scattering function for 32 angles from small to large (see Table A1.3)

Table A1.2. The columns for LISST data outputted from the WINDOWS package.

0.0018	0.0022	0.0026	0.0030	0.0036	0.0042	0.0050	0.0059
0.0069	0.0082	0.0097	0.0114	0.0135	0.0159	0.0188	0.0221
0.0261	0.0308	0.0364	0.0429	0.0506	0.0597	0.0704	0.0830
0.0979	0.1154	0.1359	0.1600	0.1882	0.2210	0.2592	0.3032

Table A1.3. The angles (in radians) for the volume scattering function measurement.